Understanding how the laminar architecture of the posterior parietal cortex supports visual behaviour

Joanita Florence D'Souza

BA & BSc(Hons)

A thesis submitted for the degree of Doctor of Philosophy at

Monash University in 2024

Department of Physiology - Faculty of Medicine, Nursing and Health Sciences

Copyright Notice

Declaration of authorship

This thesis is an original work of my research and contains no material which has been accepted for the award of any other degree or diploma at any university or equivalent institution and that, to the best of my knowledge and belief, this thesis contains no material previously published or written by another person, or any use of generative artificial intelligence technologies, except where due reference is made in the text of the thesis.

Student Name: Joanita Florence D'Souza

Main Supervisor Name: Maureen Ann Hagan

Date (original submission): 21/03/2024

Date (final submission): 28/06/2024

Publications and presentations during enrolment

Publications:

- D'Souza, J. F., Price, N. S., & Hagan, M. A. (2021). Marmosets: a promising model for probing the neural mechanisms underlying complex visual networks such as the frontal–parietal network. *Brain Structure and Function*, 1-16.

Presentations:

- Virtual Poster Presentation at the Marmoset Bioscience Symposium (October, 2020) - Spatial cueing reduces marmoset reaction times in a six-target centre-out saccade task
- People's choice award at the Monash Biomedicine Discovery Institute 3 Minute Thesis Competition (2021)
- Overall runner up at the Monash Biomedicine Discovery Institute 3 Minute Thesis Competition (2021)
- Fully financially subsidised acceptance into the European Visual Neuroscience Summer School with a poster presentation (Germany, 2022) - The marmoset posterior parietal cortex: Laminar and topographic organisation of saccade-related response field properties
- Poster Presentation at the Society for Neuroscience Annual Conference (San Diego, USA, 2022) - Laminar and topographic organisation of saccade-related responses in the marmoset posterior parietal cortex
- Poster Presentation at the Australian Neuroscience Society Annual Conference (Brisbane, 2022) - Topographic organisation of saccade-related response field properties in the marmoset posterior parietal cortex

Contents

Covid-19 Disclosure

Behavioural work in non-human primates requires long periods of time to be devoted to animal training before data collection can begin. However, lockdowns throughout 2020-2021 (a total of 267 days in lockdown) and restrictions on lab personnel severely impacted my early learning and data collection. Ethics required me to be supervised until I could be competent in animal handling and surgery techniques which was not feasible during lockdown. There were also significant shipment delays on some of the recording equipment I required for my electrophysiological experiments, which were manufactured in the U.S. To compensate for these setbacks, I diligently worked on my literature review and set up a significant portion of my data analysis pipeline with some mock data in 2020. Because of my tenacity and determination, I was able to publish a large portion of my literature review (covered in Chapter 1 and 6) as a mini review in a special edition of a high-impact journal (Brain, Structure and Function) in 2021.

Once lockdowns lifted, I worked to become competent in behavioural training and electrophysiological techniques and was quickly able to collect a world-class data set independently for the remainder of my candidature. I finished collecting full datasets from 3 marmosets at the end of 2023. Due to unforeseeable health complications, two other animals I had originally trained were not able to participate in the collection of a full data set, which required me to start training new animals. Therefore, data analyses for Chapter 5 of this thesis is still preliminary and ongoing. However, I do intend to incorporate the full data sets from three animals into future publications based on the content in my thesis chapters.

Acknowledgements

To my esteemed PhD supervisors, I extend my enduring gratitude for your support, patience, invaluable guidance and profound expertise throughout my candidature. Under your mentorship, I was able to achieve things in the academic realm that I did not think possible. With your friendship, I was able to endure some of the toughest times of my professional career.

Dr Maureen Hagan,

Thank you for your unwavering optimism throughout. Your devotion to my project and genuine vested interest in my success are the primary reasons I was able to complete this PhD. I cannot thank you enough for being the most incredible role model both, professionally and personally. When I grow up, I want to be just like you.

Associate Professor Nicholas Price,

Thank you for all your advice and inputs - both genuine and sarcastic - throughout my post-graduate career. Your blunt insistence in my competence was often far more inspiring than you will ever realise.

To my colleagues in the lab, especially *Dr Elizabeth Zavitz, Associate Professor Yan Wong, Professor Marcello Rosa, Dr Shaun Cloherty, Dr Adam Morris* and *Katrina Worthy*. Thank you for helping me, teaching me, training me and shaping me into the researcher I am today.

To the 'MBI marmo crew', especially *Ranshi, Ken, Jessima, Elysee, and the team at MARP*. Working with research animals is possibly one of the hardest things that I have ever had to endure, both morally and emotionally. Without your support and genuine care for the animals, none of this would have been possible or worth it.

To *Ranshi Samandra* in particular - we've braved the trenches together for 4 long years, often with only each other as company. Through all the challenges and triumphs, your presence was a source of strength and solidarity that I will not soon forget.

To the rest of my friends and family, you may not have all understood why I started on this academic journey, but you always supported and encouraged me and were the first to celebrate my triumphs, for which I am extremely grateful. After years of the same question, I can finally say I've submitted my thesis. I can't wait to watch you give up trying to read it by page 3.

To *Rhys Murrian*, thank you for your endless support, blind faith and oftentimes hyperbolised praise. I made it through my PhD in large part because of your love and support. Now it's your turn - allow me to return the favour.

Last, but certainly not least, I would like to extend my deepest gratitude to the invaluable research animals whose vital role in my studies cannot be overstated. *99, Bart, Hugo, Andy*, *Ollie*, and all the marmosets I've ever worked with, your resilience and cooperation were never taken for granted and your contributions to neuroscience will forever be honoured with respect and gratitude.

I also acknowledge the use of generative AIs *ChatGPT* and *Github Copilot* to assist me in writing MATLAB code for the analyses, predominantly in Chapter 5.

This research was supported by an *Australian Government Research Training Program (RTP) Scholarship*.

Abstract

Understanding the neural mechanisms underlying cognitive functions has proven to be a difficult feat for the field of neuroscience. The overwhelming majority of systems neuroscience experiments have focused on the contribution of individual brain areas to a particular behaviour or cognitive process. However, in practice, no brain area works in isolation. They are intricately wired together in networks - through precise anatomical connections - to carry out high-level brain functions. Feedforward and feedback information across these networks are integrated and processed within the laminar architecture of the cortex. In this way, the differences between neural activity in superficial and deep layers reflect the transformation of information through laminar circuits.

The frontal-parietal network is implicated in oculomotor control and visual attention. The posterior parietal cortex (PPC) is a key region within the frontal-parietal network. However, we know very little about how information is organised and processed through the cortical layers here. In higher-order primates like humans and macaques, the PPC is embedded in sulci. This makes electrophysiology experiments that target specific layers of cortex challenging. The lissencephalic cortex of the common marmoset (*Callithrix jacchus*) provides access to PPC for detailed multi-electrode recordings across the laminar circuit. In this thesis, I trained 2 marmosets on eye movement tasks including a cued saccade task, to probe attentional mechanisms in the brain. While the marmosets performed visually-guided saccades, I recorded from PPC with multichannel, semi-chronic arrays that allowed me to simultaneously record neural activity across all cortical layers. Across 12 penetrations, sampling 2415 responsive units, I demonstrated topographic organisation of saccade-direction tuning properties in PPC. Another key challenge with laminar recordings is the ability to assign recording locations to cortical layers *in vivo*. Traditional methods are unreliable in their layer estimates outside of primary sensory areas. To address this, I analytically compared several new methods. I further developed, validated, and implemented a new laminar classification method. This allowed me to perform the first layer-based analysis of attentional modulation in the PPC, which demonstrated that visual attention primarily modulates saccade-direction selective neurons within the superficial layers. This functional observation is consistent with previous anatomical studies tracing feedback connections from the frontal eye fields to the superficial layers of the PPC and suggests that the source of attention modulated signals into the PPC may come from the frontal cortex. Ultimately, this thesis lays the groundwork for understanding how cognition is supported by networks of brain areas.

List of abbreviations

CSD - current source density analysis

FEF - Frontal eye field

LFP - local field potential

LIP - Lateral intraparietal area

MT - middle temporal area

PMA - phase mean angle

PPC - Posterior parietal cortex

SPI - spike phase index

SRT - saccade reaction time

V1 - primary visual cortex

V4 - visual area 4

Chapter 1 - Introduction

Understanding the neural mechanisms underlying cognitive functions has proven to be a difficult feat for the field of neuroscience. The overwhelming majority of systems neuroscience experiments have focused on the contribution of individual brain areas to a particular behaviour or cognitive process. In practice, no brain area works in isolation. Networks of brain areas work together - wired together with precise anatomical connections - to carry out high-level brain functions. A prime example of this is the frontal-parietal network, which comprises a cluster of areas across the frontal and posterior parietal cortices (PPC), that have been tied to a wide range of behavioural and cognitive processes including oculomotor control, motor preparation, visual attention, and decision-making (Wurtz and Mohler, 1976; Colby et al., 1996; Kustov and Robinson, 1996). Within the frontal-parietal network, two key areas, frontal eye fields (FEF) and the lateral intraparietal area (area LIP), have been tied to the control of brief, rapid exploratory eye movements known as saccades. On the surface, both FEF and area LIP appear to have largely overlapping functional roles, but the contribution of each of these nodes independently, still remains unknown.

Non-invasive techniques that allow for whole brain studies, such as functional magnetic resonance imaging (fMRI) and magnetoencephalography (MEG) have been useful in looking at network interactions, but are limited either spatially or temporally, making it impossible to draw conclusions at the level of precise anatomical connectivity. While voltage and calcium-sensitive dyes have permitted valuable measurements and analysis of large populations of neural activity at once, these techniques are sub-optimal for investigations into network activity and interactions between cortical areas. In recent years, multi-area electrophysiology studies aimed at addressing this gap by recording neural activity during visual behaviours have become more common (Saalmann et al., 2007; Dean et al., 2012; Siegel et al., 2015; Wong et al., 2016). However, these techniques largely only permit correlational conclusions to be drawn about the neural activity that accompanied cognitive functions. In order to claim that a particular region plays a causal role in the generation of a cognitive function, the activity of individual neurons must be perturbed to observe the direct effects on cognitive functions and behaviour (Parker and Newsome, 1998). Traditionally, this has been achieved through invasive techniques such as electrical stimulation or cortical lesions induced via pharmacological manipulations or cooling methods. While these techniques are extremely valuable, they lack the temporal and spatial precision necessary to study functional contributions of specific cell types and their interactions with other brain regions. Often, they non-selectively involve large regions of cortex, simultaneously activating all output pathways in a region. Designer receptors exclusively activated by designer drugs (DREADDs), a technique that can control molecularly defined subsets of cells through engineered G-protein-

coupled receptors, overcomes the spatial resolution limitations of these aforementioned techniques, but sacrifices temporal resolution. DREADDs operate in the range of minutes to hours, modulating neuronal activity in a much more prolonged fashion (reviewed in Whissell et al., 2016). Currently, optogenetics is the only technique with both high temporal and spatial resolution, offering a way in which to target and control precise cell-types in vivo, on a millisecond time-scale (Boyden et al., 2005; Deisseroth, 2011). By genetically modifying specific types of neurons and causing them to express light-sensitive membrane proteins known as opsins, this technique enables precise, targeted control of neural circuits with specific wavelengths of light that can be delivered from outside an intact dura.

One current limitation in connecting these technologies to visual and cognitive behaviours is the choice of animal model. Rodents have been the primary animal model for the development of new molecular technologies, but they lack homologous cortical networks to humans and rely far less on their vision. Primates, on the other hand, predominantly use their vision and saccadic eye movements to monitor and interact with their environment. The macaque monkey in particular, has been the main source for understanding cognitive visual behaviour, because its cortical networks, including the frontal-parietal, are remarkably similar to humans. However, in macaques, many key areas of interest, including parts of FEF and area LIP, are buried within the sulci of the brain, making access challenging, particularly for precise neural stimulation, multi-electrode laminar recordings, and imaging studies.

Recently, the common marmoset, a small-bodied New World primate, has gained popularity as a primate model for neurophysiology research (Solomon and Rosa, 2014; Mitchell and Leopold, 2015). Among their many advantages, marmosets have a small body and fast reproduction cycles, making them amenable to transgenic technology (Sasaki et al., 2009). The anatomical subdivisions of cortical areas in the marmoset have also been mapped, and their anatomical connections are consistent with humans and macaques (Rosa et al., 2009; Majka et al., 2016, 2020). Furthermore, marmosets have a rich behavioural repertoire consisting of both natural (Miller and Wren Thomas, 2012) and conditioned (Mitchell et al., 2014, 2015) tasks. Marmosets also rely strongly on their sense of sight – a fact that is reflected in the large fraction of their neocortex dedicated to visual processing (Rosa et al., 2009; Majka et al., 2016, 2020) and their highly developed visual system that is homologous to higher order primates like humans and macaques (Chaplin et al., 2013; Zhu and Vanduffel, 2019). Compared to humans and other primate models, marmosets have a relatively small brain size, which may be a limitation in their use for studying cognitive behaviour. However, in the evolutionary development of primate brains, the differential expansion of cortical areas has largely been conserved across primate species relative to brain size (Chaplin et al., 2013; Zhu and Vanduffel, 2019). This means that changes in cortical expansion from marmoset to macaque in a given cortical area (Fig 1.1A, B) are predictive of the expansion expected from

macaque to human. Some areas of cortex have expanded greatly with brain size, such as the ventrolateral prefrontal cortex and temporal parietal junction, which in humans are related to high-level cognitive functions including speech and communication (Fig 1.1C, red regions). Conversely, areas of the PPC (containing area LIP), scale more modestly between marmosets and macaques (Fig 1.1C, dorsal view, arrow), and the expansion of early-developing visual areas like V1 is even more modest (Fig 1.1C, dorsal view, dark blue regions). This suggests that marmosets may still be a useful model for studying many visual behaviours, despite their small brain size.

Recent research has also confirmed that marmosets can be trained to perform a wide range of visual, oculomotor and cognitive tasks while head restrained, in a manner comparable to macaques and humans (Mitchell et al., 2014, 2015; Johnston et al., 2019; Cloherty et al., 2020). The marmoset brain also has major advantages over rodents and other primate models for neurophysiological research. Critically, the surface of the marmoset brain is lissencephalic, exposing nearly all of it's visual cortex on the lateral surface just below the skull, enabling direct access to many high-level brain areas – including important visual and oculomotor areas – that do not have clear homologues in the rodent and that are otherwise buried deep in sulci in primates like the macaque. This facilitates optical imaging and permits precise perpendicular penetrations of cortical layers for laminar analysis of local microcircuits in higher order visual areas such as FEF and area LIP, that are normally hidden in sulci. It also enables large scale neuronal recordings over entire cortical areas, uninterrupted by sulci and permits access to multiple cortical areas simultaneously (Isa, 2017). As such, marmosets serve as an important experimental bridge by which advances in the mouse community can be applied to the primate brain.

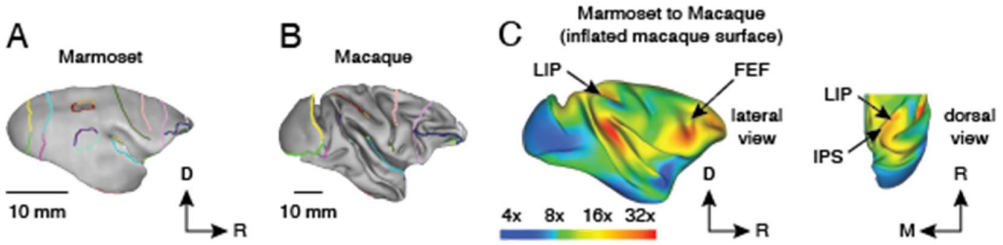

Figure 1.1 Expansion of frontal-parietal areas are conserved in primate evolution. *a) Marmoset and b) macaque brains with identified landmarks which served as anchor points to calculate expansion of cortex across species. Notably, the IPS (maroon) and anterior border of area 8aV (lavender) were used. c) Expansion map projected onto the surface of an inflated macaque brain showing the lateral view of cortex and a dorsal view of the posterior parietal cortex. Color scale indicates the factor of expansion. D, dorsal; M, medial; R, rostral. Adapted from Chaplin et al., 2013*

Acknowledging that the viability of marmosets for studies on the visual system has been previously reviewed (Solomon and Rosa, 2014; Mitchell and Leopold, 2015), here, I extend upon and update this body of knowledge, by specifically examining why marmosets are an ideal model for untangling the neural mechanisms underlying inter-area interactions in the visual system. Using the frontal parietal network as an example in marmosets, I explore what is currently known about the structure and function of key nodes in this network: namely, FEF and area LIP.

1.1 Key areas in the frontal-parietal network are conserved in marmosets and macaques

Areas of the frontal parietal network have been largely defined based on function, and do not precisely overlap with cytoarchitecturally-defined boundaries. Furthermore, sulcal folding in the brains of higher order primates, such as humans and macaques, makes precise anatomical reconstructions challenging. For example, FEF in primates is defined functionally by the ability to induce and influence saccades via microstimulation. In macaques, FEF is likely comprised of cytoarchitectural areas 45, 8aV, and 6 (Bruce et al., 1985; Stanton et al., 1989; Schall et al., 2020), which have anatomical connections with the parietal and visual cortices (Schall et al., 1995a) and connections with the superior colliculus both directly (Fries, 1984) and via the pulvinar (Sommer and Wurtz, 2006; Berman et al., 2009). Projections from FEF to the PPC are dense, feedback projections (Schall et al., 1995a; Stanton et al., 1995). Area 8aV is characterized by large pyramidal neurons in layer V, and at least partially overlaps with the region in which microstimulation evokes saccadic eye movements (Stanton et al., 1989). In marmosets, the precise anatomical boundaries of FEF are still being established. However, converging evidence suggests that a similar group of cytoarchitectural areas is involved. Anatomically, areas 8aV and 6DR form monosynaptic reciprocal connections with extrastriate visual areas and the posterior parietal cortex (Burman et al., 2006; Reser et al., 2013). One anatomical tracing study has identified neurons in the frontal cortex of the marmoset that project to the superior colliculus (Collins et al., 2005). The region appears to correspond roughly to marmoset area 8, however this study did not register to precise cytoarchitectural areas and their injections spanned superficial to deep layers of the superior colliculus. More detailed anatomical studies are needed to fully map out the marmoset cortico-collicular circuits associated with oculomotor behaviours.

In 1874, Ferrier and colleagues were the first to unilaterally stimulate FEF in anaesthetised macaques and elicit rapid contralateral eye movements known as saccades (Ferrier, 1874). This general finding that a brief stimulation of FEF produces a single contralateral saccade, of a particular amplitude, direction, latency and threshold, was reliably replicated by several other groups in the coming years, and in both humans and awake non-human primates (Robinson and Fuchs, 1969; Wurtz and Mohler, 1976; Bruce et al., 1985; Schmolesky et al., 1998; Schall et al., 2020). One notable study stimulated FEF in over 300 locations and noticed that the amplitude and direction of saccades changed in a stereotyped pattern, depending on where and how FEF was stimulated (Robinson and Fuchs, 1969). Evoked saccades in FEF also follow a visual topography - smaller, more foveal saccades are evoked from stimulation of the ventrolateral regions and larger, more peripheral saccades in the dorsomedial regions of FEF (Bruce et al., 1985).

Consistent with macaque literature, electrical stimulation of several frontal cortical sites in marmosets evokes eye and head movements (Mott et al., 1910; Blum et al., 1982). Recently, the dorsolateral prefrontal cortex of awake, free-viewing marmosets was electrically stimulated using a 96-channel Utah array (Selvanayagam et al., 2019). By co-registering their recordings with anatomical MRIs, they were able to provide precise reports of cytoarchitectural areas. In addition to evidence placing marmoset FEF in a similar relative location within oculomotor areas 45 and 8aV (Burman et al., 2006; Reser et al., 2013; Schaeffer et al., 2019), Selvanayagam and colleagues (2019) found that like human (Silver and Kastner, 2009; Jerde and Curtis, 2013) and macaque FEF (Bruce et al., 1985; Schall et al., 1995a), marmoset FEF is organised in a topographical manner, according to saccade direction and amplitude. Area 45 and the lateral portion of 8aV were associated with smaller, more foveal saccades (Fig 1.2A,B), and saccade amplitudes increased medially across the array, spanning areas 8aV and 6DR. In marmosets, the saccades evoked by area 6 stimulation tend to be goal-directed in contrast to vector coding of area 8aV, which is similar to the cortical eye fields in macaques (Selvanayagam et al., 2019). Among the few differences between marmosets, humans and macaques, saccade latencies in marmosets at low currents were noted to be longer and more variable. It is worth noting that there is some discrepancy in the cytoarchitectural definition of area 45 between humans and monkeys. Both macaque (Schall et al., 1995b) and marmoset (Selvanayagam et al., 2019) studies have suggested that as small amplitude saccades can be evoked from area 45, it likely comprises the ventral portion of the FEF. Area 45 in these studies is defined using Walker's definition (Walker, 1940), as large pyramidal cells in layers III and V (Schall et al., 1995b; Burman et al., 2006; Reser et al., 2013). In humans, area 45 is characterised by large pyramidal cells in layer III but not layer V (Petrides and Pandya, 2002). Cells in area 45 by this definition likely have non-oculomotor functions (Petrides et al., 2005).

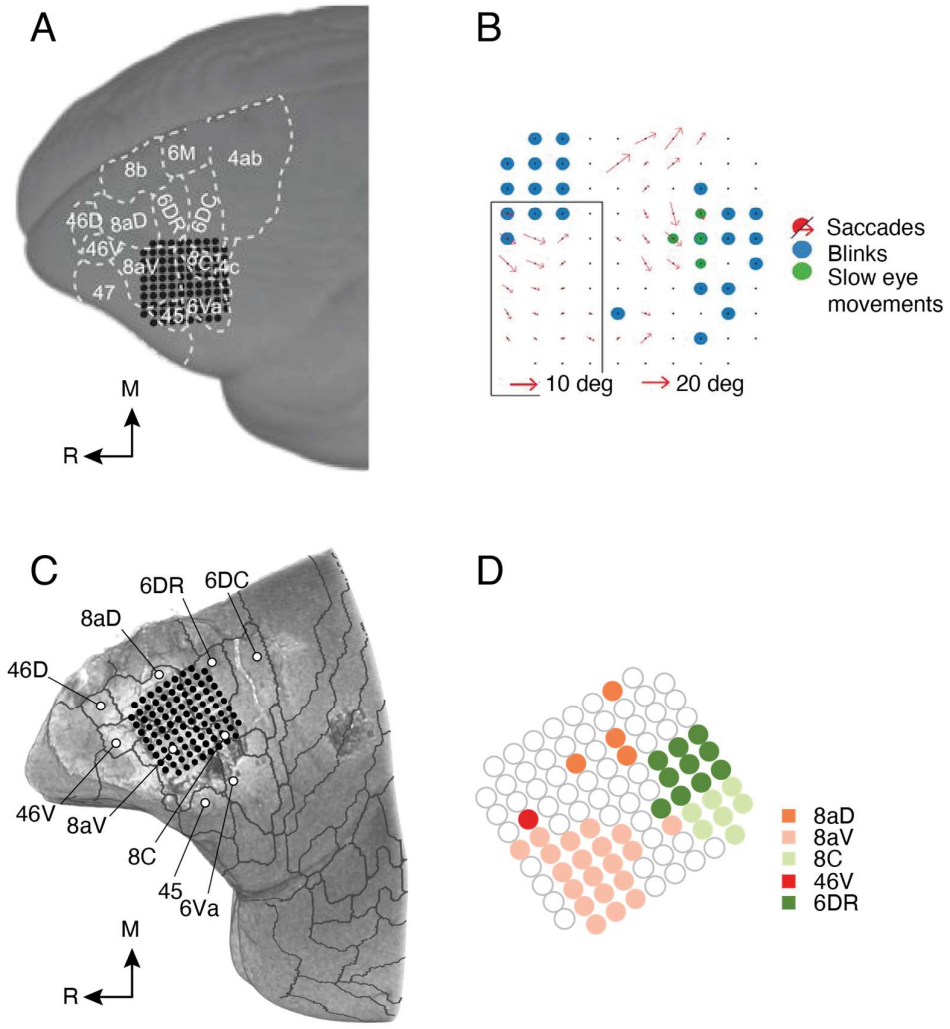

Fig 1.2 FEF-like responses in the marmoset prefrontal cortex. *a) Example marmoset MRI reconstruction of array recording locations aligned to cytoarchitectural boundaries and b) Electrode map for example showing location of saccade, blink and smooth pursuit responses in response to microstimulation. Red arrows indicate amplitude of evoked saccades. Adapted from Selvanayagam et al., 2019. c) Example marmoset MRI reconstruction of array recording locations aligned to cytoarchitectural boundaries and D, Electrode map showing location of visual responses according to cytoarchitectural area. Adapted from Feizpour et al., 2021. M, medial; R, rostral*

In addition to evoking saccades, a subset of macaque FEF neurons have visual responses, with large receptive fields (Wurtz and Mohler, 1976; Cavanaugh et al., 2012) and brisk response latencies (Mohler et al., 1973; Thompson et al., 1996; Schmolesky et al., 1998). Despite FEF's relatively late position in the visual hierarchy, visual responses in FEF have short latencies, comparable to early visual areas such as visual area 2 (V2), which may be due to direct connections with the visual cortex or connections that bypass the hierarchy from the superior colliculus via the thalamus. Similar visual responses can be found in marmosets, particularly in areas 8aV, 8C and 6DR (Fig 1.2C,D; Feizpour et al., 2021). In macaques, the lateral portion of FEF receives afferents from more foveal representations of visual cortex,

while the medial portion receives afferents from peripheral representations of visual cortex (Schall et al., 1995a). The same is true for area 8aV in marmosets (Reser et al., 2013). Consistent with this, in marmosets, the central visual field was better represented by the lateral aspect of area 8aV and the peripheral visual field was better represented by the medial aspect of area 8aV (Feizpour et al., 2021).

The FEF is not the only specialised region of the frontal parietal network that contributes towards visual behaviours. In the PPC, area LIP has been implicated in guiding saccadic eye movement control (Andersen et al., 1985, 1990b). Specifically, area LIP neurons respond to the presentation of behaviourally-relevant visual stimuli in localised regions of space (Gottlieb et al., 1998; Kusunoki et al., 2000) and saccade planning (Mazzoni et al., 1996). In macaques, area LIP is buried in the lateral bank of the intraparietal sulcus within the PPC, and has direct reciprocal anatomical connections to other nodes in the saccade control network such as FEF and the superior colliculus (Huerta et al., 1987; Andersen et al., 1990a; Blatt et al., 1990; Schall et al., 1995b; Stanton et al., 1995; Paré and Wurtz, 1997; Anderson et al., 2011). In fact, microstimulation of FEF in macaques elicits an enhanced fMRI activation of area LIP neurons (Premereur et al., 2013) during visually guided saccade tasks, fixation tasks and even in absence of any visual stimulation (Ekstrom et al., 2008). The laminar distribution of neurons and the dorsal-ventral subdivisions and myelination patterns of marmoset area LIP are similar to those in macaques (Rosa et al., 2009). Anatomical studies in marmosets have also triangulated connectivity between area LIP, FEF and the superior colliculus, reflecting observations in the macaque visual system (Collins et al., 2005; Reser et al., 2013; Ghahremani et al., 2017).

Like FEF, microstimulation of area LIP neurons evokes eye blinks and saccadic eye movements of a particular direction and amplitude in macaques (Shibutani et al., 1984; Thier and Andersen, 1998; Hanks et al., 2006) and marmosets (Ghahremani et al., 2017). Electrophysiological recordings in macaque area LIP have also revealed that most neurons discharge in the ‘planning stage’, just prior to the execution of saccades towards visible and remembered visual targets (Gnadt and Andersen, 1988; Barash et al., 1991; Colby et al., 1996; Meister et al., 2013) within their response fields. For example, during saccade tasks where the end target onset is delayed after the fixation target disappears, a “gap effect” of shorter saccade reaction times coupled with an increase in neural activity during the gap period has been recorded in macaques (Chen et al., 2013, 2016) as well as marmosets (Ma et al., 2020). Generally, area LIP neurons respond to a combination of visual stimuli, eye position and the direction and amplitude of planned eye movements, to encode the location of salient visual stimuli in eye-centered or head-centred coordinates (Andersen et al., 1985, 1990b).

Neural activity in the PPC, and notably area LIP has also been shown to be modulated by cognitive factors like visual attention (Goldberg et al., 1990; Colby et al., 1996; Snyder et al., 1997; Corbetta et al., 1998; Colby and Goldberg, 1999; Bisley and Goldberg, 2003, 2010), reward (Platt and Glimcher, 1999; Sugrue et al., 2004) and decision-making (Gold and Shadlen, 2000; Hawellek et al., 2016a; Wong et al., 2016). Area LIP is thought to integrate bottom-up sensory and top-down cognitive factors by combining and transforming visual information such as initial eye position with cognitive factors to produce a salience representation or 'priority map' of the visual field, that combines salient visual features with behavioural goals (Gottlieb et al., 1998; Bisley and Goldberg, 2010; Chen et al., 2020; Fiebelkorn and Kastner, 2020). In macaques, neurons in area LIP signal the location of the visual target rather than the saccade goal (Gottlieb and Goldberg, 1999), which has been suggested to dissociate between the locus of visual attention and the saccade motor plan. However, when visual presentation of the target and saccade execution were temporally separated, it was found that area LIP neurons first encoded the location of the visual cue, and later, some neurons also responded during saccade execution (Zhang and Barash, 2000, 2004).

Whether marmoset PPC is also modulated by such cognitive factors is yet to be determined. However, there is evidence that marmosets can perform antisaccades, a type of cognitively demanding visual task. Antisaccade tasks typically require subjects to suppress a response to a salient, peripherally appearing stimulus, in favour of saccading to a featureless, unmarked location opposite this salient stimulus (Munoz and Everling, 2004; Antoniades et al., 2013). In such tasks, the shape and/or colour of the central fixation point instructs the subject about whether the trial requires a saccade towards (prosaccade) or away from (antisaccade) the salient peripheral stimulus. Recently, (Johnston et al., 2019) observed that marmosets were capable of completing a slightly modified version of the traditional antisaccade task, and that neurons in area LIP responded to both pro- and antisaccade targets.

1.2 Marmosets are capable of a wide range of visual behaviours

The common marmoset (*Callithrix jacchus*), like the rhesus macaque (*Macaca mulatta*) and humans, displays coordinated eye-hand behaviours (Hook and Rogers, 2008), and areas of their frontal cortex suggest some anatomical similarities to macaque motor and premotor reach and grasp areas (Burman et al., 2014a, 2014b). This suggests that they may also be a suitable model for some visually-guided reaching behaviours, although with some important caveats (see Bakola et al., 2015 for a review).

Visual attention and saccadic eye movements are intimately linked from behavioural and anatomical perspectives. The spatial allocation of attention is tightly time-locked and precedes saccade execution (Filali-Sadouk et al., 2010), and in order to make a saccade towards an appropriate location, attention must be directed towards the spatial location of the saccade target. Anatomically, visual attention and saccadic behaviours recruit a common network in the primate visual system (reviewed in (Wardak et al., 2011). In humans, fMRI has demonstrated activation of similar regions in the frontal and parietal cortices during saccades and visual attention shifts (Corbetta, 1998; Nobre et al., 2000; Perry and Zeki, 2000; DeSouza et al., 2003; Munoz and Everling, 2004; de Haan et al., 2008).

Given the functional and neuro-anatomical similarities between marmosets and higher order primates like macaques and humans, it is worth examining whether marmosets are an appropriate behavioural model for probing the frontal parietal saccade network. For decades, macaques were the ideal model for psychophysical and behavioural paradigms in visual research, demonstrating an immense capacity to learn complex rules and concentrate for long periods of time. Marmosets, on the other hand, have fallen short of macaques on such behaviours - managing to complete approximately half as many trials as macaques, with sessions typically lasting 1 to 2 hours (Mitchell et al., 2014; Hung et al., 2015; Chen et al., 2021). While this can largely be attributed to the type of task being relatively unnatural for marmosets, requiring extended fixation periods and head restraint, we are still in the early stages of learning the extent of their behavioural repertoire. However, with constant improvements in the efficiency and precision of neural data collection and our ability to combine data across sessions, this is no longer a significant limitation to the marmoset model. Marmosets also tend to excel under unrestrained conditions, and in natural free-viewing or visual discrimination tasks that are more actively engaging (Mitchell et al., 2014). As such, marmosets are the ideal candidate when utilising such paradigms, especially considering the potential for using standard eye tracking to measure visual behaviour in freely moving subjects (Jendritza et al., 2021).

When considering performance under head restraint, the main sequence of saccadic eye movements in marmosets is similar to that observed in macaques and humans, with a linear relationship between the amplitude and peak velocity of saccades (Mitchell et al., 2014; Chen et al., 2021). However, the range to which marmosets can rotate their eyes away from a default central position, is far more restricted compared to macaques and humans (Mitchell et al., 2014; Chen et al., 2021). Marmosets make saccadic eye movements within ten degrees of their initial rest position (Mitchell et al., 2014). Express saccades, or saccades with very low latencies, can be elicited using a ‘gap’ saccade task, in which the central fixation point disappears prior to the saccade target onset. Humans, macaques, and marmosets all exhibit low-latency express saccades in a gap-saccade task (Ma et al., 2020; Chen et al., 2021).

Marmosets can also perform smooth pursuit eye movements, in which the eye voluntarily tracks a moving target, with similar velocity and acceleration profiles to macaques and humans (Mitchell et al., 2015). In a motion-discrimination task, marmosets displayed similar speed-accuracy tradeoffs to humans. Saccade errors and reaction times increased as the motion signal decreased (Cloherty et al., 2020). Together, these results show that the marmoset is a promising model for studying eye movement behaviour.

As previously mentioned, marmosets are capable of completing a slightly modified version of the traditional antisaccade task (Johnston et al., 2019). In this version of the task, antisaccade trials were presented in an entirely separate block from prosaccade trials, and marmosets made antisaccades towards a small, dimly lit peripheral stimulus. This version of the antisaccade task has not only been used in human studies (Barton et al., 2002; Edelman et al., 2006; Dafoe et al., 2007; Antoniades et al., 2013), it is also usually the final training stage for macaques - though (Johnston and Everling, 2011) have previously noted that some macaques have also struggled advancing past this stage. While this version of the antisaccade task did not require a geometric calculation of vector inversion of the location of the stimulus into a saccade command, it retained the most important clinical and cognitive components, such as response suppression, voluntary saccade generation, longer reaction times and higher error rates. These core components have been shown to require inhibition of the frontal parietal saccade network (O'Driscoll et al., 1995; DeSouza et al., 2003).

Saccadic eye movement behaviours are closely linked to cognitive behaviours such as decision-making and visual attention. The extent to which marmoset saccade behaviour is linked to cognitive behaviour is still poorly understood. However, their eye movements are drawn to salient features of a visual stimulus, similar to macaques and humans. Primates tend to fixate salient features of an image, which may be driven by properties of the visual stimulus like colour, luminance and motion (Chen et al., 2021) or be cognitively salient, like faces (Mitchell et al., 2014). Marmosets have also been proposed as a model for studying social behaviours (Miller et al., 2016; Nummela et al., 2017). In a free choice task, where marmosets choose between two saccade targets, marmosets were more likely to choose a target if they first viewed an image of a conspecific, with gaze oriented to one of the target locations (Spadacenta et al., 2019). This 'joint-attention' or reflexive gaze following behaviour is also observed in humans and macaques, further illustrating that cognitive visual behaviours are homologous in the marmoset.

However, it is important to note that, to date, there has been little evidence that marmosets are capable of the same level of cognitive control as their macaque counterparts. Macaque studies have relied on training subjects to fixate for long durations (on the order of 2-3 seconds) while suppressing saccades to salient stimuli, whether this is a briefly flashed

stimulus in a memory-guided saccade task (Andersen et al., 1990b), a stimulus cueing an anti-saccade away from the stimulus (Gottlieb and Goldberg, 1999), or task that requires covertly searching an array of stimuli (Thompson et al., 1996; Wardak et al., 2006). To date, marmoset studies have yet to demonstrate delayed responses to visual stimuli. Fixation durations have been shorter (approximately 1 second, for example in (Ma et al., 2020). The shorter fixation duration makes delayed-saccade tasks more challenging. Furthermore, it is still an open question whether marmosets can suppress saccades to peripheral targets for more than a few hundred milliseconds (Mitchell et al., 2014). As described above (Johnston et al., 2019), researchers settled on a modified version of the anti-saccade task. While the limits of marmoset behavioural training are still largely unknown, it is important to note that there are likely significant limitations on the types of cognitive visual tasks they can perform compared to macaques.

1.3 Bridging the gap: from brain networks to behaviour

The next frontier in systems neuroscience is understanding not just how individual areas of the brain contribute to cognitive behaviour, but how areas of the brain work together. Non-invasive imaging techniques, such as fMRI have the advantage of measuring physiological changes across the whole brain simultaneously. Functional imaging studies have revealed that FEF and area LIP are almost always coactivated in attention and saccade tasks in both humans (Corbetta, 1998; Nobre et al., 2000; Perry and Zeki, 2000; de Haan et al., 2008) and macaques (Koyama et al., 2004; Baker et al., 2006; Wardak et al., 2010). In marmosets, fMRI has revealed homologous networks for vision (Fig 1.3A) and saccadic eye movements (Fig 1.3B). A free-viewing task, in which videos of action movie trailers were displayed at different locations on a screen, revealed activation of visual cortical areas as well as frontal-parietal areas, with peaks in area LIP and area 8aV. The same task in humans confirmed that activation peaked in area LIP and the FEF (Schaeffer et al., 2019). These findings built on an earlier study which found similar results while marmosets viewed static images, although the static images did not evoke as much parietal activity (Hung et al., 2015). Together, these studies lay the foundation for establishing homologous functional networks for visual behaviour in the marmoset. Unfortunately, due to the long time-scale of the hemodynamic response, fMRI alone cannot provide insights into the cellular-level circuitry involved in inter-area communication.

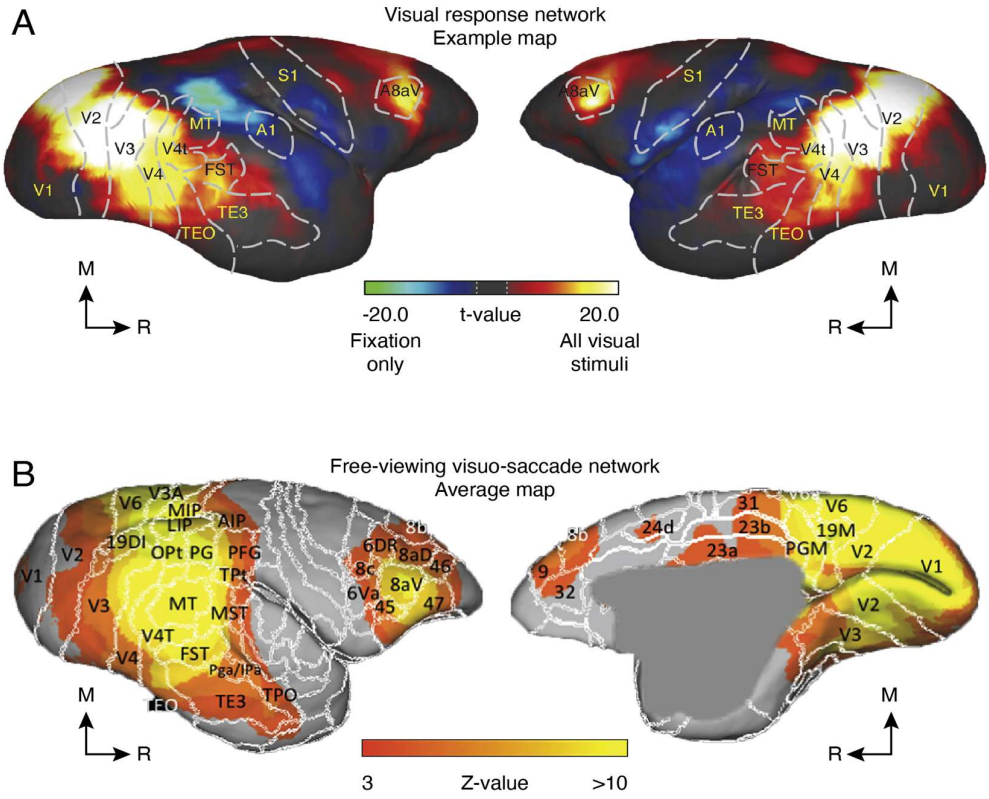

Figure 1.3 Networks for visual and saccade responses in the marmoset. *a) Visual response network in an example marmoset (left and right hemispheres shown). Functional MRI responses were compared between viewing static visual images and a fixation task (lateral, left and medial, right views shown). Adapted from (Hung et al., 2015). b) Visuo-saccade network averaged across responses of three marmosets (l. Functional MRI responses were recorded while marmosets free-viewed videos displayed at different locations on a monitor. Adapted from Schaeffer et al., 2019. M, Medial; R, Rostral*

In macaques, a growing number of studies have used multi-area extracellular recordings to look at temporal correlations in activity across nodes of the frontal parietal network. These studies have given insights into how the timing of neural activity across nodes of the network contribute to behaviour. For example, neurons in the frontal and parietal cortex signal task and choice information with the same latency (Siegel et al., 2015). Furthermore, temporally coherent neural activity across nodes of the frontal parietal network is instrumental in guiding eye-hand coordination (Dean et al., 2012; Hagan and Pesaran, 2022), decision-making (Pesaran et al., 2008; Wong et al., 2016) and visual attention (Buschman and Miller, 2007; Saalmann et al., 2007, 2012; Gregoriou et al., 2009; Bastos et al., 2015a; Fiebelkorn et al., 2018). However, large scale optical imaging, multi-electrode and multi-area recordings are challenging in macaques, because they rely on access to the entire surface of the cortical areas in question, and most high-level extrastriate areas of the macaque visual system, like FEF and area LIP, lie partially obscured within sulci. Most imaging and multi-electrode studies in macaques have been conducted on earlier visual areas like V1, because they lie exposed and unobscured on the cortical surface (for example see Chen and Seidemann, 2012) .

Typically, such studies have found a homogeneous topographical layout of the visual field across these early visual areas, where neurons in adjacent columns have receptive fields that overlap regions of the retina. However, growing evidence suggests a more fractured and twisted topography exists in extrastriate areas. Notably, the lissencephalic marmoset cortex, which is uniquely suited to such large-scale optical imaging and multi-electrode investigations, has corroborated such evidence, finding a more twisted topography with regions of rapid change in receptive field positions in extrastriate regions like the dorsomedial area (Yu et al., 2020). High-resolution fMRI maps of the macaque visual cortex have also depicted similar heterogeneous topographical layouts and retinotopic maps (Zhu and Vanduffel, 2019). The middle temporal area, an area of the brain involved in encoding visual motion, is another example of an area obscured in macaque sulci but exposed to the cortical surface in marmosets. High density electrode array recordings from the middle temporal area of the marmoset have revealed population dynamics including neural correlations (Solomon et al., 2015), spatial encoding (Chen et al., 2015), and motion adaptation (Zavitz et al., 2016). Although they did not include population analyses, similar multi-electrode arrays have been used in both the frontal (Selvanayagam et al., 2019; Feizpour et al., 2021) and parietal (Ma et al., 2020) cortices of marmosets.

Furthermore, the marmoset lissencephalic cortex is well suited for linear electrode arrays which enable simultaneous recordings across cortical layers, when inserted perpendicular to the cortical surface. Such recordings are of importance when studying inter-area networks, as a canonical microcircuit has been traced within several neocortical areas, dictating how information is hierarchically processed in a sequential manner (Wiesel et al., 1974; Douglas et al., 1989; Douglas and Martin, 2004; Shepherd, 2011). Feedforward inputs from regions lower in the visual hierarchy synapse onto the intermediate layer and project up via excitatory neurons to the superficial layers, where they are then integrated with and modulated by feedback information from the same or higher-order cortical regions, before finally projecting to deeper layers (Malach et al., 1997; Solomon et al., 2002; Majaj et al., 2007) and ultimately projecting out to other cortical areas (Thomson and Bannister, 2003). Notably, studies have often found that majority of the feedback connections terminating in superficial layers terminate in layer 1 (Rockland and Pandya, 1979; Federer et al., 2021). Figure 1.4 illustrates the typical flow of information in such microcircuits.

In macaque areas that lie on the cortical surface, such as area visual area 4 (V4), laminar-specific mechanisms have been revealed for visual attention (Nandy et al., 2017) and attention modulated V1-V4 communication in directed, laminar specific manner (Ferro et al., 2021). Specifically, layer and cell specific differences in the mean firing rate, spike count correlations and spike-spike coherence due to attentional modulation have been found within V4 colour selective columns (Nandy et al., 2017). Notably, differences between superficial and

deep layers reflect the transformation of information through the laminar circuit. Superficial layers have been found to encode feedforward sensory information like stimulus orientation, while deeper layers coded for the direction of planned eye movements (Pettine et al., 2019). Differences have also been recorded in the beta frequency range of electrical signals between layers, that corresponded to attentional states in the macaque (Westerberg et al., 2021). When attending to a stimulus inside the response field (RF), there was stronger feature-selective beta activity in deeper layers of V4, as opposed to the stronger activity recorded in superficial layers when monkeys were not attending to stimuli. Beta-frequency coherences also differ between cortical layers. Nandy et al. (2017) reported attention-dependent decreases in beta coherence in superficial and input layers of V4, and opposing increases in deeper layers.

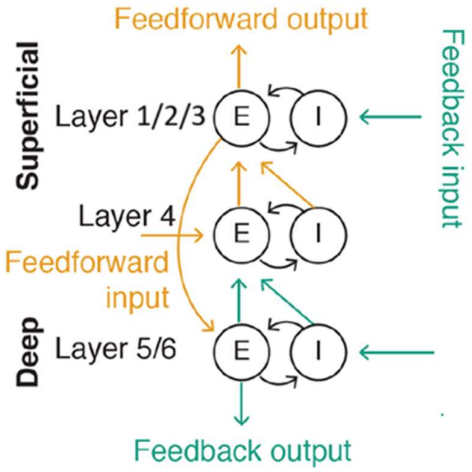

Figure 1.4. A simplified illustration of the laminar microcircuit indicating the patterns of connectivity for each cortical layer. *The connectivity between various excitatory (E; orange) and inhibitory (I; green) neurons is illustrated with directional arrows. The sequence of information flow through the cortical layers starts with feedforward inputs into layer 4, flows up through superficial layers and then down to deep layers. Local inhibitory feedback connections within and between layers are also highlighted in green and can be tracked by the arrows. Feedback inputs from other cortical areas are also highlighted in green, typically projecting to superficial and deep layers.*

Unfortunately, many areas of interest in the frontal-parietal network of macaques, including area LIP and parts of FEF, are buried in sulci. It is possible to approach the macaque sulcal cortex from an angle that traverses all layers within a column (Schroeder et al., 1998), and a handful of studies have demonstrated the importance of this technique. For example, visual information varies across cortical layers in FEF (Chen et al., 2018) and the level of a subject's consciousness modulates laminar-specific activity between the thalamus, the FEF and area LIP (Redinbaugh et al., 2020). The marmoset offers a huge advantage in this research space, as a larger proportion of the visual cortex is exposed to the surface, including

frontal and parietal areas. There are early examples of marmoset studies assessing cortical areas not accessible in the macaque for laminar recordings. For example, in the marmoset middle temporal area, such arrays have revealed different mechanisms of motion encoding in superficial and deep layers (Solomon et al., 2017). In marmoset frontal area 8aD, laminar electrodes have been used to identify potential inhibitory mechanisms in an anti-saccade task (Johnston et al., 2019). As electrode technologies are rapidly evolving, marmosets are well-positioned to address questions related to large-scale, multi-area population dynamics.

1.4 Identifying cortical layers with the local field potential

An important caveat of using laminar recording technology to study network dynamics, is that recording electrodes need to be accurately classified according to cortical depth and layer, *in vivo.* Layer-based differences in the local field potential (LFP) have commonly been used for this purpose. The LFP is a spectrally broad signal that comprises both postsynaptic neural activity in a local population of neurons as well as the spiking activity near an extracellular recording electrode (Pesaran et al., 2018). Different phases of the LFP signal can be correlated with the evoked spiking activity of neurons (Schematic Fig 1.5). Spike-LFP coherence measures how the timing of event-triggered spikes relates to the phase of the LFP waveform. When spikes are very tightly locked to a particular phase of the LFP, the two signals are described as having high coherence or correlation. Accordingly, low coherence between spiking activity and the LFP describes a situation where spikes do not occur predictably at any given phase of the LFP. The schematic in Figure 1.5 illustrates these concepts of spike-LFP phase locking, coherence and coupling. There is also evidence to suggest that the spike-LFP coherence may support communication between brain areas (Buschman and Miller, 2007; Saalmann et al., 2007, 2012; Pesaran et al., 2008; Gregoriou et al., 2009; Dean et al., 2012; Hagan and Pesaran, 2022). Notably, studies have recorded differences in components of the LFP like the spectral power or phase, between cortical layers (Davis et al., 2023; Mendoza-Halliday et al., 2024). Typically, stronger gamma band frequency components are observed in the superficial layers, and alpha-band band components in deeper layers (Bollimunta et al., 2008; Lakatos et al., 2008; Sakata and Harris, 2009; Maier et al., 2010; Buffalo et al., 2011; van Kerkoerle et al., 2014; Haegens et al., 2015; Bastos et al., 2018). These frequency bands may reflect components of the canonical microcircuit in cortical layers, where feedforward signals are integrated with feedback information (Bastos et al., 2015a).

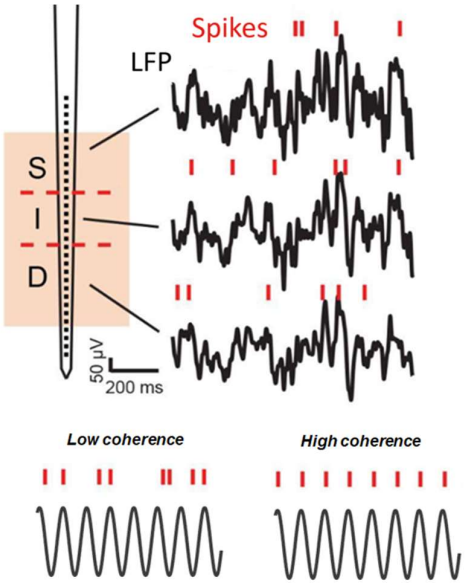

Figure 1.5. A schematic illustrating the relationship between neuronal spikes and the LFP and how this might differ between cortical layers. *Neuronal spikes and the LFP signal are thought to be correlated such that the timing of spikes can be locked to a particular phase of the LFP. When spikes are very tightly phase locked to the LFP, the two signals are said to be in high coherence. It is theorised that the relationship between spikes and LFP differ between cortical laminae (S = superficial; I = input; D = deep). Schematic adapted from Davis et al., 2023.*

Accordingly, these layer-based differences in the temporal and spectral components of the LFP have been used to define laminar boundaries. The CSD is a method that analyses the temporal dynamics of the evoked LFP across cortical depth, to provide information about the location, direction and density of extracellular current across all cortical layers (Mitzdorf and Singer, 1979; Mitzdorf, 1985; Schroeder et al., 1998). It can estimate the relative location of cortical layers based on the location of the first feedforward inputs into the laminar microcircuit. Typically, a flash stimulus is used to generate large, stereotypical feedforward signals that synchronously depolarise neurons in the visual cortex. The CSD assumes stereotypical flow of information from input to output layers (Mitzdorf, 1985; Self et al., 2013). Negative current fluctuations ('sinks') are first seen in the input granular layer IV, post stimulus onset, as this location contains the earliest inputs from upstream cortical areas (Mitzdorf and Singer, 1979; Schroeder et al., 1998; Schroeder and Lakatos, 2009; Self et al., 2013; Nandy et al., 2017). Simultaneously, the supragranular (superficial) and infragranular (deep) layers display positive current fluctuations ('sources') reflecting a homeostatic state of extracellular current, when neurons are not yet active (Mitzdorf, 1985; Self et al., 2013; Nandy et al., 2017). In time, as signals flow through the laminar circuit, the source-sink-source pattern of current across cortical depth is inverted (Self et al., 2013; Nandy et al., 2017). This is despite the subjective identification of layer IV based on depth nearest to the centre of mass on the earliest primary sink or polarity inversion in current. Unfortunately, the success of the CSD method has been largely limited to early sensory areas, where strong sensory stimuli (e.g. a

visual flash stimulus) evoke feedforward signals starting with the input layer IV (Mitzdorf and Singer, 1979; Mitzdorf, 1985). It requires repeated trials with reliably evoked responses in the input layer - something only easily achievable in early sensory areas.

The CSD has been used to define laminar compartments in some higher order cortical areas like the frontal eye fields (FEF), which receive strong retinal inputs (Bastos et al., 2018; Chen et al., 2018). However, it is generally more ambiguous in higher order cortical areas that do not have direct sensory inputs, because it is not clear what event optimally and reliably triggers feedforward signals in the input layer. Recent efforts have been made in developing alternatives to the CSD using other spectral properties of the LFP like the normalised power (Mendoza-Halliday et al., 2024) and spike-phase coherence (Davis et al., 2023). However, their efficacy in defining laminar compartments in higher order cortical areas like PPC is yet to be validated.

1.5 Conclusion

In this thesis, I focus on PPC (containing area LIP) and understanding its contribution to saccade generation and control. The overarching aim of my work is to understand the role of PPC in visual attention. Focusing on an oculomotor area like PPC is a valuable endeavour, as saccadic eye movements are one of the simplest and most effective ways of probing visual attentional behaviour. I use the marmoset as my model for studying PPC, as it offers unique advantages over previous models like the macaque. In this chapter, (Chapter One), I discussed the literature surrounding what is known about PPC and the saccade network, and presented an argument for why the marmoset is a promising model for probing the neural mechanisms underlying the complex inter-area interactions in this network. In Chapter Two, I then describe the methods by which I set up the marmoset as my experimental model: the saccade task I trained them on and how I recorded neural activity from PPC. Chapter Three presents evidence of the topographic organisation of saccade-related response field properties in PPC. Chapter Four then explores methods for defining cortical layers in PPC, as traditional methods used in early visual cortices have been notoriously unreliable here. Analytically comparing four methods for laminar classification, I settle on and present an argument in favour of using the theta-band peak phase change to define cortical layers in my PPC dataset. Using this layer classification method, I then present some preliminary results in Chapter Five, demonstrating the laminar effects of attentional modulation in PPC. To conclude, Chapter Six summarises and discusses the significance of the novel insights gained from the experimental and analytical work conducted in my candidature and detailed in this thesis. Following an acknowledgement of some of the limitations of this work, I propose the use of optogenetics in future research, to causally elucidate the neural mechanisms underlying attentional mechanisms in the frontal-parietal network

Chapter 2 - General Methodology

Two adult male marmoset monkeys (*Callithrix Jacchus*) served as subjects for the experiments in this thesis (M1, 6 years old, 440 g; M2, 4 years old, 500 g). All marmosets were born in captivity and housed in a special facility at Monash University (Clayton, Australia), where they had ad-libitum access to water and a daily diet of standard commercial pellets enriched with a selection of seasonal fruit, vegetables and mealworms. Marshmallows, popcorn, raisins and extra banana slices were used as additional positive reinforcement. The marmosets' housing facility consisted of both an indoor and connecting outdoor enclosure, which they had free access to through connecting tubing, for up to 6 hours a day, 5 days a week. The internal enclosure was maintained at approximately 27°C, 40-60% relative humidity and with a 12h light:dark cycle. Both enclosures contained a range of enriching material and where possible, marmosets were pair-housed (M2 and M3) or housed with direct visual access to other marmosets in the facility. All procedures detailed in this thesis were approved by the Monash Animal Research Platform Animal Ethics Committee and followed the Australian Code of Practice for the Care and Use of Animals for Scientific Purposes. Below I detail the general surgical, training and data collection procedures applicable to all results chapters in this thesis. The specific analytical methods and task variations relevant to addressing my research aims are detailed in their relevant results chapters.

2.1 Surgical procedures

Prior to training on the behavioural task, all marmosets were implanted with a titanium head-post to stabilise the head during recording sessions, and a titanium cranial chamber (NeurNexus, USA) over the posterior parietal cortex (PPC) in one hemisphere (Pomberger & Hage, 2019). The marmosets were first injected with atropine (0.2 mg/kg, i.m.) and diazepam (2 mg/kg, i.m.). After 30 minutes, anaesthesia was induced with alfaxalone (8 mg/kg, i.m. Jurox, Rutherford, Australia). The marmoset was then placed in a stereotaxic frame and stabilised using earbars, which had been covered in local anaesthetic (2% xylocaine jelly). After intubation, the head was further stabilised with a palate bar and eye bars. Anaesthesia was maintained by gas isoflurane (0.5-3%) in oxygen. Eyes were protected during surgery with liquid paraffin eye ointment. Once stabilised, a midline incision was made, the scalp was reflected and the temporalis muscles separated to expose the skull. Up to six titanium screws (diameter 1.5 mm, length 4 mm) were inserted 1-1.5 mm into the skull. The exposed surface of the skull was coated with a thin layer of dental adhesive (Supabond, Parkell). A head-post which would stabilise the animal's head during experiments, was then placed on the anterior part of the headcap and secured with a transparent dental acrylic (Ortho-Jet; Lang Dental Mfg.

Co.) applied to the base of the head-post, along with screws, to secure them to the skull. The margin was cleaned and the skin was sealed with surgical adhesive (VetBond; 3M) to the base of the headcap.

In either a separate surgery (M1) or the same surgery (M2), a craniotomy (9 mm in diameter) was then performed over the PPC (stereotaxic coordinates: interaural +0 mm, 6 mm medial from the midline, (Majka et al., 2016) in one hemisphere (M1: left; M2: right) leaving the dura intact. The cranial chamber was then placed over this region and secured in place on the skull with a dental adhesive (Supabond, Parkell) and dental acrylic. M2 had a second craniotomy and identical cranial chamber placed over area 8aV in the same (right) hemisphere (stereotaxic coordinates: interaural +15 mm, 7 mm medial from the midline). Following surgery, animals received oral antibiotics for 7 days (cefalexin monohydrate, 30 mg/kg) and analgesia for 5 days (meloxicam, 0.2 mg/kg).

2.2 Behavioural training

One week post-surgery, the marmosets were acclimated to sitting in a custom-designed primate chair and having their head stabilised with the surgically implanted head post (Lu et al., 2001; Mitchell et al., 2014). Visual stimuli were presented on a 24-inch Viewpixx/3D LCD monitor (VPixx Technologies Inc.,resolution: 1920 X 1080 pixels (W x H), refresh rate: 100 Hz). The stimulus monitor was positioned at a fixed viewing distance of 56 cm in front of the marmoset. All visual stimuli were generated in MATLAB (MathWorks, Inc) using Neurostim (https://klabhub.github.io/neurostim/) and the Psychophysics Toolbox extension (Brainard, 1997; Kleiner et al., 2007). Eye position was tracked monocularly with a video-based Eyelink 1000 system (SR Research). Horizontal and vertical eye positions of the right eye were recorded at 1kHz sampling rates. At the start of each session, eye positions were calibrated by presenting marmoset faces in a 3-degree Gaussian window, at different locations in the visual field, up to 10 degrees eccentricity. The marmosets were rewarded with sweetened liquids such as fruit juice at the end of every successfully completed trial (approximately 0.035 mL a trial, through a New Era syringe reward pump system up to 12 mL in a session). In the first stage of training I incrementally increased fixation durations on a small centrally located annulus (0.6 degrees visual angle), from 100 ms to 700 ms. Once the marmosets were reliably fixating on this annulus for up to 700 ms, peripheral targets were introduced at 5 degrees eccentricity, in increments of 2 deg, up to a total of 8 deg. Once they could fixate at 8 degrees, they were ready to train on the centre-out saccade task.

2.3 Centre-out saccade task design

The centre-out saccade task (Fig 3.1A), required marmosets to first fixate centrally (700 - 900 ms fixation duration for M1; 500 - 700 ms for M2) on a black and white annulus, to initiate a trial (± 2 degrees tolerance window). Thereafter, a marmoset face (2.5-degree visual angle) appeared at 5 degrees eccentricity. For M1, this was initially another annulus - however, performance reliability tended to decrease over time until the annulus was replaced with a marmoset face. Hence, this change was carried over for training M2 when he was later introduced to the project. On different days, targets could appear at one of either 8 or 36 equidistant locations. Marmosets had to saccade to this peripheral target within 500 ms (M1 mean reaction time = 124.17 ± 58.96 ms standard deviation; M2 mean reaction time = 159.54 ± 91.18 ms) and hold fixation for 200 - 400 ms to successfully complete a trial and receive a juice reward (2 deg radius tolerance window). Marmosets were able to complete an average of 280 trials per session, and each session lasted approximately an hour.

2.4 Electrophysiological recordings

Once a marmoset was performing the centre-out saccade task with at least a 70% hit rate, I implanted a semi-chronic NeuroNexus p-drive housing a 32-electrode laminar probe (100 µm electrode spacing) for up to 6 weeks. The electrode was mounted to a drive screw that allowed us to advance the electrode over the course of the implant as needed to isolate cells (each turn of the drive screw advanced the array 150 µm on the first 2 arrays in M1, and 250 µm on all other arrays, 7 - 12 mm total drive range). Typically, I would advance our probes up to at least 5 mm on the first day (recording activity up to depths of 400 µm in the brain. Thereafter, I would slowly advance 150 - 250 µm a day over the next 3-6 weeks, as needed (when I would lose signal or cell activity on the tip of the array). As such, I was able to sample from all cortical depths in PPC. The structure of the micro-drive also enabled us to remove and reimplant the probe in dozens of different orientations within the chamber and move the probe up to 4mm laterally across the surface (Pomberger and Hage, 2019). The external reference and ground wires were bridged and grounded to a silver wire that rested on the surface of the dura.

Voltage measurements from each electrode were sampled at 30 kHz (OpenEphys, USA). Multiunit spiking activity was extracted from each channel by high-pass filtering the raw voltage traces below 300 Hz and applying a 5 standard deviation threshold to identify putative spikes. To extract local field potentials (LFPs), the same raw voltage trace on every channel was low pass filtered at 300 Hz and downsampled to 1 kHz.

2.5 Inclusion and exclusion criteria

I applied specific exclusion criteria to our electrodes on a daily basis, for each recording session, as I slowly advanced our arrays into the cortex. Recording electrodes with a flat LFP signal (recorded on either the first and last trials of the saccade task or from a full-field flash stimulus) were classified as outside of the cortex and therefore excluded from further analysis for that given recording session. Units with mean firing rates of less than 5 spikes/second were also excluded from further analyses. Additionally, due to time constraints, I only included data from a subset of arrays in 2 marmosets (M1 and M2) in this thesis. Future manuscripts (and those currently drafted) will include a more comprehensive dataset. The following table details the full extent of my efforts in training and collecting data from multiple animals over the course of my candidature:

Animal	Number of days trained before first implant	Implant location	Array ID	Number of recording days
Bart	156 days	Right hemisphere	N/A	N/A
Hugo (M1)	**96 days**	**Left hemisphere**	**T659**	**19**
			X657	**7**
			X655	**13**
			X645	**37**
			105E4	**32**
			105E6	**39**
			111E5	**1**
			105E6_2	**25**
			105E4_2	**22**
			111E8	**19**
99	44 days	Left hemisphere	1067D	20
			105E3	3
			1067F	12
			105E8	8
			11EEE	6
			111EF	8

Animal	Number of days trained before first implant	Implant location	Array ID	Number of recording days
Andy	49 days	Left hemisphere	11C75	4
			111E8_2	12
			11C72_2	14
			111EE_2	17
			11C6C	16
			105E3_3	18
Ollie (M2)	**33 days**	**Right hemisphere**	**11C74**	**7**
			11C72	**13**
			11C76	**7**
			11C6E	**19**
			105E3_2	**26**
			11C6F	**28**
			12EFF	**15**
			11C75_2	**21**

Chapter 3 - Topographic organisation of saccade-related response field properties in the marmoset posterior parietal cortex

3.1 Background

Topographic maps are a ubiquitous organizational feature in the primate brain (Kaas, 1997). The fundamental feature of these maps is the way in which neurons involved in similar computations cluster together spatially. This aids in the development of functionally specialized regions (Yu et al., 2020), and is thought to reduce metabolic demands and improve the efficiency of neural processing by facilitating the brain's ability to quickly interpret and respond to stimuli in a dynamic environment. However, topographic maps do not necessarily pervade every cortex. Often, there is a more random disbursement of cells in a 'salt-and-pepper' layout, in smaller, more simpler brains, like rodents (Kaschube, 2014). This is because topographic maps have typically been thought to have emerged as an organizational aid for larger, more complex brains, like primates. Retinotopy is one important form of topography, where the spatial layout of the visual field that is directly mapped onto receptors in the retina, is also conserved throughout various cortical areas in the visual system (Wandell et al., 2007). Such topographic organization allows the brain to create a coherent representation of the visual scene, ensuring that nearby objects in our visual field are processed by nearby neurons in the brain. Other well-studied topographic maps in the primate visual system are often found in early visual areas, such as orientation maps in V1 (Bosking et al., 2002) and motion direction maps in MT (Albright et al., 1984). However, there is a growing body of evidence that suggests some form of topography, including retinotopy, persists into higher-order extrastriate areas.

The frontal eye fields (FEF) are a higher-order oculomotor coordinating area. In FEF, neurons may encode visual responses, motor responses to eye movements, or a combination of both (Bruce and Goldberg, 1985; Schall, 1991). Visually responsive neurons are biased laterally, while motor neurons are more medial (Sommer and Wurtz, 2006). The receptive fields of visually responsive neurons form a retinal topography (Mohler et al., 1973; Schmolesky et al., 1998; Cavanaugh et al., 2012; Feizpour et al., 2021). Motor responses are also topographically organized (Bruce et al., 1985; Schall, 1997; Selvanayagam et al., 2019). Electrical stimulation of neurons in ventrolateral FEF evokes smaller amplitude foveal saccades, while in the dorso-medial regions of FEF it evokes larger amplitude peripheral saccades (Bruce et al., 1985).

In the posterior parietal cortex (PPC), micro-stimulation of the lateral intraparietal area (area LIP), evokes saccadic eye movements of a particular direction and amplitude in macaques (Shibutani et al., 1984; Thier and Andersen, 1998; Hanks et al., 2006) and marmosets (Ma et al., 2020). While it has been possible to probe the response properties of PPC neurons using such techniques, little is known about the large-scale functional topography across PPC and area LIP. Most of what we know about the topographical organization in PPC comes from fMRI research (Schluppeck et al., 2005, 2006; Silver et al., 2005). In humans, there is evidence for a traveling wave of activity corresponding to saccade target locations across the contralateral visual field that systematically traverses PPC. Such activity is reflective of a topographical map of saccade target location preferences. However, fMRI data alone cannot provide robust insights into detailed topographic representations in the cortex, as it is an indirect measure of neural activity and because of spatial and temporal resolution limitations. More direct electrophysiological measures are required. Of the few electrophysiological studies in macaques, topographical mapping results have been inconsistent. Some results suggest an orderly progression of visual receptive fields in PPC when recording electrodes are tangentially inserted through cortical depths: central visual spaces represented dorsally and peripheral spaces represented ventrally (Blatt et al., 1990). However, subsequent work has struggled to reliably replicate these findings (Platt and Glimcher, 1998; Ben Hamed et al., 2001). The inconsistencies have largely been due to the fact that PPC, like many other extrastriate areas, is buried deep in the lateral bank of the intraparietal sulcus of the macaque PPC and is difficult to accurately access.

The lissencephalic marmoset cortex offers accessibility to the topography of the PPC, as homologous extrastriate areas to the macaque lie exposed to the surface (Feizpour et al., 2021). This facilitates systematic research into cortical layers with the use of multi-electrode linear arrays (Solomon et al., 2017; Johnston et al., 2019). Marmosets are also an ideal model for studying PPC, as they can be trained to perform many complex saccadic behaviours like macaques and humans (reviewed in D'Souza et al., 2021). To date, research into the marmoset homologue of area LIP in the dorsal division of PPC, has noted many similarities to the macaque. Namely, neurons in putative marmoset PPC also respond to a combination of visual stimuli and eye position in terms of the direction and amplitude of planned saccades (Ghahremani et al., 2017; Ma et al., 2020). While there are reports of saccade target responses in marmoset PPC (Ma et al., 2020; Chen et al., 2021) marmosets in these studies were only trained to make saccades to 2 targets, making detailed mapping of saccade responses impossible.

I propose that subregions of PPC, like area LIP, that are directly anatomically connected and coactivated with FEF in the frontal-parietal attentional network (Barbas and Mesulam, 1981; Schall et al., 1995a; Reser et al., 2013), have similar topographic maps of visual space. In this study, I provide the first detailed evidence of the topographic layout of saccade-direction preferences in marmoset PPC, using electrophysiological recordings from several cortical locations and depths in PPC. By training marmosets to make saccades to 8-36 directions, I detail how preferences for saccadic directions change in a systematic manner across cortical distance such that adjacent multi-units have smaller differences and how there are multiple representations of these topographic maps of saccade-direction preferences in PPC.

3.2 Methodology

This chapter presents electrophysiological data collected from 7 array penetrations in M1 (left PPC hemisphere) and 5 penetrations in M2 (right hemisphere), while the marmosets performed a centre-out saccade task described in Chapter 2. Methodological details on the animals, surgical protocol, behavioural training and data collection can be found in Chapter 2: General Methods. All analysis methods were computed in MATLAB (MathWorks, Natick, MA) using personally developed custom code and compatible toolboxes like the circular statistics toolbox (Berens, 2009).

3.2.1 Determining cortical depth of recording electrodes

To measure the distance of each electrode channel from the cortical surface, I analysed the LFP for each channel on the first and last trials of the centre-out saccade task, -300 to 500 ms around target onset, in each recording session. The shallowest electrode with a clearly defined LFP and a mean firing rate greater than 5 spikes/s in the post-target onset period was classified as the shallowest channel in the cortex. I was then able to measure the distance of every subsequent electrode in the brain relative to the shallowest electrode recorded that day, as electrodes were spaced 100 μm apart. For recording sessions where the entire probe was already in the brain and the probe was still advanced further, I ascertained the distance from the cortical surface based on the number of turns of the drive screw. In this chapter, I was only interested in assessing the topographical layout and effect of spatial proximity on saccade-direction tuning preferences in PPC. As a result, I only used measures of physical separation between electrodes (recording multi-units). In Chapter 4, I explore other methods of classifying cortical layers, like the well-known current source density (CSD) method.

3.2.2 Calculating preferred saccade direction

To calculate saccade direction tuning preferences for each multiunit, I calculated the firing rate on each trial in the first 200 ms after target onset (Fig 3.1C). The preferred direction was defined as the angle of the resultant vector from a standard vector summation calculation using the distribution of firing rates across all trials, grouped into 8 directions. Multiunits were considered significantly tuned to saccade direction if the firing rate distribution was non-uniform ($p< 0.05$, Rayleigh's test of non-uniformity, Fig 3.1D). Multiunits that were not significantly tuned to saccade direction were excluded from further analysis. Differences in preferred saccade direction across multiunits were tested using a random permutation test (10,000 permutations).

3.3 Results

I obtained extracellular electrophysiological recordings from 12 penetrations in posterior parietal cortex (PPC) in 2 marmosets (7 from M1 in the left hemisphere; 5 from M2 in the right hemisphere) while they performed a centre-out saccade task (Fig. 3.1A). Given the lissencephalic structure of the marmoset brain, I was able to record from all layers of the cortex in PPC. However, due to the curvature of the cortical surface, probes were not always inserted perpendicular to the cortical surface. Figure 3.1B schematically depicts the insertion technique of the probe through various cortical depths in PPC. I hypothesized that if there is a topographic organization to saccade tuning across the PPC, the saccade tuning preferences should change systematically across cortical distance. Alternatively, if there is no topographic organization, changes in preferred direction from one electrode to the next may be random. As expected from studies in other non-human primates (Blatt et al., 1990; Barash et al., 1991), I found multiunits in PPC that showed robust firing rate changes to saccade targets in the preferred, but not the null direction (Fig 3.3C, example cell). Firing rates decreased systematically away from the preferred saccade direction (Fig 3.3D, example cell). Across all electrodes and penetrations, I recorded a total of 1948 multiunits that were significantly tuned for saccade direction in M1, and a total of 467 units in M2 ($p<0.05$, Rayleigh's test for non-uniformity). Multiunits from each electrode contact and recording day contributed to this overall total, even if this meant some units were repeatedly counted across days. However, because statistical comparisons (Section 3.3.1; Fig 3.2C & D) were all made within a recording session (Cohen and Maunsell, 2010), I was able to control for any potentially non-independent and overlapping measurements between recording days. The majority of the multiunits had firing rate preferences for saccades into the contralateral visual field to the recording hemisphere (Fig 3.3E, M1: 87% 1696/1948 units, Fig 3.3F, M2: 75%, 349/467 units).

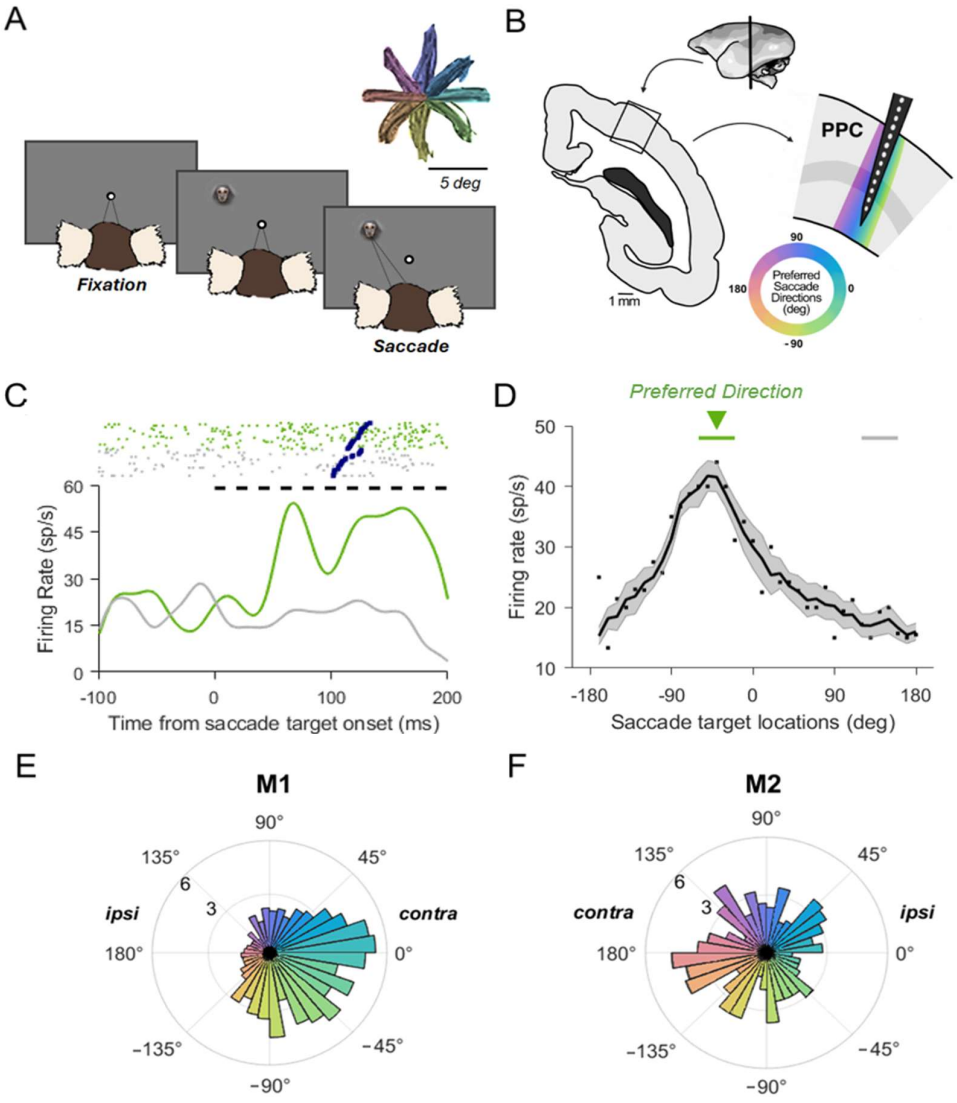

Figure 3.1. Behavioural task and experimental setup. a) *Centre-out saccade task design: initial fixation period followed by the appearance of a peripheral target (marmoset face) at 5 degrees eccentricity, at one of either 8 or 36 equidistant locations in the visual field, to which the marmoset is required to saccade to and fixate on to complete a trial successfully . Inset: Eye traces for a single example session with 8 target locations (318 trials).* ***b)*** *Implantation setup through a coronal section of PPC: The 32-channel linear array penetrates and records from cells at various cortical depths in PPC. The curved gray band in cortex depicts the approximate location of the input layer (IV) and the multi-coloured band illustrates how the arrays sample from neighboring cortical columns with graded differences in saccade direction tuning preferences.* ***c)*** *Raster plot and peri-stimulus time histogram from a single example multiunit aligned to saccade target onset, for all trials ± 20 degrees around the preferred saccade direction (-40 deg, green) and for all trials ± 20 degrees from the direction diametrically opposed to the preferred saccade direction (gray). Rasters for each trial are sorted by saccade reaction times. Saccade onset times relative to the target onset times for each trial are indicated on rasters (blue squares) and the raster trials are sorted by saccade reaction time. The analysis window in which I assess direction tuning in cells 0 - 200 ms from saccade target onset is denoted by the horizontal black dashed line.* ***d)*** *A saccade direction tuning curve for the same example multiunit depicted in C, calculated in the 0 - 200 ms time window post target onset. Each data point depicts the mean firing rate across all trials for each of the 36 target locations; the bold black line depicts the moving average ± 10 degrees from each target direction; the shaded region depicts the standard error of the mean for this moving average.* ***e)*** *Distribution of preferred saccade directions for M1 (1948 units, 7 penetrations, left hemisphere) and* ***f)*** *M2 (467 units, 5 penetrations, right hemisphere).*

3.3.1 Preferred saccade direction changes systematically across cortical depth in PPC

I recorded multiunit activity in the PPC using semi-chronically implanted microdrives that allowed us to advance our recording electrode through the cortex for weeks at a time (see Methods). As I slowly advanced the electrode into the brain, I found a systematic change in preferred saccade direction between adjacent recording electrodes across depth (Fig 3.2A, example penetration M1; Fig 3.2B, example penetration M2).

To quantify the change in preferred saccade direction across cortical distance, I compared the difference in preferred directions between pairs of multiunits, from all penetrations in PPC, at distances 100-500 μm apart. I found that pairs with the smallest differences in preferred directions were clustered at small physical separations. For pairs of units with a separation of 100 um, the majority had a difference in preferred direction 40 degrees or less in M1 (Fig 3.2C, M1: 55%, 667/1214 pairs; Fig 3.2D, M2: 41%, 117/283 pairs). As the cortical distance between pairs increased, the differences in preferred directions increased. Further analysis of the difference in preferred directions for pairs of multiunits at closer cortical distances (<100 μm apart) revealed that changes in preferred direction were significantly smaller than what could be expected by chance (M1 = 1231 pairs; M2 = 284 pairs, $p < 1x10^{-4}$, random permutation test).

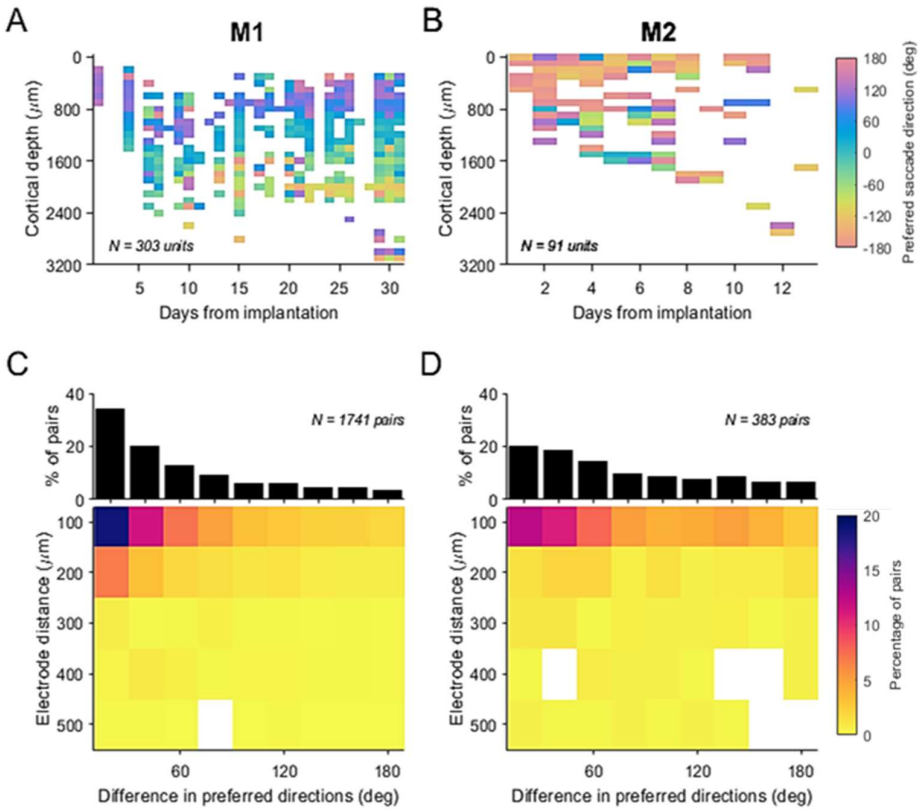

Figure 3.2. Topographic organization of saccade-related direction tuning across cortical depth in PPC. a) *Preferred saccade directions across cortical depth and recording days (31 days), from a single example penetration in M1 and* ***b)*** *M2 (13 days). Colour indicates preferred saccade direction.* ***c)*** *Distribution of the differences in preferred saccade directions for pairs of multiunits spaced 100-500 um in M1 (1741 pairs) and* ***d)*** *M2 (383 pairs).*

To visualize how preferred saccade direction changes across cortical distance and time, I calculated the circular mean of the preferred saccade direction, at each recording electrode depth, from all units across all days within a penetration (Fig 3.3A, M1, 7 penetrations, Fig 3.3B, M2, 5 penetrations). Generally, I noted minimal variation in preferred direction across time, as is evident from the consistently small standard deviation error bar range at any given recording depth (± 20 degrees). I also observed a systematic and slow drift in the estimated preferred direction with advancing electrode depth. In M1, P2 - P6 displayed a change of around 100 degrees over a total depth range of 3500 μm. This may be due to changes in the curvature of the brain, which affects how orthogonal the electrode is to the cortical surface. The slightly greater variability across recording depths observed in P1, P5 and P6 in M1, as well as P1 - P5 in M2, can be further attributed to the fewer data points averaged together here.

.

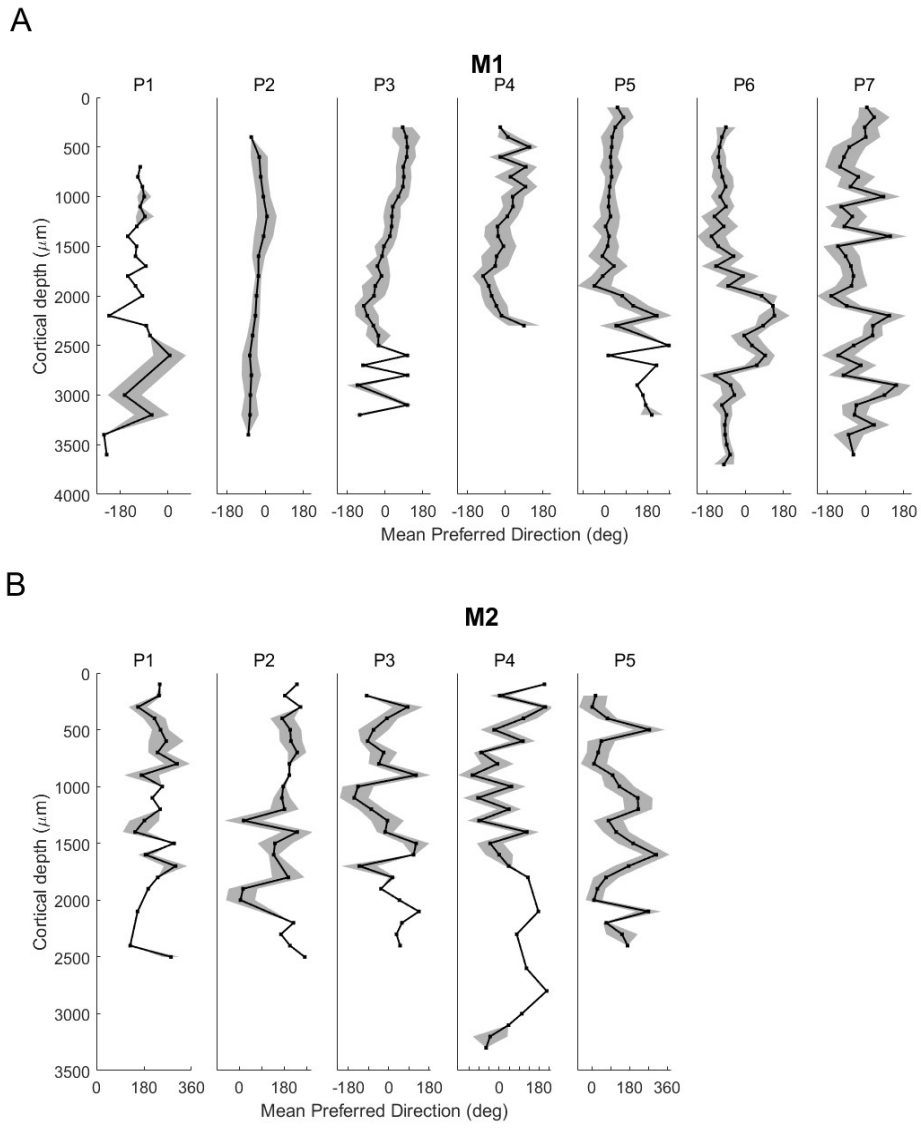

Figure 3.3. Preferred saccade directions averaged across cortical depth a) *Preferred saccade directions at each cortical depth (0 - 4000 μm), averaged across time. Shaded region depicts standard deviation from the mean at each depth. M1 (7 penetrations, left hemisphere) and* ***b)*** *M2 (five penetrations, right hemisphere).*

As shown in Fig 3.1E and F, there was a trend for preferred saccade directions to be in the contralateral visual field. M1, implanted in the left hemisphere, yielded multiunits with preferences for rightward directions (0 ± 90 degrees), and M2, implanted on the right, yielded preferences for leftward directions (180 ± 90 degrees). Together, these results suggest that saccade tuning preferences are topographically organized in the PPC.

3.3.2 Multiple representations of saccade-direction topographic maps across PPC

Evidence from humans (Schluppeck et al., 2005, 2006; Silver et al., 2005) and macaques (Andersen and Buneo, 2002) suggests multiple representations of the visual field exist across areas of the PPC. Indeed, in humans, multiple representations of visual space can be found along the intraparietal sulcus (Silver and Kastner, 2009). To test whether the organization of saccade direction preferences suggested the presence of one or multiple representations of the visual field, I organized the recording penetrations relative to their spatial locations within the recording chamber (Fig 3.4A: M1, Fig 3.4B, M2). The semichronic recording drives allowed submillimeter changes in electrode position within the chamber. Fig 3.4 shows the organization of the mean saccade preferred direction, organized by the electrode's entry position to the cortical surface. The arrangement of electrodes shows that the same parts of the visual field are represented at different spatial locations in the brain. For example, representations of rightward saccades (~0 deg) can be seen in several locations in M1 (Fig 3.4A). While the density of penetrations is insufficient to fully map topographic maps across the PPC, these results suggest that the representations of the visual field repeat across the cortical surface, consistent with macaque and human studies.

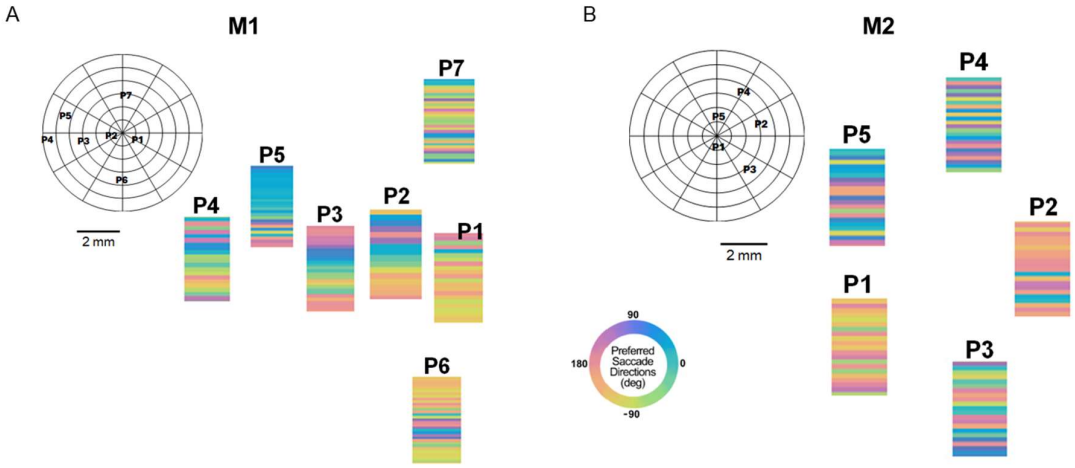

Figure 3.4. Spatial organization of the topographic maps of saccade-related direction preferences across PPC. a) *Average preferred saccade directions from each penetration organized by the location of each array penetration across the cortical surface of PPC (M1, 7 penetrations) and* ***b)*** *M2 (5 penetrations).*

3.4 Discussion

To our knowledge, this is the first detailed evidence of the topographic layout of saccade-direction preferences in PPC across depth. Our results demonstrate how preferences for saccadic directions in PPC favour the contralateral visual field and are topographically organized. Furthermore, I found multiple representations of topographic maps across PPC where saccade direction preferences in PPC changed systematically across cortical distance such that adjacent multi-units had smaller differences.

I found that PPC in marmosets is topographically organized in a manner similar to humans and macaques. Unlike the randomly dispersed 'salt-and-pepper' ensemble of orientation tuned cells observed in rodents (Kaschybe, 2014), marmosets display a topographic layout, where neurons with similar computations cluster together spatially, across depth. Topographic organization and the functional specialization of cortical areas go hand in hand in the brain. However, as is evident from the salt-and-pepper arrangement of neurons in the rodent brain, it is not necessary for yielding strong selectivity and tuning for stimulus features. Typically, we have understood topographic maps to have emerged from efficient connectivity constraints in larger brains - spatially clustering neurons with similar computations reduces the number of long-range connections across the brain, thereby reducing metabolic energy demands, reducing processing latencies and facilitating synaptic plasticity.

However, given that topographic maps also exist in the smaller brains of marmosets, we are left to wonder whether this organizational feature is reflective of some more complex mechanism. Spatial clustering could permit top-down feedback signals, such as those affiliated with the attentional network, to modulate the activity of populations of neurons. In area LIP, a specialized subregion of PPC within the fronto-parietal attentional network, studies have noted that neural activity is modulated by cognitive factors like visual attention (Goldberg et al., 1990; Colby et al., 1996; Snyder et al., 1997; Corbetta, 1998; Colby and Goldberg, 1999; Bisley and Goldberg, 2003, 2010), reward (Platt and Glimcher, 1998; Sugrue et al., 2004) and decision-making (Gold and Shadlen, 2000; Hawellek et al., 2016b; Wong et al., 2016). In fact, most PPC areas are spatially specific, responding more strongly when attention is directed to the contralateral visual field compared.

Our success in simultaneously and systematically sampling all layers of PPC is largely credited to the lissencephalic structure of the marmoset brain, which exposes PPC on the surface of the cortex. In line with previous work in other primates (Blatt et al., 1990; Barash et al., 1991; Snyder et al., 1997), I found a greater proportion of multiunits in PPC that had direction preferences to the contralateral visual field (Fig 3.1E and 1F). I also found systematic changes in preferred saccade direction across cortical depths in PPC (see example penetrations in Fig 3.2A and 3.2B), that I attributed to the oblique angle of insertion of our recording probes. I did not use fMRI guided implantation techniques or histological staining of insertion tracts. Therefore, it is difficult to ascertain whether saccade preferences are organized in cortical columns. Future research would benefit from histological images marking the insertion points and tracts of probes. However, the curvature of the marmoset brain and the depth of some of our recorded units (~2.4 mm below the cortical surface) suggests that I was recording multiunits at oblique angles to the surface. The pattern of changing saccade preferences is consistent with the idea that our electrode is traversing multiple columns with

slightly differing saccade direction preferences. Furthermore, in some of our penetrations (P2 - P5 in M1, Fig 3.3A) there is evidence for consistent preferred directions across cortical depth, which suggests a topographic organization.

Area LIP within PPC is directly and reciprocally connected to FEF and the superior colliculus within the fronto-parietal attentional network (Collins et al., 2005; Reser et al., 2013; Ghahremani et al., 2017). Area LIP is thought to be an integrative hub, combining and transforming bottom-up visual information such as eye position, with top-down cognitive factors like attention. In fact, micro-stimulation of FEF in macaques has been shown to enhance the responses of area LIP neurons during visually guided saccade tasks, through feedback signals, as it does so even in the absence of any bottom-up visual stimulation (Ekstrom et al., 2008). Based on the evidence of previous work reporting the differences in stimulus encoding mechanisms between cortical layers in FEF (Chen et al., 2018), I hypothesized that within cortical areas, there would be greater similarity in encoding stimulus mechanisms. Substantiating this hypothesis, I found that the closer two neural multiunits were spatially, the smaller the difference in their preferred directions (Fig 3.2C and 3.2D). This meant that units within 100 - 200 μm, that were likely recorded from the same functional cortical layer, shared very similar, if not identical saccade direction preferences. This may also reflect the principle of cortical columns observed in earlier visual areas like V1 and MT, where neurons with similar preferences for particular stimulus properties like orientation and motion, are arranged into functional layers. However, to gain a more comprehensive understanding of the large-scale topographic organisation in PPC, future research would benefit from utilising imaging methods with high temporal resolution (e.g. calcium or voltage imaging).

I also found multiple representations of the visual field in PPC (Fig 3.4A and B). Previous work in humans corroborates these findings, noting reversals in the orientation of the visual field on the boundaries between functional subregions in PPC (reviewed in Silver and Kastner, 2009). Subregions of the PPC encode for different motor functions including smooth and saccadic eye movements, reaching movements, hand and grip movements (Andersen and Buneo, 2002). While I did not test for representations other than preferred saccade direction, distinct representations of the visual field may reflect different areas of functional specialization.

Ultimately, in this study, I demonstrated that PPC neurons around area LIP are topographically organized by saccade-direction preferences. However, the nature of this organization and the way information is transformed between cortical layers remains unknown. I posit that statistically identifying the boundary between laminar compartments in PPC would allow us to further our understanding of how information is transformed and modulated by top-down feedback information into area LIP.

Chapter 4 - An analytical comparison of current methodologies used to define cortical layers

4.1 Background

Despite the diversity of functional computations carried out by different cortical areas, a ubiquitous organisational feature of the primate brain is the six anatomical cell layers that make up almost all areas of the neocortex. Cell type, size and composition differ between these layers (Douglas et al., 1989; Douglas and Martin, 2004, 2007), giving rise to distinct laminar activity patterns: initial feedforward sensory activation of input layer IV, followed by excitation in superficial layers 2 and 3 and finally in deep layers 5 and 6 (refer to the simplified schematic illustration in Fig 1.4; Malach et al., 1997; Solomon et al., 2002; Majaj et al., 2007). Understanding the principles of this canonical laminar microcircuit is essential for understanding how such cortical areas process information and accomplish their functions. Histological staining of cells is the most effective and reliable method for revealing the boundaries of laminar compartments (Balaram et al., 2014; Majka et al., 2016). In fact, from his artistic drawings, Ramon y Cajal depicted the laminar structure of the cortex over a century ago (Swanson et al., 2017). However, it requires post-mortem tissue processing and is not a feasible way to identify cortical layers in ongoing *in vivo* experiments.

Several analytical methods have been developed to identify laminar boundaries by considering different features of the local field potential (LFP) and how they differ between cortical layers. Until recently, the current source density (CSD) analysis of the LFP has been the standard for laminar identification in primary sensory cortices (Mitzdorf and Singer, 1979; Mitzdorf, 1985; Schroeder et al., 1998). It relates the timing of evoked LFP responses to the order of information flow through the laminar microcircuit. Typically, a flash stimulus is used to generate large, stereotypical feedforward signals that synchronously depolarise neurons in the visual cortex. The CSD assumes stereotypical flow of information from input to output layers (Mitzdorf, 1985; Self et al., 2013). Negative current fluctuations (‘sinks’) are first seen in the input granular layer IV, after stimulus onset, as this layer receives input projections from the thalamus (in the case of primary visual cortex) or earlier areas in the cortical hierarchy (Mitzdorf and Singer, 1979; Schroeder et al., 1998; Schroeder and Lakatos, 2009; Self et al., 2013; Nandy et al., 2017). However, the CSD has numerous caveats limiting its reliability and generalisability as a laminar identification method outside of early sensory areas.

Recently, two alternative techniques for estimating laminar boundaries have been developed, using the generalised linear phase of the spike-LFP signal coherence (Davis et

al., 2023) and the relative spectral power of the LFP (Mendoza-Halliday et al., 2024). Mendoza-Halliday et al. (2024) describe observing a ubiquitous spectrolaminar pattern of LFP power across multiple cortical areas (V1, V4, 7A, PFC, MT, MST), including the lateral intraparietal area (area LIP) in the posterior parietal cortex (PPC), and in multiple primate species from macaques, to marmosets and even humans. In areas anatomically organised into the six-layered motif, they reported observing a canonical pattern of a peak in LFP power in the gamma frequency band (50 - 150 Hz) in superficial layers and a peak in power in the alpha-beta band (10 - 30 Hz) in deeper layers. They found that the crossover between normalised gamma and alpha-beta power marked the lower boundary of input layer IV. The estimates from the relative power method were validated by a comparison to estimates from histological methods performed on a subset of the data, using electrolytic lesions.

The second alternative method to the CSD, developed by Davis et al. (2023), describes estimating laminar compartments using spike-LFP phase coupling patterns. The timing of spiking activity coinciding with a particular phase of the LFP has been thought to represent the excitability of local populations of neurons (Davis et al., 2022). Davis et al., (2023), repeatedly observed that the preferred phase angle of this spike-LFP relationship reliably reverses at the depth that corresponded to the CSD sink marking layer IV, such that superficial layers were almost 180 deg different from deep layers. Their layer IV identification method closely tracked estimates from the CSD method in several cortical areas (V4, MT and PFC) and animal models (macques and marmosets). However, given that they only analysed this method in areas where CSDs could be reliably recorded, the question of whether their method can be used to identify layers in higher order cortical areas like PPC, where it is difficult to obtain a CSD, remains unknown.

Neither of these methods require specific sensory stimuli like the CSD method - both have been tested with a number of behavioural tasks, as well as during fixation behaviours and passive viewing paradigms. Therefore, they can be measured concurrently with the experimental conditions of interest. Another key advantage of these methods over the CSD is that one can develop statistical tools to quantitatively define the layer IV estimate. Traditionally, CSD is often ‘hand marked’ to identify the sink corresponding to layer IV. This subjective approach makes it challenging to compare results between experimenters or labs. While Mendoza-Halliday et al. (2024) offer an example of how quantitative layer estimates may be made using the spectral power of the LFP. Davis et al., (2023), surprisingly, do not. Generalised phase takes a wider-band estimation of the LFP, giving a more global estimate of activity (Davis et al., 2020). However, the LFP is spectrally broad and can be decomposed into many narrow-band components that have been aligned with spiking activity in relation to various functions such as attention (Fries et al., 2001, 2008; Gregoriou et al., 2009; Fiebelkorn and Kastner, 2019), motor planning (Sanes and Donoghue, 1993; Rubino et al., 2006) and

cross-cortical communication (Fries, 2015). Narrow-band phase estimates, particularly at high frequencies, have even been reported as hyper-localised in cortical regions (Pesaran et al., 2002) and layers (Buffalo et al., 2011). Hence, I implemented another approach to estimating LFP phase using multitaper spectral estimation (Mitra and Pesaran, 1999), to allow for narrow-band phase estimations of the spike-LFP relationship. I also developed statistical measures for quantifying layer IV estimates from this spike-LFP phase method (detailed in Chapter 4.2.5).

In this chapter, I applied all four of the aforementioned methods for estimating the depth of layer IV (CSD, relative power, general phase, multitaper phase), using data collected from the marmoset lateral intraparietal area within PPC, across 5 penetrations in two animals. Furthermore, for three of the methods (relative power, general phase, multitaper phase), I developed quantitative tests to objectively identify the layer IV estimate. I compared the output of these tests to layer IV estimates from the CSD where the earliest 'sink' was identified subjectively. By statistically comparing the layer IV estimates from the CSD, relative power of the LFP, spike-LFP coupled general phase and multi-taper spike-LFP phase methods (in the theta, alpha, beta and gamma frequency ranges), I found that phase coupling in the theta-band frequency range most closely reflects the layer estimates yielded by the CSD method. Like the Davis paper, I found that relative power yielded consistently deeper estimates of layer IV than the CSD or spike-phase methods, but it was the most likely of all the methods to yield a statistically significant estimate of layer IV.

4.2 Methodology

In this chapter, I analysed extracellular electrophysiological recordings from 5 penetrations in the lateral intraparietal area (area LIP) within the posterior parietal cortex (PPC), in 2 marmosets (3 penetrations from M1 in the left hemisphere; 2 from M2 in the right hemisphere). All analysis methods were computed in MATLAB (MathWorks, Natick, MA) using personally developed custom code and compatible toolboxes like the circular statistics toolbox (Berens, 2009). The current source density (CSD) was estimated using a specific task described below. All other methods used trials from our center-out saccade task (see Chapter 2.3 for details). For details regarding the extraction of spiking and LFP activity (see the Chapter 2: General methods).

4.2.1 Inclusion criteria

Out of the 32 electrodes on our laminar arrays, I only included electrodes determined to be in the brain, according to criteria described in Chapter 2.5 & 3.2.1, for our layer IV estimation methods.

4.2.1 Determining cortical depth of recording electrodes

As detailed in Chapter 3.2.1, to measure the distance of each electrode channel from the cortical surface, I used the LFP recorded on the first and last trials of the centre-out saccade task, -300 to 500 ms around target onset, in each recording session. The shallowest electrode with a clearly defined LFP and a mean firing rate greater than 5 spikes/s in the post-target onset period was set at 0 μm. The distance of every subsequent electrode was determined relative to this, based on the 100 μm spacing between each channel. For recording sessions where the entire probe was already in the brain and the probe was still advanced further, I ascertained the distance from the cortical surface based on the number of turns of the drive screw (either 150 or 250 μm per turn).

4.2.2 Current source density analysis for estimating layer IV

At the end of every recording session, head-fixed marmosets maintained fixation while a full screen 100% luminance flash was presented (600 ms flicker interval) for 5 - 10 minutes. The CSD was calculated as the second spatial derivative of the stimulus-triggered LFP in the 200 ms period post flash-offset using code available from the MATLAB file exchange (https://au.mathworks.com/matlabcentral/fileexchange/69399-current-source-density-csd). Flash responses were trial averaged and temporally smoothed over 15 ms (Fig 4.1). For visualisation, the CSD was plotted as a spatial map after smoothing using bicubic (2D) interpolation (MATLAB function interp2 with option cubic). Electrodes corresponding to layer IV were identified as those nearest to the centre of mass of the earliest primary sink or polarity inversion in current, through visual inspection (Schroeder et al., 1998; Hansen et al., 2012; Self et al., 2013; Nandy et al., 2017). The same observer, blind to other recording details, classified all CSD layer IV boundaries based on this criterion.

4.2.3 Relative power of the LFP for estimating layer IV

I extracted the LFP on electrodes meeting the inclusion criteria from each trial, ± 500 ms around the onset of the peripheral saccade target (a 1s analysis window) in the centre-out saccade task (see Fig 2.1A). The power spectrum of the LFP was computed using multitaper methods (1- 150 Hz; with 2 Hz smoothing) on each electrode, according to

Mendoza-Halliday et al., (2024). At each frequency, power was normalised by dividing the power at each electrode by the maximum power at that frequency across all electrodes. To test how the relative power changed for the alpha-beta band and the gamma band across depth, I averaged the normalized spectrum across the alpha-beta band (10 - 30 Hz) and the gamma band (50 - 150 Hz). The depth or electrode at which the two normalized power spectrums (alpha-beta and gamma) crossover was taken to represent layer IV (see Fig 4.2 for an example session). In cases where there was ambiguity due to signal noise or a double crossing of the power spectra, the crossing at the lower depth was marked as layer IV. To test whether the cross-over between alpha-beta and gamma bands was significant, I compared the difference in normalized power above and below the crossover point to the difference in normalized power that would be expected by chance ($P < 0.05$, random permutation test, 10,000 permutations). Recording days where the change in relative power was insignificant were excluded from further analysis.

4.2.4 Generalised linear phase of the spike-LFP coherence for estimating layer IV

I calculated the general phase of the LFP in the same manner as described in Davis et al., (2023), using their publicly accessible code (Github.com/mullerlab). I first extracted the LFP ±500 ms around the onset of the saccade target, and then filtered this signal using a wideband filter (5 - 50 Hz, fourth-order zero-phase Butterworth filter). A single-sided Fourier transform approach (Marple, 1999) on the wideband signal was to compute the phase derivatives as finite differences. For each spike that occurred in the analysis window, I found the corresponding general phase to the nearest millisecond (as the LFP is sampled at 1kHz). As described in Davis et al. (2023), I used metrics to describe spike-LFP coherence: the spike phase index (SPI) and the phase mean angle (PMA). The SPI measures the strength of the spike-LFP phase coherence and is defined as the length of the resultant vector of all of the spike-LFP phases across trials (scale of 0 - 1, using circ_r in the MATLAB circular statistics toolbox). The PMA measures the circular mean angle of all the spike-LFP phases across trials (circ_mean in the MATLAB circular statistics toolbox). I then generated a matrix of SPI and PMA sorted by electrode depth order (example session in Fig 4.3)

To quantitatively define the LFP electrode at which the spike-LFP phase shifted, I devised a simple, conservative statistical method. I first calculated the change in spike-LFP phase across adjacent electrode pairs (circ_dist in the MATLAB circular statistics toolbox) and found the pair of electrodes that exhibited the largest phase change and the deeper of the pair was defined as the layer IV boundary electrode. I then tested whether the spike-LFP phase difference between superficial and deep electrodes was significantly greater than what would be expected by chance ($P <0.05$ random permutation test, 10,000 permutations). Recording days with an insignificant spike-LFP phase change were excluded from further analyses.

4.2.5 Mutli-tapered phase of the spike-LFP coherence for estimating layer IV

I also estimated the LFP phase using multitaper analysis (Mitra and Pesaran, 1999; Pesaran et al., 2002). As with the other methods, I first extracted the LFP ± 500 ms around the onset of the peripheral saccade target. I then band-pass filtered the LFP at four frequencies (4 Hz, 12 Hz, 20 Hz, and 40 Hz). Band-pass filtering was performed using multitaper methods (T= 250 ms, W = 10 Hz, Mitra and Pesaran 1999). After filtering, the same analysis steps were performed as with the general phase method previously described. For each spike that occurred, I took the phase of the LFP at each frequency band to identify the layer IV boundary as the spike-LFP phase changes across LFP electrodes. See Figure 4.4 for the multi-taper PMA distribution at each frequency. To quantitatively identify the layer IV boundary I performed the same permutation test described above (Chapter 4.2.5). This was performed at each frequency band, and as with other methods, recording days with non-significant results were excluded from further analysis. For the multitaper method, I also tried a second method for quantitatively identifying the spike-LFP phase change. For each spiking electrode, I fit a sigmoid function to the PMA across LFP electrodes. The median inflection point of the sigmoid across spiking electrodes was taken as the layer IV boundary. To test whether the sigmoid was a significant fit, I took the p-value of the F-statistic, comparing the sigmoid fit to a flat line. As with other methods, recording days with non-significant fits ($p > 0.05$) were excluded from further analysis.

4.3 Results

Here, I present layer IV estimates from 4 established methods: CSD, LFP relative power, spike-LFP coupled general phase and spike-LFP coupled multi-tapered phase. I used 5 electrode penetrations from the lateral intraparietal area (area LIP) in the posterior parietal cortex (PPC) in 2 marmosets (3 penetrations from M1 in the left hemisphere; 2 from M2 in the right hemisphere). Each method of estimating layer IV is first illustrated using data from the same example recording session from M1 (Sections 4.3.1-4.3.4). In Section 4.3.5, I then compare the estimates from all recording days and all methods, in both marmosets and in Section 4.3.6 focus on two specific approaches to using the multi-taper phase estimation.

4.3.1 Current source density analysis estimates of layer IV

Figure 4.1 illustrates the LFP trace and corresponding CSD plot from an example recording session in M1. I attempted to estimate layer IV from CSDs in every recording session where the CSD stimulus was run (N = 112 recording days, 70 M1, 42 M2). The voltage reversal occurs approximately 50 ms post flash offset in the evoked LFP between electrodes 16 and 19 (Fig 4.2A) and corresponds to the bounds of the layer IV 'sink' in the CSD (Fig 4.1B). The estimate of the layer IV 'sink' in the CSD (Figure 4.1) was annotated by an observer who was blind to other details of the recording. However, on some recordings, a 'sink' could not be convincingly detected. Overall, I found approximately 73% of all recording sessions with a CSD stimulus (51/70 across 3 penetrations) in M1 yielded clear layer IV estimates from the CSD method; 17% in M2 (7/42 across 2 penetrations).

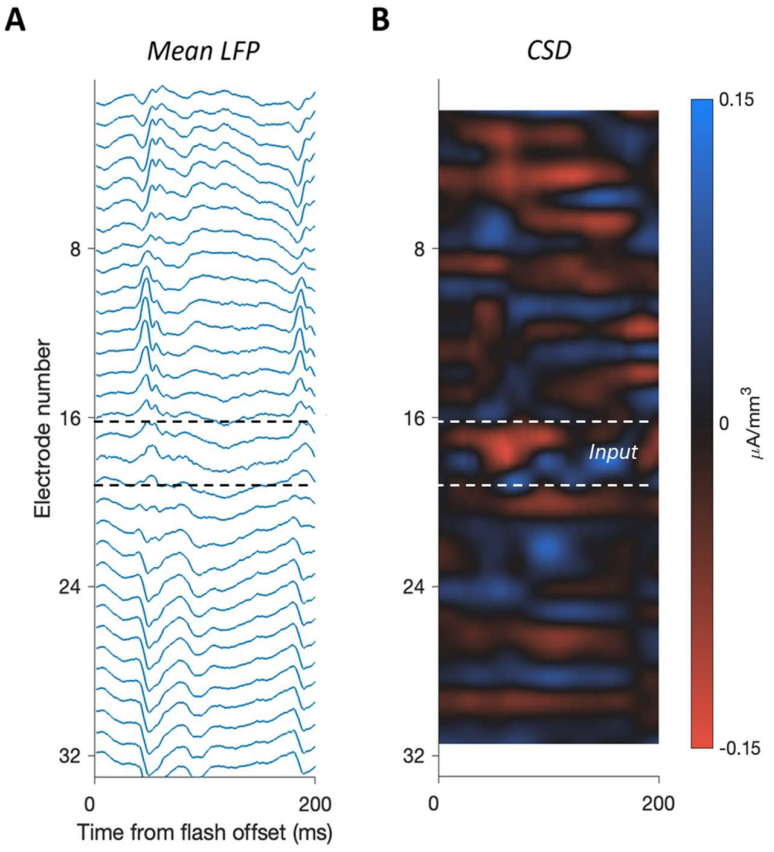

Figure 4.1. Current source density analysis reveals the layer IV boundary in a single example recording session. A) *The average evoked LFP response in the time window 200 ms post flash offset to the full field stimulus flash in an example recording session in PPC, in M1. Each line is the response measured on a single electrode on the linear array. The electrodes are ordered from shallowest/most superficial (1), to deepest in cortex (32).* ***B)*** *Current source density (CSD) measurement from the same example recording session in a. The input layer is defined by the bounds of the earliest current sink (red; electrodes 16 - 19), which corresponds with the voltage reversal in the LFP, while the superficial and deep layers are defined above and below this input layer respectively.*

4.3.2 Relative power of the LFP estimates of layer IV

Prior work has often reported differences in the power spectra of the LFP across cortical areas (Mendoza-Halliday et al., 2024), where superficial layers display higher power for frequencies in the gamma range and deeper layers favour lower frequencies around the alpha-beta range (Bastos et al., 2015b; Johnston et al., 2019; Senzai et al., 2019). Corroborating these findings, I observed similar patterns across recording sessions in M1 and M2. Fig 4.2A shows the normalised LFP power across frequencies same example recording day in M1 (see example in Fig 4.2A). Power in the alpha-beta range (10 - 30 Hz, blue line) peaked on the deeper electrodes while power in the gamma power (40-150 Hz, red line) peaked on the most superficial layers. I took the mean normalized power of these frequency ranges across electrodes (Fig 4.2B). The electrode at which normalized power in the alpha-beta and gamma range crossed over was taken as the layer IV estimate. Overall, 58% of all recording sessions (45/78 across 3 penetrations) in M1 yielded significant layer IV estimates and 29% in M2 (13/42 across 2 penetrations).

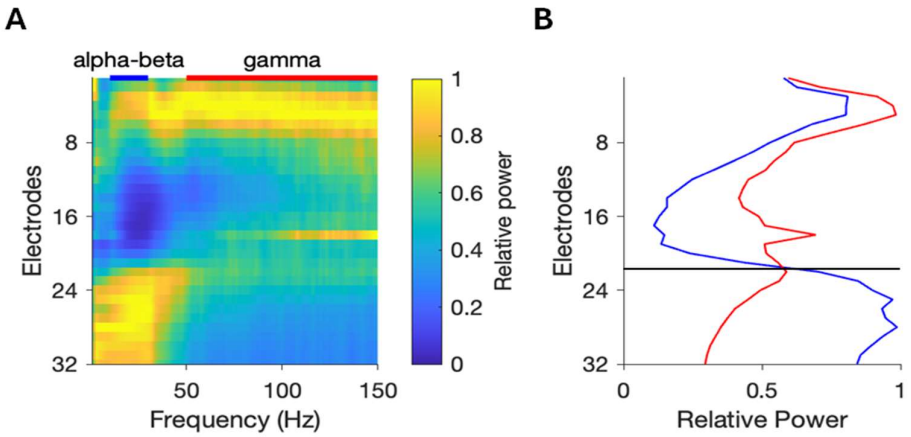

Figure 4.2. LFP relative power spectrum analysis for a single example recording session, revealing the layer IV electrode estimate. *LFP power is calculated over the time window 500 ms before and after stimulus onset, from a single recording session in M1, over PPC.* ***A)*** *LFP relative power plotted for each frequency and depth aligned electrodes (electrode 1 is superficial; electrode 32 is deep).* ***B)*** *Mean relative power in the alpha-beta (10 - 30 Hz, blue) and gamma (50 -150 Hz, red) frequency bands as a function of electrode depth for the example recording session. The electrode corresponding to the bottom of input layer IV is marked (horizontal black line at electrode 22) with respect to the alpha-beta/gamma relative power crossover.*

4.3.3 Spike-LFP coupled general phase estimates of layer IV

I next measured the Spike phase Index (SPI) and Phase mean angle (PMA) using the general phase of the spike-LFP relationship, as described in Davis et al., (2023), and according to their custom code. In their results, Davis et al., (2023) noted a slight trend towards superficial electrodes having higher SPI, although they note that this was highly inconsistent

across recording sessions. I too found inconsistent distributions of SPI across electrode depth. The example recording day shows a dip in SPI (Fig 4.3A) around the middle of the array, but no clear difference between the more superficial and deep electrodes. The PMA on the other hand showed a systematic shift in mean angle across LFP electrode depth (Fig 4.3B), reflecting the findings of Davis et al., (2023). However, where Davis et al. (2023) recorded superficial LFP electrodes with a preferred phase angle of 0 degrees and deeper LFP electrodes with a preferred angle of ± 180 degrees, I noted superficial LFP electrodes closer to -45 degrees and deeper LFP electrodes with preferred angles between 100 - 120 degrees. Calculating the peak change in spike-LFP PMA between adjacent LFP electrodes and testing for significance using a permutation test (detailed in Chapter 4.2.5), I defined the layer IV boundary electrode for every recording session in both marmosets. Overall, 47% of all recording sessions (37/88, across 3 penetrations) in M1 yielded significant layer IV estimates and 16% in M2 (7/45, across 2 penetrations).

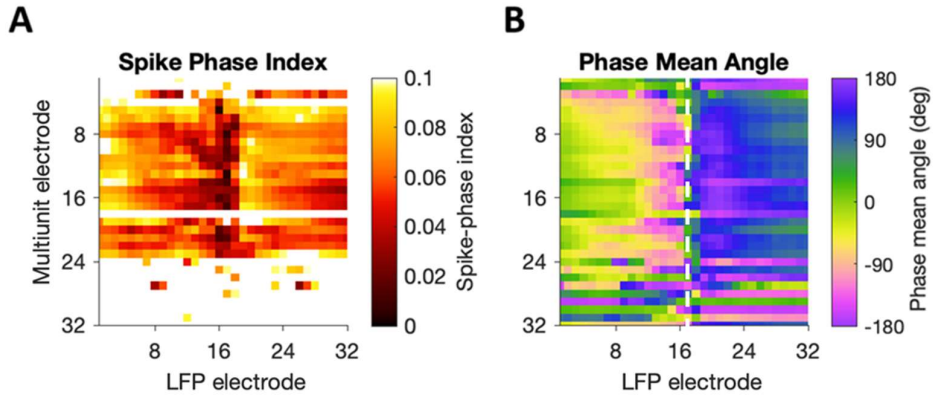

Figure 4.3. Spike-LFP general phase coupling analysis for a single example recording session reveals the layer IV electrode estimate from the phase mean angle reversal. A) *Distribution of spike phase index values from spike-LFP coupling in PPC, from a single session in M1, across all 32 depth aligned electrodes (electrode 1 is superficial; electrode 32 is deepest).* ***B)*** *Corresponding distribution of preferred phase mean angles from spike-LFP coupling from the same example day as in A. The LFP phase reversal (white dashed line) indicates the layer IV estimate, calculated as the peak in the distribution of phase mean angles along the LFP electrodes.*

4.3.4 Spike-LFP coupled multi-tapered phase estimates of layer IV

Finally, I calculated the spike-LFP coupled phase using the multi-taper method at four component frequencies centred on 4 Hz (theta), 12 Hz (alpha), 20 Hz (beta) and 40 Hz (gamma). Figure 4.4A depicts the SPI distributions and the PMA distributions across all frequency bands, within a single example recording session. Reflecting the general phase results described previously, I found no clear difference between superficial and deep electrodes in SPI distributions in any of the frequency bands - though I still noted a dip in SPI

around the middle of the array in theta, alpha and beta bands (Figure 4.4A). Unlike what was observed in Davis et al. (2023), I found different phase relationships across our four frequency bands of interest (Fig 4.4B). Notably, the PMA distribution in the theta band most closely reflected the observed pattern reported by Davis et al., (2023) for the generalised PMA, where superficial LFP electrodes preferred phase angles closer to ±180 degrees and deeper LFP electrodes preferred 0 degrees. Alpha and beta bands reflected a fairly different pattern to theta, with superficial LFP electrodes preferring phase angles closer to 0 and deeper electrodes preferring angles closer to ±180 degrees. Of the two, the PMA results in the beta band most closely resembled our generalised phase results. The phase consistency (both SPI and PMA measures) was generally quite weak in the gamma band.

For consistency, I calculated the peak change in spike-LFP PMA between adjacent LFP electrodes and tested for significance using a permutation test in the same way as was done for the generalised phase (Chapter 4.3.3; see Chapter 4.2.5 for methodological details). I first identified the electrode that exhibited the greatest change in PMA (for each recording session in both marmosets and for each frequency band) and tested whether the mean phase angle of electrodes superficial and deep to that change point was significantly different from what could be expected by chance ($p < 0.05$, random permutation test).

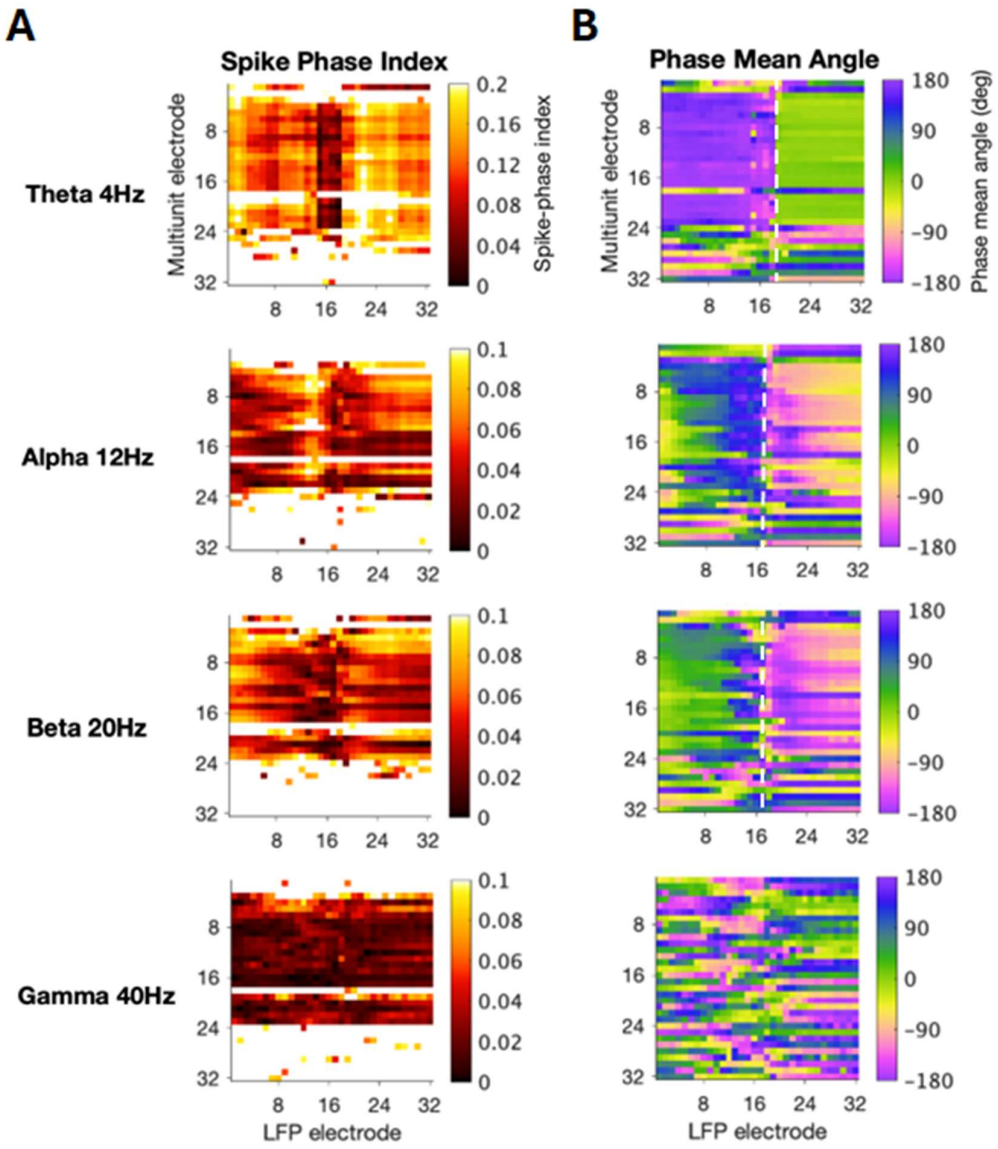

Figure 4.4. Multi-taper spike-LFP phase coupling analysis for a single example recording session, reveals the impact on layer IV electrode estimates. *Data in column* ***A)*** *depicts the distribution of spike phase index values from spike-LFP coupling in PPC, from a single session in M1, across all 32 electrodes (electrode 1 shallowest; electrode 32 deepest) and at 4 central frequencies: 4 Hz, 12 Hz, 20 Hz and 40 Hz. Data in column* ***B)*** *depicts the corresponding distribution of phase mean angles from spike-LFP coupling from the same example day as in A, at the same frequencies. The LFP phase shift (white dashed line) indicates the layer IV estimate at each frequency,*

4.3.5 Statistical comparison of layer IV depth estimates

Here, I compare the layer IV estimates from all four of the methods described in this chapter. Figure 4.5 depicts the comparison of estimates that were significant on every recording day from a single array penetration in M1. As I advanced our arrays slowly through the cortex, there were several days when the array was only partially in the brain. As a result, fewer methods passed statistical tests of significance and there are fewer data points in the first 5 days corresponding to estimates of the depth of layer IV electrodes. Advancing the array deeper into the cortex tended to stabilise the estimates over time for the general phase, multitaper phase and relative power methods. However, estimates from the CSD method displayed a larger variability in layer IV estimates across days, and for a longer period of time.

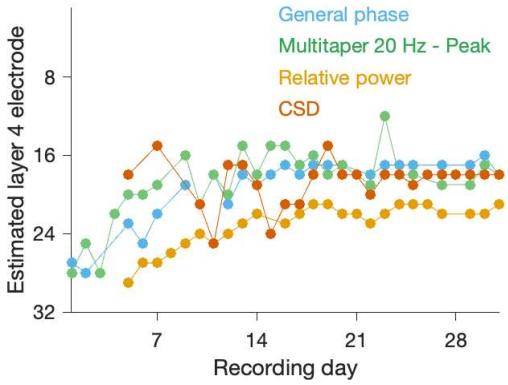

Figure 4.5. A comparison of the estimated electrode depth of layer IV between methods, within a single array penetration in M1. *CSD (orange), the relative power of the LFP (yellow), spike-LFP general phase coupling (blue) and spike-LFP multi-tapered phase coupling at 20 Hz (green; single example frequency chosen for visualisation). Significant layer IV estimates are depicted for each recording day (N = 78 recording days).*

I then statistically compared the layer IV estimates from all 3 of the methods described in this chapter to the estimates from the CSD method, using Wilcoxon's rank sum tests, in 3 arrays for M1 (Fig 4.6A) and 2 arrays in M2 (Fig 4.6B). Firstly, in M1, the layer IV depth estimates from the relative power of the LFP (median depth estimate 2000 μm) were significantly deeper ($p = 3.59e-08$) than those from the CSD (median depth estimate 1700 μm). However, they were not significantly different in M2 (relative power median depth estimate 1700 μm; CSD median depth estimate 1500 μm). A similar trend was observed when comparing the spike-LFP coupled general phase method layer IV estimates to the CSD in both marmosets. In M1, general phase estimates (median depth 1600 μm) were significantly more superficially located ($p = 0.048$), whereas in M2, they were not significantly different (median general phase depth of 600; p - 0.06 μm) from the location of the CSD estimates. layer IV depth estimates for each of the frequency ranges for the spike-LFP coupled multi-

tapered phase method were compared to the CSD estimates. All but the muti-taper frequency band at 4Hz were significantly different from CSD estimates: 4 Hz (M1: median depth of 1700 μm, p = 0.147; M2: median depth of 800 μm, p = 0.25), 12 Hz (M1: median depth of 1600 μm, p = 0.031; M2: median depth of 400 μm, p = 0.04), 20 Hz (M1: median depth of 1500 μm, p = 0.003; M2: median depth of 600 μm, p = 0.034), 40 Hz (M1: median depth of 1312.5 μm, p = 0.0005; M2: median depth of 600 μm, p = 0.03). Unfortunately, with all methods, M2 yielded very few significant layer IV estimates.

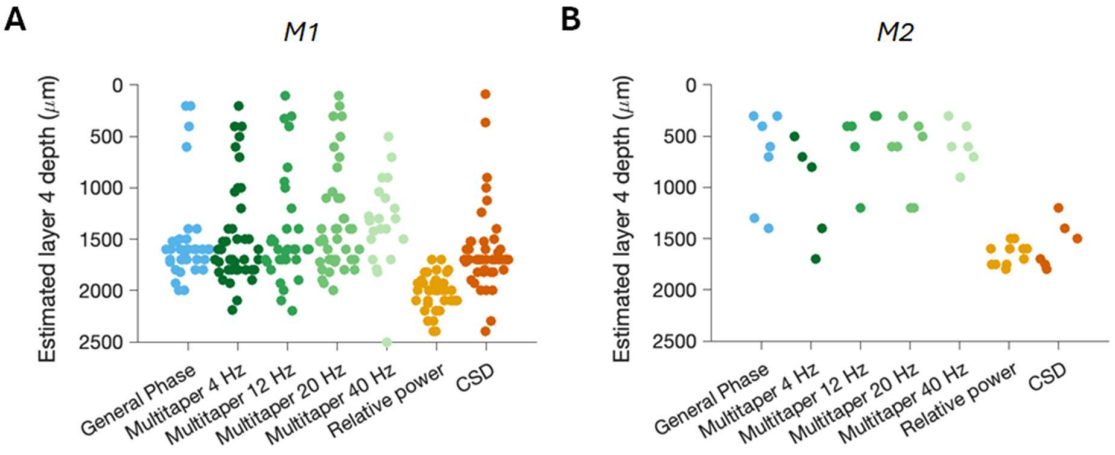

Figure 4.6. A comparison of the estimated depth of layer IV between methods. *CSD (orange), the relative power of the LFP (yellow), spike-LFP general phase coupling (blue) and spike-LFP multi-tapered phase coupling (shades of green) at 4Hz, 12 Hz, 20 Hz and 40 Hz.* ***A)*** *the estimated depths of layer IV from each of the 4 methods for M1 (3 arrays, N = 78 recording days) and* ***B)*** *M2 (2 arrays, 45 days).*

4.3.6 A comparison of two statistical measures identifying layer IV from the spike-LFP coupled multi-taper phase method

Given the tail of shallow layer IV estimates from the phase change peak calculation (especially in the multi-taper method), I suspected a higher rate of false positives in the initial few days of each array implant. Hence, I plotted the layer IV estimates over time for each frequency band using the multi-taper method (Fig 4.7A), as the results of this method most closely resembled the CSD. In the first 7 - 10 days, in all frequency bands, I observed a greater degree of variability in layer IV estimates from the phase change peak estimates, but also estimates at much shallower electrodes. This was a result of the array being only partially inserted into the cortex in the first days of the implant, as I slowly advanced through cortex. As the array advanced into deeper layers of cortex over the course of the implant, the estimated layer IV electrode shifted.

In an attempt to overcome this, I developed a second method to quantitatively identify the spike-LFP phase shift, by fitting a sigmoid function to the multi-tapered data. For this method, I fit each spiking electrode with a sigmoid function across the LFP electrode PMA and tested whether the median fit was significantly better than a flat line ($p < 0.05$, F-test statistic). Fig 4.7A depicts the statistically significant layer IV estimates across all multitaper frequency bands, from both of these tests, for a single electrode penetration from M1. Fig 4.7B depicts the same as A, but for all recording days combined across 3 penetrations in M1. This gives us a direct way to compare the distribution of layer 4 estimates between the two methods. Focusing on the trends within a single array (Fig 4.7A), I noted that as the array is advanced into deeper layers of cortex over the course of the implant, the estimated layer IV electrode, from both methods, shifts higher on the array (electrode 32 marks the tip of the array).

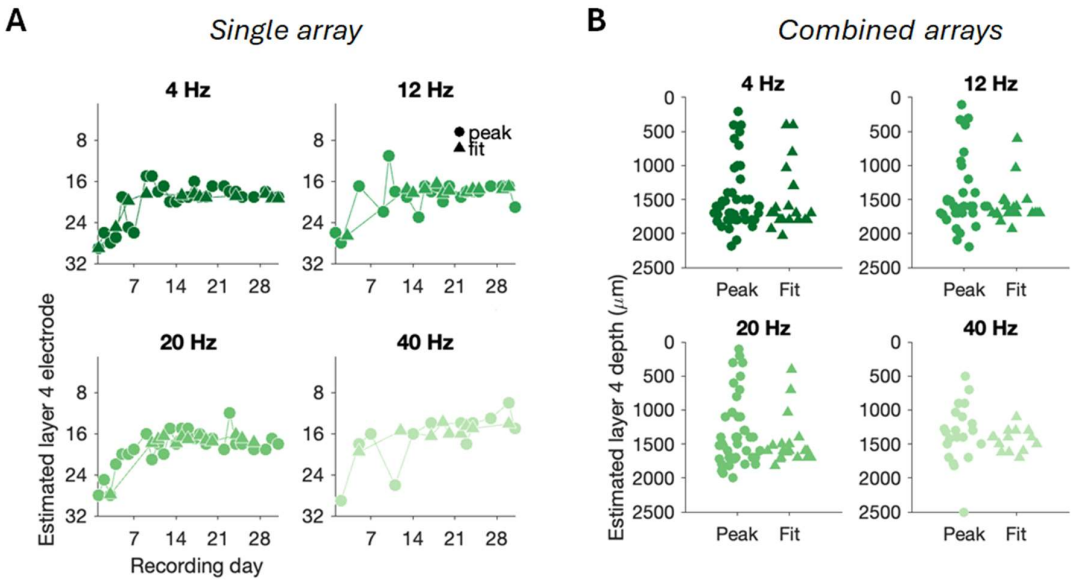

Figure 4.7. A comparison of the layer IV estimates from the peak phase change and sigmoidal fit statistical tests using the spike-LFP multi-taper method. A) *Depicts the daily layer IV electrode estimates at each of the 4 central frequencies for a single penetration in M1 (electrode 32 is located on the tip of the array).* ***B)*** *Depicts the estimates as seen in* ***A****, but by cortical depth and for all recording days across all 3 penetrations in M1. Circles represent the layer IV estimates based on the peak of the distribution of phase mean angles, tested using a random permutation test (10,000 permutations). Triangles represent the layer IV estimates based on the goodness of fit for the distribution of phase mean angles, to a sigmoidal curve.*

When combining the statistically significant layer IV estimates across all frequency bands and from all 3 arrays in M1 (Fig 4.7B), the discrepancies between the two statistical tests are more apparent. Despite the two tests converging on similar median layer IV estimates within 100 μm difference, for all frequency bands (4 Hz: peak median 1700 μm, fit median 1700 μm; 12 Hz: peak median 1600 μm, fit median 1700 μm; 20 Hz: peak median 1500 μm, fit median 1600 μm; 40 Hz: peak median 1312.5 μm, fit median 1400 μm), table 2.1 reveals that the two tests have vastly different success rates in estimating a significant layer IV boundary at each multi-taper frequency band. Across almost all frequency ranges, the permutation test yields a greater percentage of significant layer IV estimates compared to the sigmoidal fit.

Animal	**Multi-taper frequency band**	**Statistical test**	**% of all layer IV estimates in this frequency**
M1 (3 arrays)	**4 Hz**	Permutation **'peak'**	56%
		Sigmoidal **'fit'**	27%
	12 Hz	Permutation **'peak'**	45%
		Sigmoidal **'fit'**	27%
	20 Hz	Permutation **'peak'**	55%
		Sigmoidal **'fit'**	26%
	40 Hz	Permutation **'peak'**	28%
		Sigmoidal **'fit'**	19%
M2 (2 arrays)	**4 Hz**	Permutation **'peak'**	12%
		Sigmoidal **'fit'**	2%
	12 Hz	Permutation **'peak'**	14%
		Sigmoidal **'fit'**	4%
	20 Hz	Permutation **'peak'**	18%
		Sigmoidal **'fit'**	5%
	40 Hz	Permutation **'peak'**	11%
		Sigmoidal **'fit'**	11%

Table 4.1. Layer IV estimation success rates from two statistical tests: the phase change peak permutation test and the point of inflection from a sigmoidal fit. *The percentage of all recording days across all arrays for M1 (3 arrays, 78 days) and M2 (2 arrays, 57 days) with significant layer IV estimates from the preferred phase mean distribution, using either a permutation test or a goodness of fit test to a sigmoidal curve.*

4.4 Discussion

In this chapter, I applied four methods of laminar classification to a dataset from the lateral intraparietal area (area LIP) located within the posterior parietal cortex (PPC), in two marmosets (M1, 3 arrays, 78 days; M2, 2 arrays, 45 days). After obtaining layer IV estimates from each recording day, I then statistically compared the distribution of estimates between these methods. M2 overall yielded very few significant layer IV estimates from any of the methods (Figure 4.6B), due to an unclear LFP signal and significantly fewer electrodes with spiking activity. Therefore, most of our conclusions are drawn from M1 in this discussion (Figure 4.6A). Three of the laminar classification methods: the current source density analysis (CSD), the relative power of the LFP and the generalised linear phase of spike-LFP coupling, were previously developed and tested in other cortical areas and under different contexts. I proposed the fourth method using the multi-tapered phase of spike-LFP coupling (Pesaran et al., 2002, 2008; Hagan and Pesaran, 2022) in the theta, alpha, beta and gamma frequency ranges. I conducted a comparative analysis of estimates from these four methods because the traditional CSD method of laminar classification has been notoriously unreliable in higher-order cortical areas with more complex microcircuitry. I was also seeking a quantitative method of laminar classification that the CSD method lacks. Through our comparative analysis (Figure 4.6), I found that the multi-tapered theta phase of the spike-LFP coherence yielded estimates of the depth of layer IV that most closely tracked estimates from the CSD in our PPC data. However, Mendoza-Halliday et al.'s (2024) method using the relative power of the LFP, yielded the largest number of significant layer IV estimates - though these estimates were systematically deeper than estimates from the CSD (a finding replicated in Davis et al., 2023).

The CSD analysis was the standard of laminar identification until recently, when research into laminar microcircuitry started expanding beyond sensory cortices. This is because higher-order cortical areas receive multiple inputs, including modulatory feedback signals, from multiple sources. When there aren't direct sensory inputs into layer IV in such areas, the entire basis of the CSD defining the boundaries of the input layer from the earliest current 'sink' after stimulus onset collapses. Further to the point, the CSD analysis requires the array to traverse all cortical layers in a single penetration to map the 'sink-source' pattern across depth. When insertion is too angular, this pattern has often been much less visible (Chen et al., 2018). This has been a major limitation of the CSD in previous work, given that many higher-order cortical areas like area LIP in PPC are buried in sulci in macaques. The lissencephalic cortex of the marmoset does alleviate this struggle a little, as areas like PPC are exposed on the surface of the brain. However, due to the high degree of curvature of the marmoset brain over PPC, probes were not always inserted perpendicular to the cortical surface (Figure 3.1B). As observed in our data, the CSD method was still less than ideal in such cases, and when slowly advancing arrays through the cortex. In the initial days of each

penetration, there was a higher degree of ambiguity in identifying the 'sink' that defined layer IV. Given that layer IV is 'hand marked' in the CSD method, this can result in several inaccurate estimates (see high degree of variability in CSD distribution of estimates in Fig 4.5 compared to other methods).

For all of the aforementioned reasons, recent efforts have been focused on developing alternative methods for defining laminar boundaries using other spectral features of the LFP. The focus has remained on using the LFP, as there has been a growing body of evidence reporting laminar differences in the LFP under different contexts. Two recent methods involve utilising the relative spectral power of the LFP (Mendoza-Halliday et al., 2024) the phase of spike-LFP coupling (Davis et al., 2023). Both of these methods directly address many of the limitations of the CSD method. For instance, they can be conducted on data collected during a variety of experimental conditions such as the centre-out saccade task, and do not require a separate, specialised paradigm to evoke relevant LFP activity like in the CSD method. Davis et al., (2023) also reported that the generalised phase and relative power methods required far fewer trial numbers and durations, compared to the CSD, to yield adequate signals. Here, I demonstrate that the location of layer IV estimated from the three alternative methods can also be clearly quantified using statistical methods, unlike in the CSD. In fact, it is this statistical quantification that reduces the variability in their layer IV estimates, compared to the CSD. During the initial days of array implants, when the array is only partially in the brain, many of these methods do not pass statistical tests of significance in defining layer IV boundaries, thereby reducing the rate of erroneous layer IV estimations. However, as I observed, there are still some false positive layer estimates in the first few days of an implant (Figure 4.5 and 4.7A). Advancing the array deeper into the cortex tended to stabilise these estimates over time.

Corroborating the findings of Mendoza-Halliday et al., (2024), in areas V1, V4, 7A, PFC, MT, MST and area LIP in macaques, marmosets, humans and even mice, I was able to reliably identify a crossover point between the relative gamma power in superficial layers and the relative alpha-beta power in deeper layers in marmoset PPC (Figure 4.2). It was this crossover that I identified as layer IV. On days when the arrays were only partially penetrating cortical layers, I found that this method yielded the lowest number of significantly defined layer IV estimates and hence the lowest number of false positive estimates (Figure 4.6A). Additionally, as seen in Figure 4.6A, I observed that the median depth of layer IV for the relative power method was much deeper than estimates from the CSD and phase methods (a finding corroborated in Davis et al., 2023). Further analysis revealed that the depth of this median was often even deeper than where I recorded the most spiking activity. Given that our analyses included all electrodes in an array, no matter how deep, and only excluded electrodes based on a flat LFP signal, it is possible that the relative power cross-over I was

observing was at the bottom of layer VI and not layer IV. A future analysis would benefit from excluding electrodes that are too deep (potentially in white matter) based on the additional criterion of a minimum firing rate of neurons, as this property is notably different in white matter.

I also reported success in defining layer IV in PPC, using the generalised linear phase of the spike-LFP relationship (Davis et al., 2023). The phase of the LFP is thought to be a useful measure for tracking neuronal fluctuations, which are indicative of the transition between excitation and inhibition across cortical areas and layers (Atallah and Scanziani, 2009; Isaacson and Scanziani, 2011). I expanded on the Davis et al. (2023) paper result by developing two methods to quantitatively detect a significant change in spike-LFP phase across the array. However, I did note that the phase mean angles in superficial and deep layers in PPC (Figure 4.3B) were quite different to those reported in Davis et al. (2023). Davis et al. (2023) reported that the phase of spike-LFP coherence in superficial and deep layers was remarkably consistent across brain areas (V4, MT and PFC), independent of task or filtering window. Using their same method of calculating spike-LFP phase, I found a different phase relationship between superficial and deep layers in PPC. While methodologically consistent with Davis et al., (2023), the differences in our results may be explained by the fact that we recorded from PPC, , an area not tested by Davis et al. (2023). This could reflect fundamental differences in PPC, compared to the aforementioned areas, attributable to modulatory attentional effects. Importantly, the phase change we observed in PPC still tracked the earliest sink in the CSD and other layer IV identification methods described here. This supports the idea that phase changes reflect underlying differences in laminar processing.

Given that the generalised phase provides a more global estimate of neural activity, I also investigated narrow-band phase estimates for their potential localised representation of neuronal activity (Pesaran et al., 2002). Using multi-tapered LFP signals, I defined layer IV using the phase of the spike-LFP coupling in the theta (4 Hz), alpha (12 Hz), beta (20 Hz) and gamma (40 Hz) frequency ranges (Figure 4.4). These frequency components of the LFP have been linked to many different functions such as attentional modulation, working memory, motor planning and inter-area communication. Arguably, the layer IV estimates I obtained from these 4 frequency ranges using the multitaper method in PPC yielded the most interesting results of all methods. This is because, despite theta, beta and alpha phases all yielding similar layer IV estimates, the direction of the phase mean angle shift between superficial and deep layers was notably different in the theta band compared to the alpha and beta bands. The direction of the phase shift in the theta band from our data most closely resembled the shift observed in Davis et al's (2023) generalised phase results. However, it was strikingly different to the direction of the shift in our own generalised phase results. In our data, the phase shifts in the alpha and beta frequency ranges most closely reflected the direction of the generalised phase shift. This is not entirely surprising, as alpha and beta bands are dominant components

of the LFP, and as such will be weighted more heavily in the generalised phase calculation. Given that Davis et al., (2023) did not study the parietal cortex, I posit that the differences observed between our data and theirs may reflect unique features of the PPC. Ultimately, the layer IV estimates I obtained from the multi-taper method in the theta band most closely tracked the estimates from the CSD method (Figure 4.6A). Despite the caveat of the multi-taper method requiring sufficient spiking data, I argue in favour of its use to estimate layer IV boundaries in PPC. For the arrays (mostly in M1) where cells were more clearly tuned to saccade direction (see Chapter 3, Fig 3.3), I obtained much clearer layer IV estimates from the spike-LFP coupled multi-taper theta phase. Future research would benefit from applying this novel multi-taper method of layer identification to other cortical regions, in other primate models and in an anaesthetised state, to assess its robustness and generalisability.

Across all methods, I acknowledge the caveat that the depth of layer IV is almost certainly overestimated. This is due to the fact that all the methods are indirectly estimating depth. The only direct method of measuring depth is histological staining. From the histologically stained sections portrayed in the marmoset atlas (Majka et al., 2020), the cortical depth of area LIP in PPC measures out to approximately 2.4 mm, with the granular layer IV at around 1.2 mm. However, the median range of layer IV estimates gathered from the data in M1 was much deeper, lying between 1.5 - 1.7 mm below the surface of the cortex. This suggests that our estimate of the dura was likely inaccurate. Moreover, our inclusion criteria (detailed in Chap 2.5) was to include any electrode with a visually identifiable LFP signal. Even when not in direct contact with neural tissue, EEG, ECoG and MEG sensors placed on the surface of the skull can detect LFP activity from just above the surface of the brain (Buzsáki et al., 2012). Therefore, our estimate of layer IV depth is almost certainly overestimated. However, the remarkable consistency of layer IV depth estimates across electrode arrays suggests that our methods are reproducible. A future analysis could put the additional constraint of firing rate on the electrodes included. Setting a minimum firing rate for inclusion would remove electrodes potentially above the surface of the brain or in the white matter. Histological staining of cortex around insertion points is one of the best ways to overcome this limitation and remains the only way to gain ground truth about the depth of recording electrodes. Hence, I propose that is the natural next step in validating our laminar classification results. Mendoza-Halliday et al. (2024) have already validated their method using the relative power of the LFP with histology in a subset of their data. However, there is yet to be any histological confirmation of the validity of the spike-LFP coupled phase estimates (generalised or multi-taper).

Overall, I conclude that there are promising alternatives to the CSD method of laminar identification in higher order areas like area LIP in PPC. The relative power of the LFP yields the lowest number of false positive layer IV estimates when the array is only partially

penetrating cortical layers, though estimates are often much deeper than other methods. The phase mean angle of spike-LFP coupling also demonstrated robust layer IV estimates in PPC, in the same way as previously reported in macaque V4, and marmoset MT and PPC (Davis et al., 2023). However, the direction of the phase shift in specific mutli-tapered frequency bands like theta, alpha and beta, were uniquely different in PPC compared to other previously tested cortical areas. Nonetheless, I decided to use multi-taper phase coupling in the theta-band frequency range to define superficial and deep layers relative to the layer IV estimate, in our PPC data in the following chapter. The theta band phase estimates not only more closely reflected the pattern of phase shift between superficial and deep layers observed in other cortical areas and species (Davis et al., 2023), it also most closely tracked layer IV estimates from the traditionally held CSD method.

Chapter 5 - Laminar effects of attentional modulation in the marmoset posterior parietal cortex

5.1 Background

In a sea of overwhelming visual information, spatial attention is a cognitive process that enables the selective focus and efficient processing of behaviourally relevant stimuli. In foveate animals, saccadic eye movements are the primary way in which visual attention is directed spatially. There is a growing body of evidence that implicates the frontal-parietal network and key areas within it, such as the frontal eye-fields (FEF) and the lateral intraparietal area (area LIP) in the posterior parietal cortex (PPC), in the mediation of such attentional gaze shifts in primates (see reviews Johnston and Everling, 2008; D'Souza et al., 2021). When paying attention to the location of a behaviourally relevant stimulus, an overall enhancement of activity has been observed in these areas (Moran and Desimone, 1985; Motter, 1993; Connor et al., 1997; Treue and Maunsell, 1999; Corbetta and Shulman, 2002; Bisley and Goldberg, 2003; Serences and Yantis, 2006). However, the specific computations involved in these attentional processes across cortical layers are still not fully understood. In the traditional primate model, the rhesus macaque (*Macaca mulatta*), oculomotor areas are typically buried in sulci and are difficult to access. The common marmoset (*Callithrix jacchus*), offers a solution to this problem, with its lissencephalic cortical surface, homologous cortical networks, and rich behavioural repertoire (see D'Souza et al., 2021 review).

When attention is directed to a specific location in the visual field, the latency of saccades to that location are faster than to unattended locations. This is true whether visual attention is endogenous, or self-directed (Herrington and Assad, 2009), or exogenously captured by salient stimuli (Posner and Cohen, 1984; Bell et al., 2004; Fecteau et al., 2004). Saccadic reaction times (SRTs) refer to the time it takes to initiate a saccade from the time of stimulus appearance. SRTs are thought to be modulated by attentional facilitation through oculomotor control pathways, rather than sensory pathways. From the use of saccadic adaptation experiments, in which participants make a sequence of eye movements guided by visual targets, SRTs to the final target are faster when attention is cued to this endpoint goal, rather than to any of the intermediate visual target locations (Khan et al., 2010). The validity of attentional cues also greatly impacts SRTs. For example, manipulating the likelihood that a visual cue predicts an upcoming saccade target affects SRT. When the cue is less predictive, SRTs are significantly longer (Nagel-Leiby et al., 1990). This is likely due to the disruption of attentional processes.

Convergent evidence from anatomical, lesion, imaging and neurophysiological studies have implicated the frontal-parietal network in the mediation of attentional gaze shifts in primates (Johnston and Everling, 2008; McDowell et al., 2008; D'Souza et al., 2021). Independently, studies have demonstrated how both FEF and PPC activity are crucial to saccadic eye movements (Schlag-Rey et al., 1997; Everling and Munoz, 2000; Zhang and Barash, 2000; Johnston and Everling, 2006). In both areas, topographical maps have been demonstrated organised according to visual location or saccadic responses of a particular amplitude and direction (see Chapter 3 results; (Bruce et al., 1985; Blanke et al., 2000), and stimulation of each area also reliably evokes saccades to the contralateral visual field (Moore and Fallah, 2004; Szczepanski et al., 2010; Ghahremani et al., 2019). Notably, activity in both FEF and PPC has been recorded in anticipation of a stimulus (Corbetta and Shulman, 2002; Serences and Yantis, 2006; Bressler et al., 2008). In fact, an enhancement of neural activity is commonly seen in these areas when directing attention to a behaviourally relevant stimulus, before a saccade is even made (Moran and Desimone, 1985; Motter, 1993; Connor et al., 1997; Treue and Maunsell, 1999; Bisley and Goldberg, 2003).

The reciprocal connections between FEF and PPC are thought to be where spatial attention emerges (Lynch et al., 1985; Andersen et al., 1990b; Baizer et al., 1991; Schall, 1995; Lewis and Van Essen, 2000; Burman et al., 2006; Reser et al., 2013; Ghahremani et al., 2017, 2019). This theory is founded on the anatomical evidence of laminar divisions in both areas, where cells of different types, sizes and compositions are organised into 6 layers or 3 functional groups (Douglas et al., 1989; Malach et al., 1997; Solomon et al., 2002; Douglas and Martin, 2004; Majaj et al., 2007; Shepherd, 2011). To understand the mechanisms that give rise to attentional modulation in these areas, it is therefore important to understand how attentional modulation varies across layers. Typically, feedforward sensory inputs project to input layer IV, while feedback projections terminate in the superficial and deeper layers (see simplified schematic of laminar circuit in Fig 1.4; Mountcastle, 1997; Harris and Mrsic-Flogel, 2013). FEF feedback projections terminate in the superficial layers of PPC (Schall et al., 1995a; Stanton et al., 1995). Unfortunately, because FEF and PPC are normally buried in sulci in primate models like the macaque, it has been difficult to access and rigorously study the circuit dynamics in these areas. However, the lissencephalic marmoset cortex offers accessibility to homologs of the macaque PPC. In the marmoset, PPC neurons are tuned to specific saccade directions (Ma et al., 2020) and depict a topographic organisation of preferred saccade directions across cortex (Chapter 3). To our knowledge, only one study to date has alluded to any laminar differences in neural activity in marmoset PPC. In 2023, Selvanayagam et al. (2023), reported significantly more stimulus and target related activity in the superficial layers of PPC, reflective of earlier visual areas, while deeper layers had more post-saccadic oculomotor-related activity. However, they did not examine the effects of attentional modulation on neural activity across cortical layers in the marmoset PPC.

In this chapter, I explore the impact of spatial attention on the activity of saccade-direction tuned neurons in marmoset PPC. I trained marmosets on a cued saccade task that directed their attention to an upcoming saccade target with 85% validity. I first show that marmosets can learn a cued saccade task, as evidenced by their saccade behaviour. Next, I demonstrated that the cue modulated firing rates in the PPC. This modulation was dependent on the preferred direction of the neuron, as well as the cortical layer (superficial or deep) that the neuron was located in. Together, these provide the first laminar descriptions of encoding visual attention in the PPC.

5.2 Methodology

In this chapter, I detail the analytical methods pertaining to the behavioural and electrophysiological data recorded in the lateral intraparietal area (area LIP) located within the posterior parietal cortex (PPC), from 3 penetrations in M1 (left hemisphere implant). All analysis methods were computed in MATLAB (MathWorks, Natick, MA) using personally developed custom code and compatible toolboxes like the circular statistics toolbox (Berens, 2009). Further methodological details on the animals, surgical protocol, behavioural training and data collection can be found in Chapter 2: general methods.

5.2.1 Cued centre-out saccade task design

After learning the standard centre-out saccade task to 8 or 36 peripheral target locations (described in detail in Chapter 2: General Methods; Figure 3.1A), marmosets were introduced to a spatial cue (small grey bar flashed for 50 ms, at 1 deg eccentricity) that indicated the location of the upcoming saccade target with 85% accuracy (Figure 5.1A). 'Informative cue trials' refer to those trials where the cue indicated the location of the upcoming target; 'uninformative cue trials' were those where the peripheral target appeared at another location from that indicated by the cue (15 % of all cue trials). Whilst maintaining central fixation, marmosets covertly attended to the spatial cue, which appeared 200 - 400 ms prior to the peripheral saccade target. They were rewarded for saccading to the peripheral target within 500 ms of its appearance. The location of the cue was selected based on the response field (preferred saccade direction) of the majority of cells, on the first few days of recording. Cued trials were randomly interleaved with uncued trials (65:35, uncued:cued). Within the same penetration, marmosets were always cued to the same location so as to reinforce the purpose and validity of the cue. In this chapter, M1 was cued to targets at 0 degrees for all recording sessions across the 3 penetrations. Saccade reaction times (SRTs) were defined as the time it took for the marmoset to saccade to and fixate on the peripheral target, once the target appeared in their periphery.

5.2.2 Calculating the preferred saccade direction of multi-units

Preferred saccade direction was calculated in the same manner as previously described in chapter 3.2.2. Briefly, saccade direction tuning was calculated based on firing rates across within the first 250 ms after target onset, on uncued trials. The mean firing rate was calculated at each target location and the circular mean of the defined the preferred direction. Significance of tuning was based on Rayleigh's test for non-uniformity (see Figure 3.1C & D).

5.2.3 Defining the cortical depth of recording electrodes

To define the cortical depth of our recording electrodes, I used a combination of methods described in chapters 3 and 4, to first define layer 4. For every recording session, I identified the shallowest electrode on the array that was in the brain as the electrode that had a clearly defined LFP (based on the first and last trials of the centre-out saccade task, -300 to 500 ms around target onset), and a firing rate greater than 5 spikes/s in the post target onset period. Excluding all electrodes that were not in the brain, I then extracted the LFP ± 500 ms around the onset of the peripheral saccade target and used a multitaper analysis to extract the LFP signal centred at 4 Hz (T= 250 ms, W = 10 Hz, (Mitra and Pesaran, 1999). In the same time window, I also calculated spike times for each electrode. Comparing the spike times on each electrode to the phase of the multi-tapered LFP on every other electrode, I calculated a matrix of phase mean angles (PMA, see Figure 4.4 example) using the circ_mean function (MATLAB, circular statistics toolbox). Extracting the distribution of PMAs along the LFP axis, I then identified the layer 4 boundary based on the peak of this distribution (the largest change in preferred phase angle between 2 adjacent electrodes), and statistically validated it based on permutation test (10,000 permutations). Where I could not identify a statistically valid layer 4 boundary, I considered the boundary identified from the next nearest recording session. Finally, the superficial and deep layers were defined as above and below the layer IV boundary, respectively (see Chapter 4).

5.2.4 Assessing the effects of attention on firing rates aligned to the preferred direction and cue direction

I aligned trials to the preferred saccade direction of every multiunit. I first calculated the difference between the saccade target direction presented on each trial (cued and uncued separately) and the preferred saccade direction of every multi-unit (see Chapter 5.2.2 for details). Trials across multi-units were then grouped into eight equidistant direction bins (centred at -180, -135, -90, -45, 0, 45, 90, 135), inclusive of trials ± 20 degrees around bin centres. Next, I calculated the average firing rate across all trials in each direction bin, over 50 ms time-windows, ± 500 ms around the onset of the saccade target. This resulted in two dimensional tuning matrices (8 direction bins x 20 time bins), plotted in Figure 5.3.

To align trials to the cued direction for every session (0 degrees), I followed the same procedure as above, but initially calculated the difference between the actual saccade target direction presented on every trial (cued and uncued separately) and the cued direction (Figure 5.5). Because only one cue direction was presented on each day, I was able to align uncued trials to the cued direction on that day, even though no cue appeared on those trials.

5.2.1 Assessing the effects of attention on the relationship between cue direction and preferred direction

I tested how the relationship between the preferred direction and the cue direction influenced firing rates. First, for each multiunit, the firing rates on each trial were normalised to the 500 ms preceding saccade target onset (across cued and uncued trials). Trials were then aligned by the relationship between preferred direction and target direction as well as preferred direction and cue direction. For each multiunit, trials were grouped into eight bins (centred at -135, -90, -45, 0, 45, 90, 135, 180) and averaged. As each multiunit only has one preferred direction, each multiunit contributes to one column of the matrix. Colour matrices in Figure 5.12 show the mean normalised firing rate across the population of multi units.

I tested how the population mean normalised firing rates were modulated by target direction, cued direction and preferred direction by fitting the firing rates with a von Mises function. A maximum likelihood estimation (‘mle’ function in MATLAB) was used to estimate the parameters of the von Mises function fit to our data. I compared the fit of the von Mises function against that of a flat line ($p < 0.05$, chi-squared distribution).

5.3 Results

5.3.1 Effects of the spatial cue on saccade reaction times

By adding a visual cue to a subset of trials within the centre out saccade task first described in chapter 2.3, I introduced an element of spatial attention to the task (Fig 5.1A) that I hypothesised would influence the marmoset's performance. The cue predicted the upcoming saccade target with 85% accuracy. This gave us three trial types: uncued trials, informative cued trials, and informative cue trials. In general, M1 displayed remarkably fast saccade reaction times (SRTs) across all trial types (Fig 5.1B, range of daily medians 105 - 187 ms). Analysing the trend in SRTs between trial types for every recording day across the 3 arrays (*N* = 83 days), I discovered on 54% (45/83) of days, informative cue trials had a faster median SRT compared to uncued trials. On 81% (67/83) of recording days uninformative cue trials had a slower SRT compared to uncued trials (Fig 5.1B). In general, across all saccade target locations, I also noted that despite cued trial SRTs being slightly slower than uncued trials, that the SRTs for both cued and uncued trials were faster at the cued location (0 degrees) compared to the other 7 saccade locations (Fig 5.1C). Note, the median SRT on cued trials is slightly higher at each direction, as it includes SRTs from both informative and uninformative cued trials. Across the entire distribution of trials (Fig 5.1D) I also found that SRTs on uninformative cue trials (*median* = 127.2 ms) were slower than both informative cue trials (*median* = 114.9 ms) and uncued trials (*median* = 114.6 ms). Statistically comparing the SRTs between each trial type using Wilcoxon rank sum tests, I discovered that SRTs on uninformative cue trials were significantly slower than on uninformative cue trials ($p < 0.0001$, Fig 5.1E) and uncued trials ($p < 0.0001$, Fig 5.1G). SRTs on informative cue trials were not significantly different from uncued trials ($p = 0.516$, Fig 5.1F).

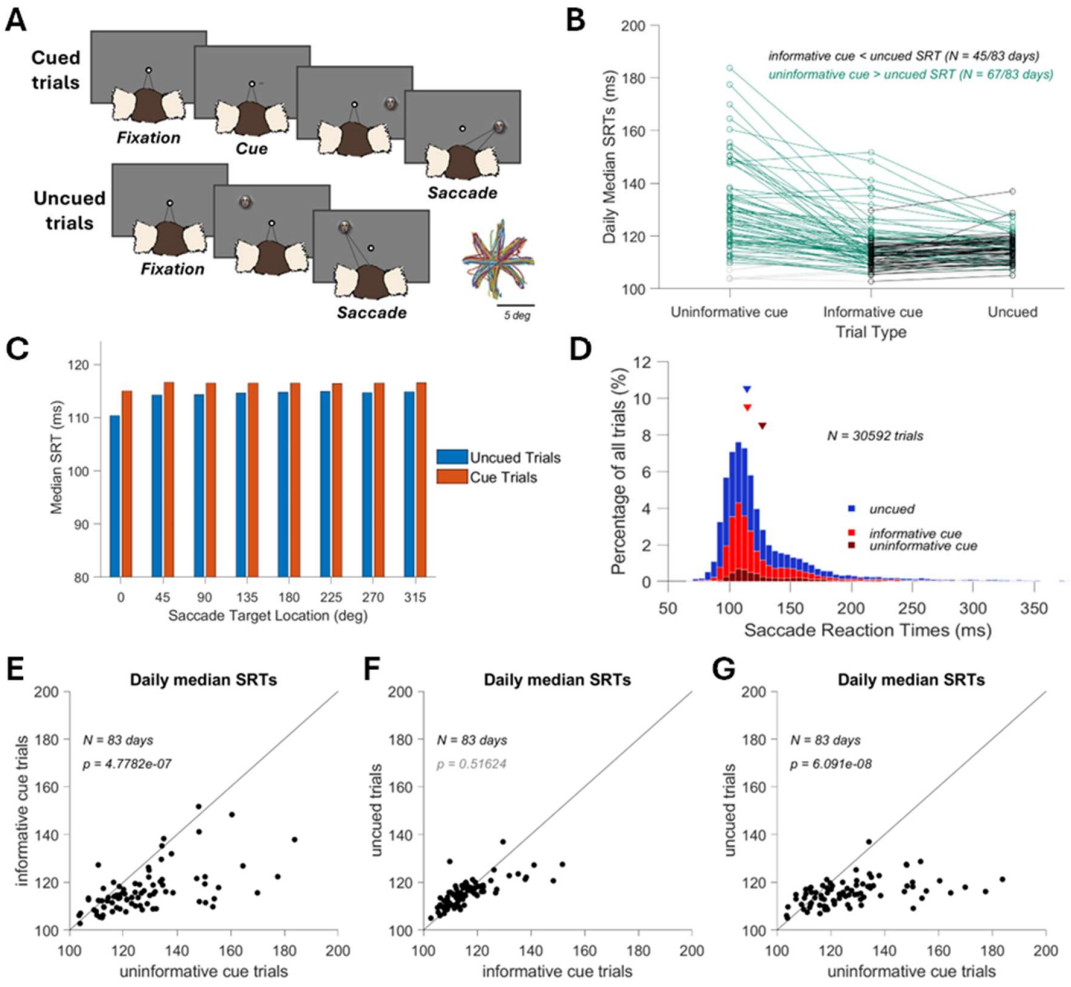

Figure 5.1: Behavioural effects of the spatial cue. A) *Schematic of the centre-out saccade task design with cued trials. On cued trials, while marmosets maintain central fixation, a cue (1 deg eccentricity) flashes for 50 ms, indicating the location of the peripheral saccade target (marmoset face; 5 deg eccentricity), which appears 200 - 400 ms later, at one of either 8 or 36 equidistant locations in the visual field (Inset shows an eye trace pattern for a single example session with 318 trials at 8 target locations). Marmosets are required to saccade to and fixate on to successfully complete a trial.* ***B)*** *A comparison of the daily median SRTs on each of the 3 trial types: uninformative cued, informative cued and uncued. Uninformative cued trials with slower SRTs than uncued trials shown in green; Informative cued trials with faster SRTs than uncued trials shown in black; remaining trials in grey.* ***C)*** *Median SRTs on all uncued and all cued trials, at each of 8 peripheral saccade target locations.* ***D)*** *Frequency distribution of SRTs by trial type, for all trials across 3 arrays in M1, with medians denoted by the coloured triangles (uncued = blue; informative cued = red; uninformative cued = maroon) across all trials. Scatter plots statistically comparing the daily median SRTs (Wilcoxon Rank sum test) between:* ***E)*** *uninformative and informative cued trials;* ***F)*** *informative and uncued trials;* ***G)*** *uninformative cued and uncued trials.*

5.3.2 Effects of the spatial cue on saccade direction tuning

As discussed in Chapter 3, neurons in PPC are tuned to a range of saccade directions, predominantly in the contralateral visual field. Preferred saccade directions were calculated based on the circular mean of responses to uncued stimuli (see chapter 5.2.2 and 3.2.2 for further methodological details). Across 3 arrays in M1 (*N* = 83 days), I collected *N = 640 multi-units* that were saccade-direction tuned. The marmoset was spatially cued to 0 degrees on all recording days. Figure 5.2 presents two example multi-units recorded in PPC: the first with a preferred direction at 0 degrees, matching the cued direction (Fig 5.2A), and the second with a preferred direction -120 degrees away (Fig 5.2C). Given that multi-units respond maximally to their preferred saccade direction, this direction can be thought of as the centre of their response field. When the cue is near the preferred direction, it is likely that it falls within the multi-unit's response field. Aligning the firing rates of the example cells to the cued direction (Fig 5.2,C,D), suggests that the effect of the cue on firing rates may depend on the relationship between the cued direction and the preferred direction. Therefore, in our analysis of how the cue might affect firing rates in PPC, we need to consider three variables: the preferred direction of each multiunit, the cued direction on that day, and the saccade target direction on each trial.

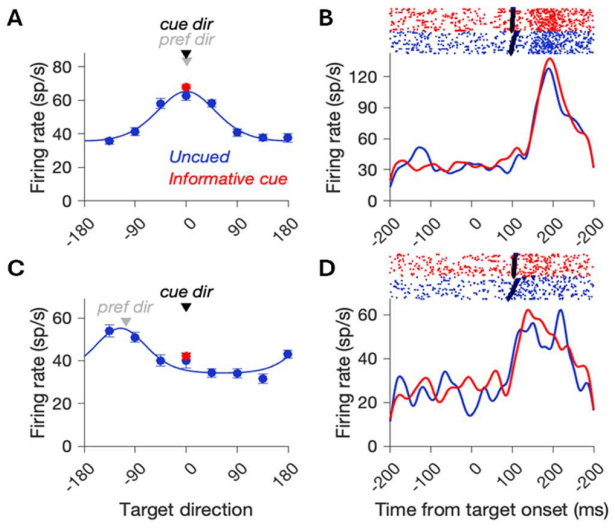

Figure 5.2. Two example recording units in PPC with different saccade direction tuning preferences. *The preferred saccade direction of multi-units was calculated based on the resultant vector on uncued trials and the significance of this tuning preference was based on Rayleigh's test for non-uniformity.* ***(A)*** *The tuning curve for a recording unit with an average saccade direction preference close to 0, matching the direction of the cue (± SEM error bars).* ***(B)*** *A raster plot and peri-stimulus time histogram (PSTH) from the same example multi-unit as in A, aligned to saccade target onset for the cued direction, showing responses to the uncued trials (blue), and informative cue trials (red).* ***(C)*** *A tuning curve as seen in A and raster plot plus PSTH as seen in B* ***(D)*** *but for a second multi-unit recorded in PPC, with an average saccade direction preference of 240 degrees (-120 degrees), but the same cued direction (0 degrees).*

To test how responses to the preferred saccade direction were modulated by attention, I first aligned responses to the preferred direction of each recorded multi-unit (methods detailed in Chapter 5.2.2) and then compared the average firing rates of all multi-units between cued and uncued trials. I first plotted the response field maps (Fig 5.3) for saccade directions aligned to the preferred direction of multi-units, for uncued and cued trials separately. Figure 5.3A, B and C depict the response field maps for each of the 3 arrays in M1 individually, and then Fig 5.3D depicts the average across all 3 of these arrays.

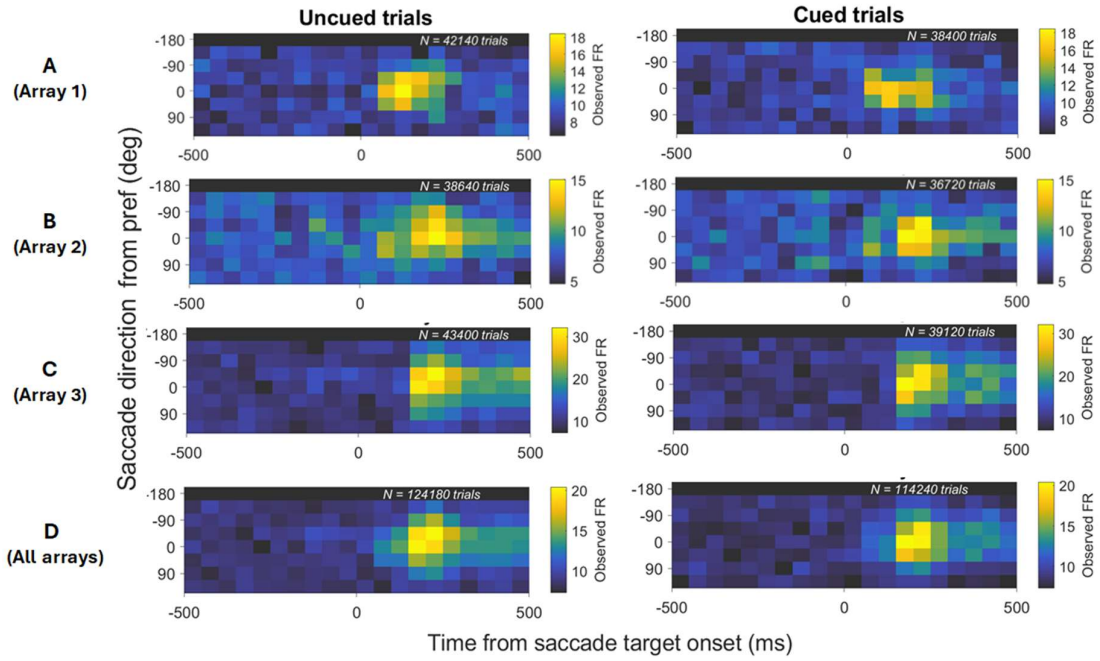

Figure 5.3. Response field maps in PPC on cued and uncued trials, aligned to the preferred direction of cells. *Firing rates of N = 640 recorded multi-units averaged over 50 ms bins, ± 500 ms around the onset of the peripheral saccade target, for target locations grouped into 8 equidistant bins (0 ± 180 degrees). For each multi unit, saccade directions were aligned to the preferred direction of that multiunit. Colour scale represents mean firing rate. Response field maps for uncued (left column) and cued (right column) trials presented separately for each array individually (rows **A, B** & **C**) and averaged over all arrays (row **D**).*

To gain insight into the time window when attentional modulation was greatest, I next assessed how firing rates changed over time between cued and uncued trials. (Fig 5.4A). This time window was then used to assess the impact of attentional modulation on tuning across preferred directions (Fig 5.4B). I extracted the distribution of firing rates across time (± 500 ms from target onset), for trials when the preferred direction equaled the saccade direction (i.e. saccade direction - preferred direction = 0 degrees) in the response field maps averaged over all 3 arrays. I observed a peak in firing rate in both the cued (*N = 16480 trials*) and uncued (*N = 17740 trials*) trial distributions, in the time window from 200 - 250 ms post target onset.

I then extracted the preferred direction aligned responses from both cued and uncued trials, across all 8 direction bins, in the time window (200 - 250 ms post target onset). By doing this, I was able to examine the effects of attentional modulation on saccade direction tuning in PPC. Comparing the cued (*N = 5712 trials*) and uncued (*N = 6209 trials*) trial distributions with a two-sample t-test, I only observed a significant difference in mean firing rates between the two, at saccade directions -90 degrees from the preferred direction (Fig 5.4B, *t(1721) = -2.00, p = 0.045*). The fact that I did not observe any difference between cued and uncued trials at the preferred saccade direction, and that our data contained a large distribution of preferred saccade directions, suggests that there may be an additional effect that is dependent on the cued direction.

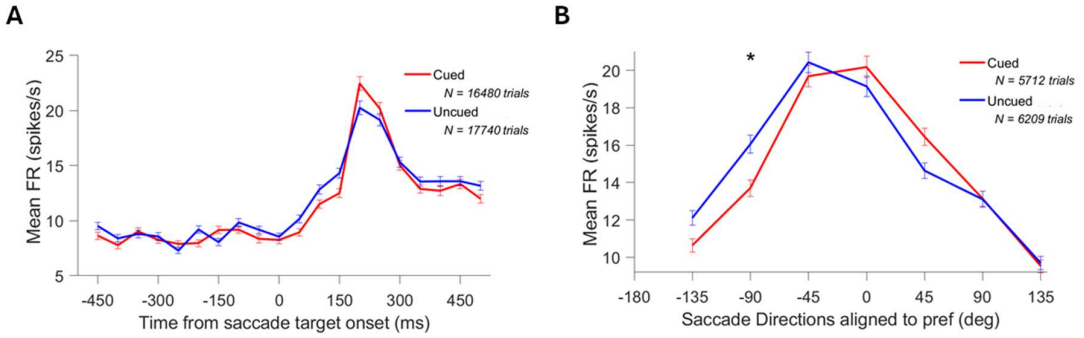

Figure 5.4: A comparison of the distribution of firing rates between cued and uncued trials in time and across saccadic locations aligned to the preferred direction of PPC cells. (A) *Cued (red) and uncued (blue) distributions of firing rates across time (50 ms bins, ± 500 ms around target onset), at the saccade location that equates to the preferred direction (0 degrees).* ***(B)*** *Cued and uncued distributions of firing rates for saccade directions aligned to the preferred direction of multi-units (45 degree bins), 200 - 250 ms post target onset. ± SEM error bars. * denotes a significant difference (p < 0.05, two-sample t-test) between cued and uncued trials in that time (A) or direction (B) bin.*

In the previous analysis, neural responses were averaged after aligning to each neuron's preferred direction. However, this likely masks the effect of the cue. To address this, here I test how responses aligned to the cued direction were modulated by attention. All multi-unit responses were first aligned to the cued direction presented in that recording session (0 degrees across all 3 arrays), and then average firing rates of all multi-units on uncued trials were compared to those on cued trials. The response field maps were plotted (Fig 5.3) for saccade directions aligned to the cued direction, for uncued and cued trials separately. Figure 5.5A, B and C depict the response field maps for each of the 3 arrays in M1 individually, and then Fig 5.5D depicts the average across all 3 of these arrays.

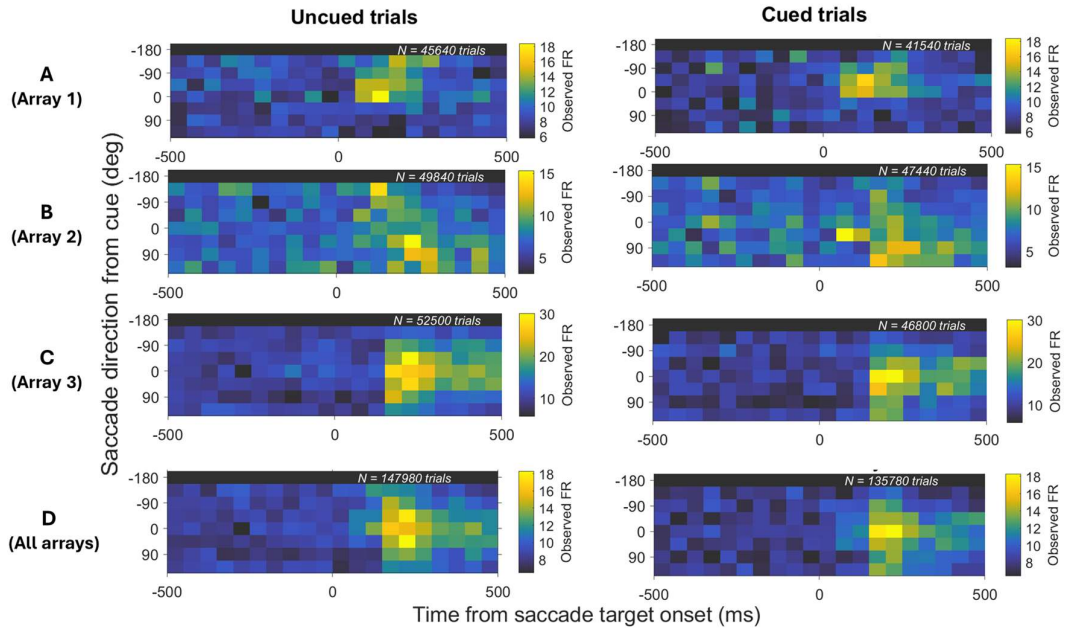

Figure 5.5: Response field maps in PPC on cued and uncued trials, aligned to the cued direction. *Cued direction on all 3 arrays here was at 0 degrees. Firing rates of N = 640 recorded multi-units averaged over 50 ms bins, ± 500 ms around the onset of the peripheral saccade target, for target locations grouped into 8 equidistant bins (0 ± 180 degrees). Higher firing rates are represented in yellow; lower firing rates in blue. Response field maps for uncued (left column) and cued (right column) trials presented separately for each array individually (rows **A, B** & **C**) and averaged over all arrays (row **D**).*

To assess how the cued direction affected neural responses across time, I first needed to select the time window when attentional modulation was greatest. To do this, I first extracted the distribution of firing rates across time (± 500 ms around target onset), for the trial where the cue direction was equal to the saccade target direction (Fig 5.6A). I again observed a peak in firing rate in both the cued (*N = 21140 trials*) and uncued (*N = 21140 trials*) trial distributions, in the time window from 200 - 250 ms post target onset.

I then extracted the cued and uncued distribution of firing rates across all saccade directions (aligned to the cued direction), across all 8 direction bins, in the time window (200 - 250 ms post target onset). This allowed us to test whether attention modulated firing rates around the cued direction, regardless of the preferred direction of the PPC neurons. Our null hypothesis was that there should be no effect at the cued direction on uncued trials. Comparing the cued (*N = 6789 trials*) and uncued (*N = 7399 trials*) trial distributions using a two-sample t-test (Fig 5.6B), I found that cued trials had a significantly higher firing rate than uncued trials (*p*

< *0.05*) at cue - target difference of 0 degrees. This trend reversed, ± 45 degrees from the cued direction (0 degrees): the firing rate on uncued trials at 45 degrees and 315 degrees (- 45 degrees) was significantly higher than cued trials ($p < 0.05$). This suggests that even on uncued trials, the cued direction is having an influence on firing rates, although that influence is significantly different to that on cued trials. In essence, there was a significant attentional enhancement of responses at the cued direction and a significant inhibition of responses to saccade directions ± 45 degrees away from the cued direction.

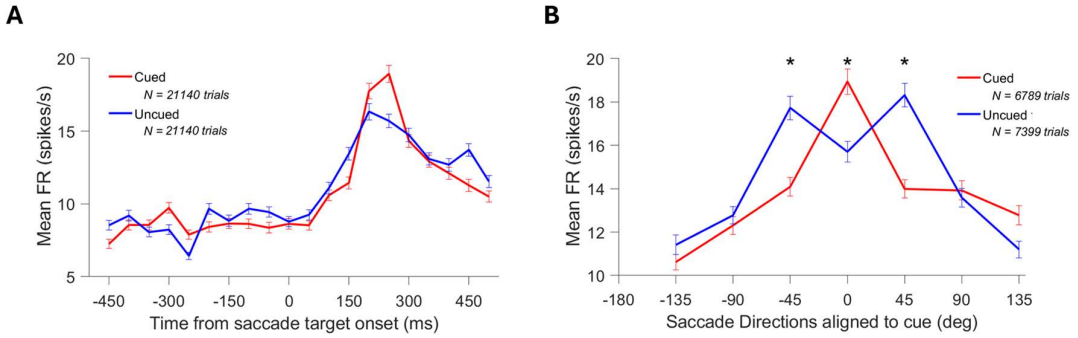

Figure 5.6: A comparison of the distribution of firing rates between cued and uncued trials in time and across saccadic locations aligned to the cue direction. *(Cued direction on all 3 arrays here was at 0 degrees).* ***(A)*** *Cued (red) and uncued (blue) distributions of firing rates across time (in 50 ms bins, ± 500 ms around target onset), at the saccade location that equates to the cued direction (i.e. 0 degrees).* ***(B)*** *Cued and uncued distributions of firing rates for saccade directions aligned to the cued direction (in 45 degree bins), 200 - 250 ms post target onset. ± SEM error bars. * denotes a significant difference (p < 0.05, two-sample t-test) between cued and uncued trials within that time (A) or direction (B) bin.*

5.3.3 Laminar differences in the effects of the spatial cue on saccade direction tuning

To determine the laminar differences in attentional modulation of PPC responses, I separated PPC multi-units into superficial (*N = 277 multi units*) and deep (*N = 88 multi-units*) layers. Superficial and deep layers were defined based on the boundary of the input layer IV (detailed in Chapter 5.2.3). To assess the laminar-dependent effects of attentional modulation on responses aligned to the preferred direction, I aligned each recorded multi-unit, in each layer, to the preferred direction (Fig 5.7 & 5.8). Figure 5.7 depicts the average response field maps aligned to the preferred direction, across all 3 arrays in M1, plotted by trial type (uncued and cued) and laminar compartment (superficial and deep). For responses aligned to the preferred direction, I observed little difference in the distribution of peak firing rates between trial types or between laminar compartments.

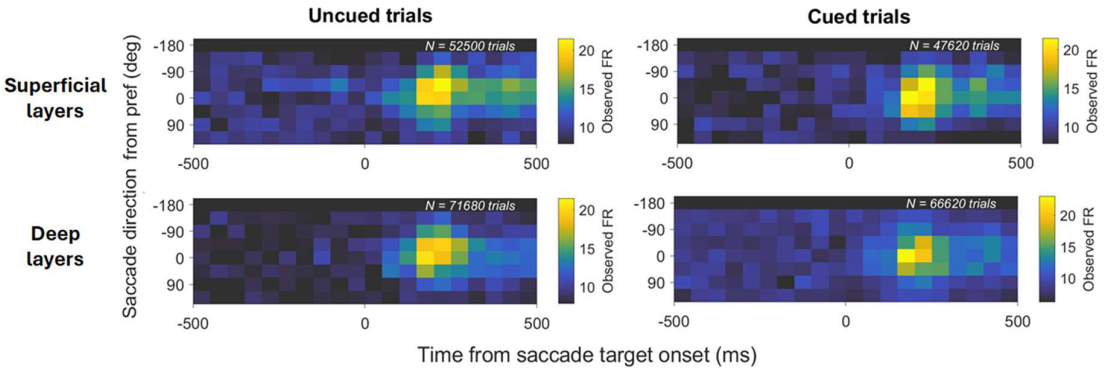

Figure 5.7: Response field maps for cued and uncued trials, aligned to the preferred direction of cells, in the superficial and deep layers of PPC. *Firing rates of multi-units averaged over 50 ms bins, ± 500 ms around the onset of the peripheral saccade target, for target locations grouped into 8 equidistant bins (0 ± 180 degrees). Higher firing rates are represented in yellow; lower firing rates in blue. Superficial (top row, N = 227 units) and deep (bottom row, N = 88 units) laminar compartments were categorised around the point of greatest change in the phase mean angle from the spike-phase coupling relationship using a 4Hz multi-tapered LFP. These response field maps (averaged over 3 arrays in M1) for uncued (left column) and cued (right column) trials were also presented separately.*

To determine the time window when attentional modulation was greatest, I assessed how firing rates changed over time, between cued and uncued trials, across both superficial and deep layers (Fig 5.8A). I extracted the distributions (by trial type and layer) of firing rates across time (± 500 ms around target onset) for when the preferred direction equaled the saccade direction (i.e. saccade direction - preferred direction = 0 degrees). I did this for both cued and uncued trials, as well as in both superficial and deep layers of PPC. I observed a peak in firing rate across all distributions in the time window from 200 - 250 ms post target onset.

Extracting the responses, aligned to the preferred saccade direction, on both trials and from both layers in this time window (Fig 5.8B), I examined the laminar-dependent effects of attentional modulation on saccade direction tuning in PPC using a two-sample t-test (Bonferroni corrected for multiple comparisons, $\alpha = 0.025$). I found no statistically significant differences between trial types in either superficial or deep layers ($p > 0.025$).

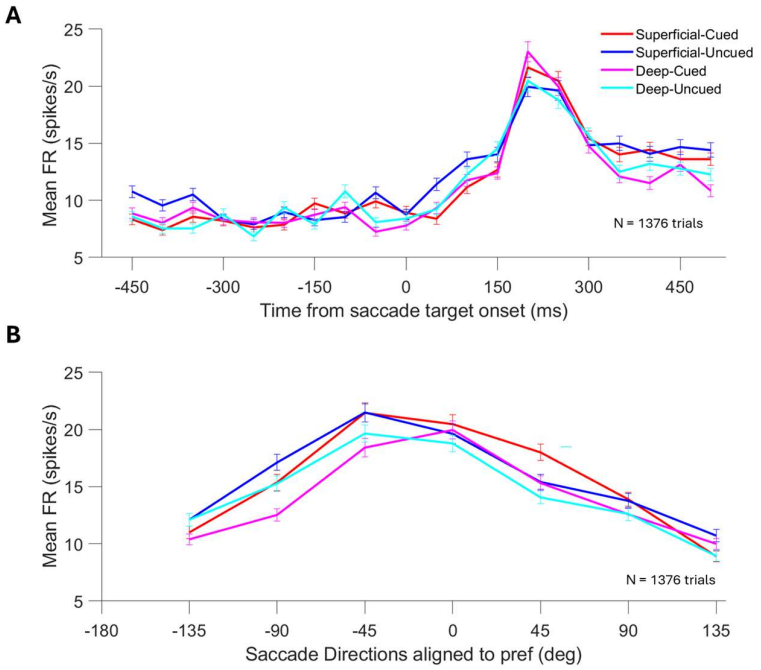

Figure 5.8: Laminar differences in the firing rates between cued and uncued trials, for distributions across time and saccade locations aligned to the preferred direction of PPC cells. *Superficial and deep laminar compartments were categorised around the point of greatest change in the phase mean angle from the spike-phase coupling relationship using a 4Hz multi-tapered LFP. Cued distribution in superficial layers (red); uncued distribution in superficial layers (blue); cued distribution in deep layers (magenta), uncued distribution in deep layers (cyan).* ***(A)*** *Distributions of firing rates across time (in 50 ms bins, ± 500 ms around target onset), at the saccade location that equates to the preferred direction (i.e. 0 degrees).* ***(B)*** *Distributions of firing rates for saccade directions aligned to the preferred direction of multi-units (in 45 degree bins), 200 - 250 ms post target onset. ± SEM error bars. Within each layer, cued and uncued trial distributions were compared using a two-sample t-test (Bonferroni corrected for multiple comparisons, α = 0.025)*

Next, I assessed the laminar-dependent effects of attentional modulation on responses aligned to the cued direction (0 degrees). Figure 5.9 depicts the average response field maps aligned to the cued direction, across all 3 arrays in M1 (in the same way as was done for the preferred saccade direction above), plotted by trial type (uncued and cued) and laminar compartment (superficial and deep). This time I observed a notable reduction in the spread of firing rates across space in deeper layers compared to superficial layers, and an obvious concentration of activity around 0 degrees on cued compared to uncued trials.

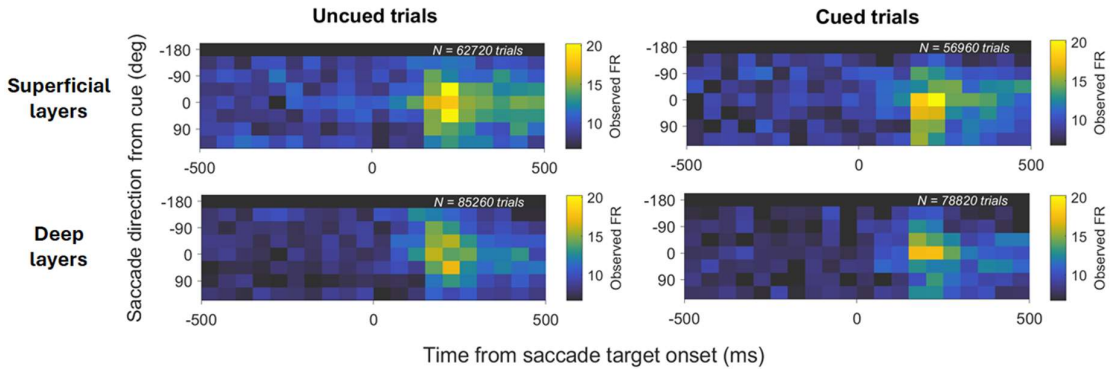

Figure 5.9: Response field maps for cued and uncued trials, aligned to the cued direction, in the superficial and deep layers of PPC *Cued direction on all 3 arrays here was at 0 degrees. Firing rates of multi-units averaged over 50 ms bins, ± 500 ms around the onset of the peripheral saccade target, for target locations grouped into 8 equidistant bins (0 ± 180 degrees). Higher firing rates are represented in yellow; lower firing rates in blue. Superficial (top row) and deep (bottom row) laminar compartments were categorised around the point of greatest change in the phase mean angle from the spike-phase coupling relationship using a 4Hz multi-tapered LFP. These response field maps (averaged over 3 arrays in M1) for uncued (left column) and cued (right column) trials were also presented separately.*

Once again, to determine the time window when attentional modulation was greatest, I assessed how firing rates changed over time, between cued and uncued trials, across both superficial and deep layers (Fig 5.10A). I extracted the distributions (by trial type and layer) of firing rates across time (± 500 ms around target onset) for when the cued direction equaled the saccade direction (i.e. saccade direction - cued direction = 0 degrees). I did this for both cued and uncued trials, as well as in both superficial and deep layers of PPC. Like the distributions aligned to preferred saccade directions, I observed a peak in firing rate across all distributions, in the time window from 200 - 250 ms post target onset.

Finally, by extracting the responses, aligned to the cued saccade direction, on both trials and from both layers in this time window (Fig 5.10B), I examined the cue-direction dependent differences in attentional modulation across laminar compartments in PPC. A two-sample t-test (Bonferroni corrected for multiple comparisons, $\alpha = 0.025$) revealed that in the superficial layers, responses to uncued trials were significantly larger than cued trials, at -45 degrees ($p = 0.004$). In deeper layers, responses on cued trials were significantly larger at the uncued direction (0 degrees) and 135 degrees away ($p = 0.012$), while responses on uncued trials were significantly larger than cued trials at 45 degrees away from the cued direction ($p = 0.0003$). This suggests attention-related inhibition of responses in superficial layers at -45 degrees from the cued direction. In deep layers, it suggests that there is a facilitatory effect of attention on responses at the cued direction, but an inhibitory effect on responses 45 degrees away from the cued direction.

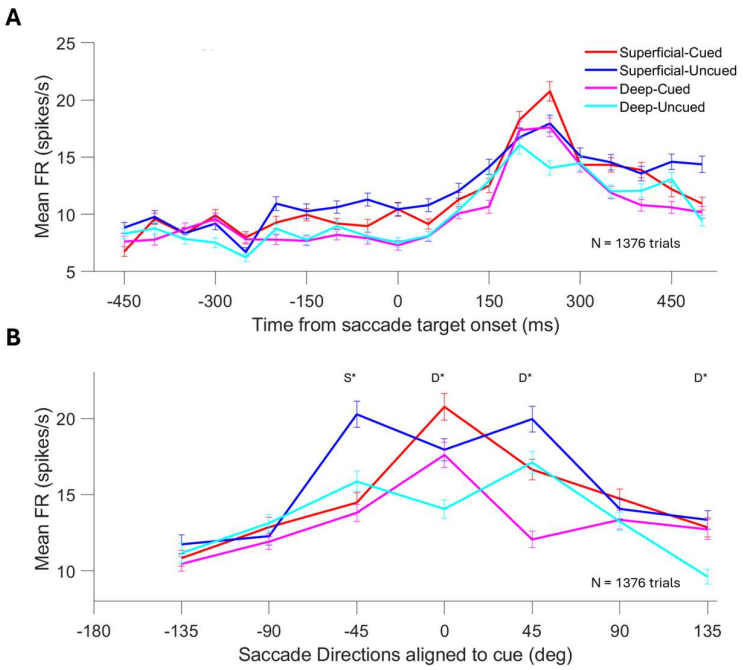

Figure 5.10: Laminar differences in the firing rates between cued and uncued trials, for distributions across time and saccade locations aligned to the cued direction. *Cued direction on all 3 arrays here was at 0 degrees. Superficial and deep laminar compartments were categorised around the point of greatest change in the phase mean angle from the spike-phase coupling relationship using a 4Hz multi-tapered LFP. Cued distribution in superficial layers (red); uncued distribution in superficial layers (blue); cued distribution in deep layers (magenta), uncued distribution in deep layers (cyan).* ***(A)*** *Distributions of firing rates across time (in 50 ms bins, ± 500 ms around target onset), at the saccade location that equates to the cued direction (i.e. 0 degrees).* ***(B)*** *Distributions of firing rates for saccade directions aligned to the cued direction (in 45 degree bins), 200 - 250 ms post target onset. ± SEM error bars. * denotes significance ($p < 0.025$, two-sample t-test with Bonferroni corrections for multiple comparisons) between firing rates within each time (A) or direction (B) bin. S* denotes a significant difference between superficial-cued and superficial-uncued; D* denotes a significant difference between deep-cued and deep-uncued.*

5.3.4 The relationship between the cue direction and the preferred direction

Thus far, I have examined the effects of the attentional cue on neuronal activity in PPC, aligned to the preferred saccade direction and to the cued direction separately. To recap, I found no significant laminar or attentionally-dependent differences between responses on cued and uncued trials, aligned to the preferred saccade direction of cells alone. However, when responses were aligned to the cued direction, I found both significant laminar and attentionally-driven differences. Surprisingly, I also found modulation around the cue direction on uncued trials, although the effect was significantly different than what was seen on cued trials (Fig 5.6 and Fig 5.10). One potential explanation for this could be the underlying distribution of preferred directions. If the distribution of preferred directions is biassed towards the cue direction, it could explain the effects of the cue direction seen on uncued trials. Furthermore, on cued trials, the influence of the cue could vary depending on the relationship between the cued direction and the preferred direction.

Therefore, for the next stage of inquiry, I sought to understand the relationship between a cell's preferred saccade direction and the direction of the cue. The null hypothesis is that there is no interaction between the cue direction and the preferred direction (Figure 5.11A). This means that the target direction, but not the cue direction, influences the neuron's response. I hypothesised that direction-selective neurons in PPC respond optimally when the cued direction matches their preferred direction, as the preferred direction represents the centre of a neuron's response field (where they respond optimally). Figure 5.11B visually illustrates this hypothesis, demonstrating how PPC neurons respond optimally to a preferred saccade direction (previously explored in chapter 5.3.2), and how this tuning is influenced by the direction of the cue. Responses are maximal when the cued direction is near the preferred direction (i.e. inside the response field), and gradually reduces as the cue gets further from the preferred direction.

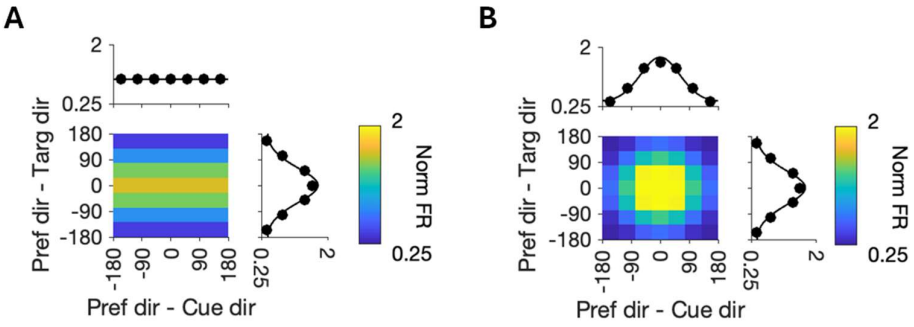

Figure 5.11. Hypothesis schematic depicting the effects of the cue on neuronal activity in and out of the response field, as a tuning matrix. *Tuning matrices relating the distribution of responses to each saccade target location, aligned to the preferred saccade direction (pref dir - targ dir), to the distribution of responses aligned to the direction of the cue, relative to the preferred direction (pref dir - cue dir).* ***(A)*** *Null hypothesis tuning matrix illustrating the pattern of activity when direction tuned responses are not influenced by the direction of the cue and how far away it is from the preferred saccade direction. There is tuning along the axis aligned to the preferred saccade direction (significant von mises fit for distribution of responses across the pref dir - targ dir y-axis, plotted on the right marginal) but none along the axis measuring how far the cued direction is from the response field (non-significant von mises fit for distribution of responses across the pref dir - cue dir x-axis plotted on the upper marginal).* ***(B)*** *Saccade direction tuning in PPC is significantly affected by the cued direction in relation to how far away the cue is from the neuron's response field (significant tuning along the pref-dir - cue dir x-axis). Here, blue indicates lower neuronal firing rates and yellow indicates higher.*

Firstly, the average preferred direction from 3 arrays implanted in PPC in M1 (*N = 640 multi-units*) was centred on 0 degrees, as 31% of units preferred a saccade target direction at 0 degrees (Fig 5.12A), and less than 5% preferred directions further than 90 degrees beyond this. This may explain the modulation of firing rates by the cue, on uncued trials observed in Fig 5.6 and 5.10. Indeed, when I factor in the relationship between the preferred direction and the cue direction on uncued trials (Fig 5.12B), I see no effect of the cue direction on firing rates (p = 0.59, von Mises fit, see Methods). On cued trials (Fig 5.12C), I found that the direction of the cue significantly influenced responses when the cue was near the preferred direction. Responses aligned to the cued direction, relative to the distance from the preferred direction (right marginal in Fig 5.12C), were significantly tuned on cued trials (p = 2.4×10^{-5}, von Mises fit).

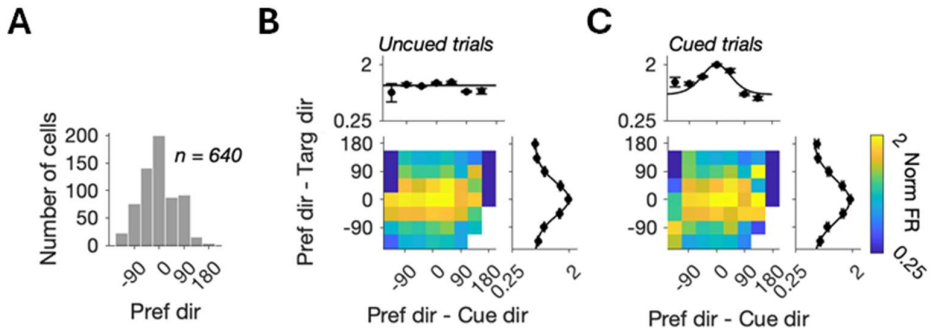

Figure 5.12. The direction of attentional cueing, when within the response field, enhances PPC responses on cued trials. (A) *A frequency histogram of preferred directions across all recorded PPC multi-units, from 3 arrays in M1.* ***(B)*** *A tuning matrix relating the distribution of normalised responses aligned to the preferred saccade direction, with the distribution of normalised responses aligned to the direction of the cue, relative to the preferred direction (pref dir - cue dir), on uncued trials.* ***(C)*** *A tuning matrix as seen in B, but for normalised responses on cued trials. Tuning curves on the marginals of each axis depict the average normalised response at each direction bin ± SEM (error bars). The significance of tuning on was determined by fitting these distributions to a von Mises curve.*

Next, I investigated the source of this cue-driven effect in relation to laminar compartments in PPC. I first categorised our multi-unit responses into superficial (*N = 277 units*) and deep (*N = 88 units*) layers based on the boundary of the input layer (see Chapter 5.2.3 for details). As detailed in Chapter 4, layers were defined based on a significant peak change in spike-LFP phase mean angle between adjacent electrodes. Not every recording day yielded a significant peak change, hence why there were fewer tuned PPC units assigned

to these 2 laminar compartments (*N = 365 units*) layers than recorded in total (*N = 640 units*). In Figure 5.13A, I observed that the distribution of preferred saccade directions for multi-units located in the superficial layers was split between two main saccade directions. 36% of the response units preferred saccade targets at 0 degrees and approximately 20% preferred targets at 90 degrees. As observed in the responses across layers in PPC (figure 5.12), in superficial layers I found no relationship between the cue and preferred direction on uncued trials (Fig 5.13B marginal; von Mises fit, $p = 0.2$) and found a facilitatory effect of the cue direction when it closer to the preferred direction on cued trials (Fig 5.13C marginal; von Mises fit, $p = 6.8 \times 10^{-5}$). In the deeper layers (Fig 5.13D), the distribution of preferred directions was concentrated between -90 to 0 degrees. No relationship between the cue direction and preferred direction was found on either uncued (Fig 5.13E marginal; von Mises fit, $p > 0.05$) or cued trials (Fig 5.13F marginal; von Mises fit, $p > 0.05$).

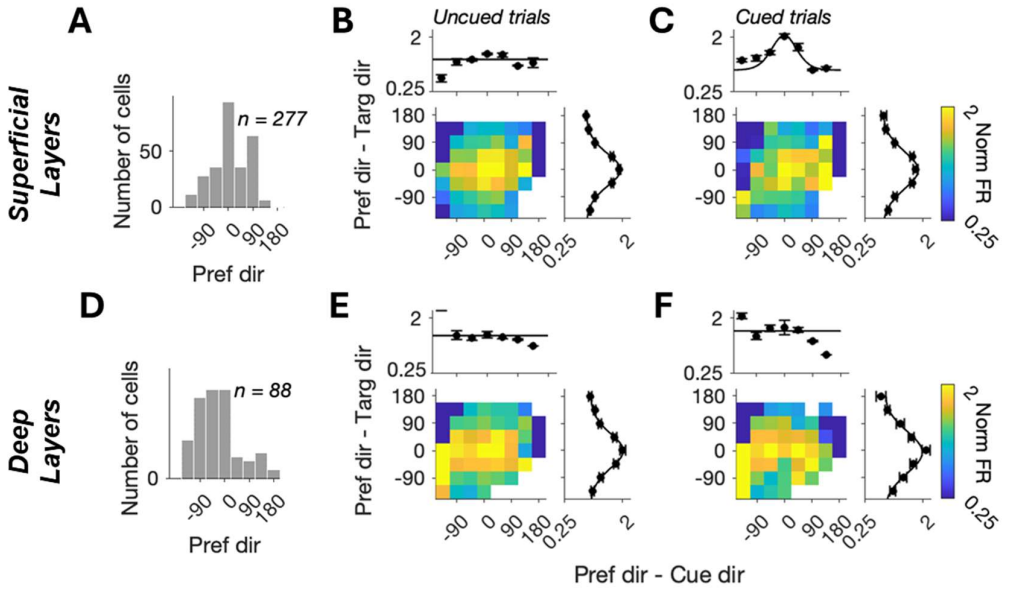

Figure 5.13. Laminar differences in the effect of attentional cueing to the response field of saccade-direction tuned PPC neurons. *Top row (panel A-C) displays data from superficial layers; Bottom row (panel D - F) displays data from deep layers, collected from 3 arrays in M1. Frequency histograms of the preferred directions across multi-units in PPC, recorded in superficial* ***(A)*** *and deep layers* ***(D)****.* ***(B)*** *A tuning matrix relating the distribution of normalised responses aligned to the preferred saccade direction, with the distribution of normalised responses aligned to the direction of the cue, relative to the preferred direction (pref dir - cue dir), on uncued trials in the superficial layers.* ***(C)*** *A tuning matrix as seen in B, but for normalised responses on cued trials in superficial layers.* ***(E)*** *A tuning matrix as seen in B, but for normalised responses to uncued trials in deep layers.* ***(F)*** *A tuning matrix as seen in C, but for normalised responses on cued trials in deep layers. Tuning curves on the marginals of each axis on the tuning matrices in B,C,E and F depict the average normalised response at each direction bin ± SEM (error bars). The significance of tuning on was determined by fitting these distributions to a von Mises curve.*

5.4 Discussion

In this chapter, I explored the impact of spatial attention on the activity of saccade-direction tuned multi-units in the posterior parietal cortex (PPC). By comparing the saccade reaction times (SRTs) between the three trial types in the cued centre out saccade task (uncued, informative cue and uninformative cue), I demonstrated that the marmoset can successfully learn the intention of the spatial cue (Fig 5.1). I then demonstrated that spatial attention modulated firing rates in PPC. This modulation was dependent on the preferred direction of neurons, the positioning of the cue relative to the preferred direction, and the cortical layer (superficial or deep). This is the first description of the modulatory effects of spatial attention across cortical layers in PPC.

Analysis of SRTs validated that the cue was probing attentional mechanisms. As predicted, the cue influenced performance on the saccade task. When faced with an uninformative cue (i.e. the saccade target did not match the location they were cued to attend to), the marmoset was, on average, significantly slower at saccading to the target than if the cue was valid (Fig 5.1E) or even in the absence of a cue (Fig 5.1G). I did not find a significant facilitatory behavioural effect of the cue on informative cue trials compared to uncued trials (Fig 5.1F). This is likely due to the marmoset's extremely fast SRTs (see also Ma et al., 2020; Chen et al., 2021). I noted here that while over 80% of recording days showed a slowing of SRT on informative cue trials, there is a fair amount of variance across days in median SRTs. It is a current limitation of our work, but future analyses will benefit from exploration of this variance and its correlation with neural activity patterns.

In the past, it has been reported that humans demonstrate a 3% (10 ms) reduction in SRTs on informative cue trials, and a 14% (40 ms) increase in SRTs on uninformative cue trials, compared to uncued trials, (Crawford and Muller, 1992). These trends are reflected in our dataset, though the SRTs reported in humans can be up to 2.5 times longer than marmosets (Crawford and Muller, 1992; Chen et al., 2021). Further assessment of the saccade kinematics in our dataset revealed that, on average, SRTs were slightly faster towards the cued direction, regardless of the presence of the cue (0 degrees; Fig 5.1C). This was likely a reflection of the cue being in the same position for several months. Previous research has not indicated that marmosets display bias towards a portion of the visual field (Chen et al., 2021).

I expected an attentional modulation on cued trials to result in an enhancement of PPC responses, based on the findings of previous research (Corbetta and Shulman, 2002; Serences and Yantis, 2006; Bressler et al., 2008). I specifically examined the effects of attention on saccade direction tuning, as others (including myself in Chapter 3) I have shown

that neurons in PPC are tuned to saccadic eye movements of a particular direction (Ghahremani et al., 2017; Ma et al., 2020). As PPC neurons respond maximally to their preferred saccade direction, this preferred direction can be viewed as the centre of their response field (Andersen et al., 1985). Aligning multi-unit responses to the preferred direction of cells (Fig 5.3 and 5.4), I observed no significant attentional modulation of responses at the preferred direction (Fig 5.4B). I did, however, observe a significant difference between responses on cued and uncued trials, to saccade directions -90 degrees from the preferred direction of neurons (Fig 5.4B). Our data contained a large distribution of preferred saccade directions (Figure 5.12) and the concentration of preferred directions was between -90 and 0 degrees. Therefore, the significant difference between cued and uncued responses at -90 degrees from the preferred direction, likely alluded to attentional effects at the cued direction. To test this theory, I then aligned our multi-unit responses to the cued direction (Fig 5.5 and 5.6), and observed a significant attentional enhancement of responses at the cued direction. On trials where the saccade target location was ± 45 degrees away from the cued direction, I also observed significant inhibitory attentional modulation of firing rates. This suppressive neuronal effect was directly reflected in the behavioural performance of the marmoset, where SRTs on uninformative trials (target location ≠ cue location) were significantly slower. Our findings reflect the idea that the facilitatory behavioural effects of the cue are often restricted to the cued location (Crawford and Muller, 1992).

The apparent modulation of firing rates away from the preferred direction (Fig 5.12) and on uncued trials aligned to the cue (Fig 5.6), indicated that I needed to take into account the relationship between the preferred direction and the cued direction. By taking into consideration the relationship between the cue and preferred direction, I found there was no modulation by the cue on uncued trials (Fig 5.12). On cued trials, however, I found enhanced firing rates when the cue was near the preferred direction (5.13). Our results supported the hypothesis that the effects of attentional modulation are enhanced in a spatially localised manner.

I next sought to gain insights into the neuronal effects of spatial attention modulation dependent on the cortical layer. In the frontal-parietal saccade network, FEF and area LIP within PPC are reciprocally connected, with FEF sending feedback projections that terminate in the superficial layers of PPC (Schall et al., 1995a; Stanton et al., 1995). In line with this, I hypothesised that attentional modulation would predominantly affect the superficial layers of PPC. When responses were aligned to the preferred direction, I did not detect any significant laminar-dependent differences in attentional modulation of PPC responses (Figs 5.7 & 5.8B). This was understandable given that I did not see much attentional modulation of the general population of PPC multi-units aligned to preferred direction. I did, however, observe significant laminar-dependent differences in the impact of attentional modulation on responses aligned

to the cue direction (Figs 5.9 & 5.10B). Overall, the same trend in attentional modulation between cued and uncued trials, as observed in the general population of PPC neurons, was also observed across superficial and deep layers of PPC, although firing rates were generally higher in the superficial layers (Fig 5.10B). When assessing the effects of spatial attention on the relationship between the preferred direction of a cell and the cued direction, across cortical layers, I again found no modulation of the cue on uncued trials, in either superficial or deep layers. On cued trials, the facilitatory effect of the cue was observed in superficial layers only (Fig 5.13). Consistent with our hypothesis, attentional modulation enhanced the responses of superficial multi-units on cued trials when the direction of the cue was near the preferred saccade direction.

PPC neurons are known to have reward-modulated neuronal responses (Bendiksby and Platt, 2006; Peck et al., 2009; Leathers and Olson, 2012; Wu, Chen and Cai, 2023). As such, it was vital that I control for the influence of reward-modulated responses in PPC in the design of the cued saccade task, by carefully ensuring that I did not vary reward in a way that influenced the marmosets behavioural performance. Marmosets received a uniform volume of reward for correct completion of a trial (see Fig 5.1A), right from the onset of their training - they were never rewarded any differently for faster reaction times on a given trial. Therefore, we could be certain that any influence on their reaction times, specifically on cued trials, were due to the facilitatory effects of attention. If the training regimen were to deviate from this, it is likely that an analysis of neuronal responses across training and recording sessions would reveal a modulatory effect on PPC neuronal responses and it would be difficult to dissociate neural effects driven by the cue from neural effects driven by expectancy of different rewards.

While this is the first account of the modulatory effects of spatial attention across cortical layers in PPC, there has been extensive work done in other cortical areas, like visual area 4 (V4). The superficial layers of V4 have been found to encode feedforward sensory information like stimulus orientation, while deeper layers coded for the direction of planned eye movements (Pettine et al., 2019). Feedback signals project to the deeper layers in V4 (Ungerleider et al., 2008). As a result, studies have recorded differences in the beta-frequency range of the LFP between cortical layers in V4 (Nandy et al., 2017; Westerberg et al., 2021). Stronger beta-coherence is observed in deeper layers, in relation to feature selectivity during attentional states (Nandy et al., 2017; Westerberg et al., 2021), while superficial and input layers demonstrate the opposite effect. Given that I found differences in spike-LFP phase with cortical depth (Chapter 4), a next logical step for this dataset will be to analyse effects of spatial attention on spike-LFP coherence across superficial and deep layers.

In this study, I demonstrated that marmosets could learn a cued saccade task, and that the spatial attention cue modulated firing rates in PPC. The modulation was dependent on the preferred direction of the neuron, the positioning of the cue relative to the preferred direction, and the cortical layer. The superficial layers of PPC, which receive feedback signals from FEF,

saw the greatest effect of attentional modulation in the way of an enhancement of neuronal responses to the cued direction, when it was near the preferred saccade direction. I would, however, like to note that the findings of this study are preliminary, and the interpretation of these results are limited by the analysis of data collected from only one monkey, and a select few arrays that presented the cue in the same direction. Data collection and analyses are ongoing, and future work will expand the data in both of these areas. Ultimately, I would like to connect the observed changes in our neural dataset, to the behavioural manipulations of visual attention.

Chapter 6. General Discussion

In this thesis, I demonstrate the value of the common marmoset (*Callithrix Jacchus*) as a model for studying complex cognitive functions like visual attention. Visual attention is a modulatory mechanism controlled by networks of cortical areas, like the frontal-parietal saccadic network (Bisley and Goldberg, 2010). In this network, specific nodes including the frontal eye fields (FEF) within the frontal cortex and the lateral intraparietal area (area LIP) within the posterior parietal cortex (PPC), are directly and reciprocally connected (Huerta et al., 1987; Andersen et al., 1990a; Blatt et al., 1990; Schall et al., 1995b; Stanton et al., 1995; Paré and Wurtz, 1997; Anderson et al., 2011), and appear to have overlapping functions (Corbetta, 1998; Nobre et al., 2000; Perry and Zeki, 2000; DeSouza et al., 2003; Munoz and Everling, 2004; de Haan et al., 2008). Here, I argue that investigating the laminar organisation of brain areas like PPC is an important step in dissecting the individual contributions of these areas to the wider network. Reiterating some of the limitations of this line of inquiry in previous research (discussed in greater detail in Chapter One), I describe how the experimental evidence presented in this thesis, from the marmoset PPC, is ideally suited for addressing them. Firstly, the lissencephalic structure of the marmoset cortex permitted me to, for the first time, access PPC and map the fine topographic organisation of saccade-direction preferences here. Through multi-electrode recordings, I also performed the first layer-based analysis of attentional modulation in PPC, demonstrating that visual attention primarily modulates activity within the superficial layers. Given that previous anatomical studies have traced feedback connections from the frontal eye fields to these same superficial layers in PPC (Schall et al., 1995a; Stanton et al., 1995), the functional observations in this thesis suggest that the source of modulatory attentional signals in PPC may come from the frontal cortex.

6.1 Marmosets as a model for studying cortical networks

In humans and macaques, many higher order cortical areas like PPC are buried in sulci. This can make accessibility for electrophysiological recordings challenging, and determining the layer of the recording extremely difficult. Marmosets, on the other hand, have a lissencephalic cortex with a large and highly developed visual system (Rosa et al., 2009; Chaplin et al., 2013; Majka et al., 2016, 2020; Zhu and Vanduffel, 2019) that is mostly exposed on the lateral surface. In Chapter 3, I demonstrate the advantages of this, by using multi-electrode laminar arrays to record from multiple depths and sites across PPC. By doing so, I gain insight into the way in which PPC neurons represent the visual field, and provide the first detailed evidence of the topographic layout of saccade-direction preferences here.

As discussed in Chapter 1, cortical areas like PPC do not work in isolation - they are wired together in networks. Feedback projections within networks are theorised to be one of the main mechanisms of attentional modulation. In fact, many studies have reported differences in attentional modulation between superficial and deep layers, dependent on the location of feedback projections (Nandy et al., 2017; Pettine et al., 2019; Westerberg et al., 2021). In the frontal parietal network, FEF feedback projections terminate in the superficial layers of PPC (Reser et al., 2013). Therefore, we would be remiss if we did not consider laminar level circuit interactions between cortical areas when studying network-level cognitive functions like attention. However, due to a lack of accessibility of cortical layers in the macaque PPC, it has been difficult to test this theory - particularly in relation to the hypothesised laminar-dependent differences in attentional modulation seen in other brain areas.

Laminar-dependent attentional research in higher-order cortical areas like PPC is further complicated by the difficulty in identifying laminar boundaries using traditional methods like the current source density analysis (CSD). This is because the CSD relies heavily on precisely-timed feedforward circuit dynamics (Mitzdorf, 1985; Self et al., 2013; Nandy et al., 2017), whereas PPC receives a complex mix of feedforward and feedback projections from multiple areas (Andersen et al., 1990a; Schall, 1991). In Chapter 4, I analytically compared recently developed alternatives (Davis et al., 2023; Mendoza-Halliday et al., 2024) to the CSD, which utilised different spectral features of the LFP signal. I found that the theta-band peak phase change in the spike-LFP coherence relationship was the best alternative for defining cortical layers in my PPC data.

Consequently, I was able to demonstrate the laminar dependent effects of attentional modulation in PPC for the first time (Chapter 5). In this final chapter, I describe success in training a marmoset to perform a cued centre-out saccade task, which enabled me to probe the neuronal correlates of attention. I found that attentional modulation was greatest in the superficial layers of PPC, where we previously noted FEF feedback projections terminate. I also observed that in the general PPC neuronal population, the magnitude of attentional modulation was dependent on the preferred saccade direction of neurons, as well as the location to which attention was directed.

There is still a lot we don’t know about marmoset neurophysiology and the extent of their behavioural capabilities. Future research would greatly benefit from such investigations clarifying these gaps in our knowledge. Marmosets are likely restricted to more simple visual and cognitive behaviours. Some research groups have shifted from traditional, trial based visual tasks in favour of more naturalistic visual foraging tasks (Yates et al., 2023). Previous studies of the PPC in marmosets have also focused on two saccade target directions to simplify training procedures (Ma et al., 2020). Here, we demonstrate marmosets can be

trained to complete more sophisticated visual behaviour. By training marmosets to make saccades to up to 36 visual targets, we were able to create the first detailed maps of saccade tuning in the PPC (Chapter 3). Furthermore, we demonstrate that they can be trained to learn a spatial cue that influences their saccade reaction times, indicating that they are directed spatial attention in the cued direction (Chapter 5). While it is true that our marmosets performed far fewer daily trials than typically reported in macaques, I argue that the benefits of their neuroanatomical and lissencephalic brain structure still provide important opportunities for the application of more complex techniques. Nonetheless, trial number and complexity are considerations that will limit the types of cognitive tasks that can be tested in this animal model.

Overall, the work in my thesis has provided insight into how PPC neurons encode saccade-related properties and how attention modulates activity here. This work would not have been possible without the unique advantages that the marmoset brain provided over previously used animal models. Ultimately, understanding the unique function of PPC in the frontal-parietal network is essential for disentangling it from FEF, and revealing the underlying mechanisms of attention in the primate visual system.

6.2 Future directions: optogenetics as tool for dissecting neural circuits

A next logical step in this line of work is to causally manipulate activity across the frontal parietal network to understand how information is integrated across brain areas and cortical layers. Over the last few decades, several methods for inferring how information is communicated across areas have been proposed. One method is to measure the coherence in neural activity across brain areas. In Chapter 4, I measured how the coherence between spiking activity and the phase of the LFP changed over cortical depth. Spike-LFP coherence has also been measured in communication between LIP and FEF (Buschman and Miller, 2007). Given that FEF and area LIP both receive input from several extrastriate visual areas (Andersen et al., 1990a; Schall, 1991), conclusions about the temporal coherence of neural activity between areas of the frontal parietal network are limited. It is difficult to dissociate functionally relevant signals from irrelevant ones, and to determine whether coherent fluctuations in two regions are simply due to common input. Furthermore, it is difficult to ascertain directionality in the flow of information across areas.

Consequently, there is a need to perturb activity in one area, while recording from the other, to better understand the interactions between directly connected areas. One way to address this is by observing functional changes in a network associated with inactivation (pharmacologically or through cooling) or electrical microstimulation. Inactivating either FEF or area LIP (via cooling) while recording from the other changed the firing rate of over 70% of neurons during a memory-guided saccade task (Chafee and Goldman-Rakic, 2000). Neurons in each area were equally likely to have firing rates augmented or suppressed, suggesting a

fairly equal exchange of information across areas, while neural latencies to the cue response remained unchanged. Likewise, microstimulation of FEF results in widespread activation of neurons in area LIP (Ekstrom et al., 2008). Inactivation of both area LIP (Wardak et al., 2002) and FEF (Wardak et al., 2006) results in an increase in reaction time for the selection of a saccade target amongst distractors. However, the deficits increased with task difficulty only in area LIP (Wardak et al., 2002), suggesting a role in encoding visual salience. Representations of visual salience emerge earlier in area LIP than in FEF (Buschman and Miller, 2007), suggesting that these signals may propagate from parietal to frontal cortices. Indeed, a recent study found that representations of visual salience in FEF disappeared when the PPC was pharmacologically inactivated (Chen et al., 2020). While these studies have provided invaluable insights, both inactivation and microstimulation are spatially crude and non-selectively engage large regions of cortex around the site of stimulation or inhibition. As a result, any observed effects from these techniques could encompass indirect pathways through neighbouring cortical regions. Furthermore, inactivation studies are temporally limited by the time course of the drug or cooling procedure. Therefore, there is a need for techniques that can manipulate neural activity with both spatial and temporal precision to tie neural activity of individual cells to the anatomical projections across areas.

Optogenetics offers a way to modulate direct functional links between anatomically connected areas through precise stimulation or inhibition of specific cell types within an area, while recording from another (Boyden et al., 2005). The technique operates under the same general principle of electrical stimulation, chemical cooling or chemical lesioning agents, but targets specific types of neurons made to express light-sensitive ion channels or pumps, called opsins, to change the polarisation of the cell in response to specific wavelengths of light (Deisseroth, 2015). Commonly, illumination of bacteriorhodopsins and halorhodopsins results in hyperpolarisation, which inhibits neural activity, while illumination of channelrhodopsins typically results in depolarisation and action potentials. Briefly, these microbial opsin genes, incorporated into stable and non-replicating viral vectors such as adeno-associated viral (AAV) vectors, are injected into regions of interest, where they are able to efficiently transduce specific types of postmitotic neurons in the vicinity of the injection. Optogenetic techniques have been predominantly implemented in mouse models, however their use in primates is growing (as reviewed in El-Shamayleh and Horwitz, 2019 and Diester et al., 2011). By exploiting viruses incorporating cell-specific promoters, it has been possible to determine the contribution of different cell types, particularly excitatory and inhibitory cells (Cardin et al., 2009; De et al., 2020). This is important because computational modelling has suggested that temporally coherent neural activity is driven by windows of neural excitation and inhibition (Shewcraft et al., 2020). This opens the door to using optogenetics to probe network dynamics and their cellular origins. Rodent models have already been used to investigate how projections from the frontal cortex to thalamus modulate visual attention (Wimmer et al., 2015;

Schmitt et al., 2017). However, the neurophysiology and behaviour of rodents and primates differ in many ways, making it difficult to translate discoveries in rodents to higher order primates. Furthermore, while still in it's nascent stages, recent work describes optogenetic G protein-coupled receptors (optoGPCRs) which more directly target the synaptic terminals of long-range neuronal projections (reviewed in Wietek et al., 2024). The precision of traditional opsins in targeting such synaptic terminals are limited, as they typically rely on manipulating neuronal soma, which can result in undesirable secondary effects on downstream regions, to which they are often connected. OptoGPCRs effectively perturb intracellular signalling cascade pathways and inhibit synaptic transmission through the inhibition of voltage-gated calcium channels or the inhibition of neurotransmitter release from axon terminals.

In macaques, optogenetics has been used to reveal causal links between neural activity and cognitive behaviours in a manner that effectively extends the result of previous electrical microstimulation studies. For example, in macaques trained to saccade to a salient target among distractors, optogenetic stimulation of area LIP increases the number of saccades to targets within the stimulated neurons' receptive field, and decreases those saccades' latency (Dai et al., 2014). Gerits et al., (2012) observed a similar decrease in saccade latencies when optogenetically stimulating the arcuate nucleus in macaques performing a visually guided saccade discrimination task, but reported little to no change in performance accuracy or other saccade metrics such as amplitude. Optical stimulation of V1 neurons transfected with channelrhodopsin (ChR2) variants can generate saccades towards the receptive field of stimulated neurons in macaques trained to perform saccade-dependent visual discrimination tasks (Jazayeri et al., 2012). However, optogenetic stimulation of saccade modulation centres like FEF in macaques (Ohayon et al., 2013; Inoue et al., 2015), is often suboptimal at evoking eye movements with metrics identical to visual or electrical stimulation protocols. Optogenetically-evoked saccades in macaques often do not reach the desired eccentricity and are not entirely accurate in their direction trajectories. This is because it is difficult to target all relevant cells in these areas, as optogenetic injections activate a smaller volume of tissue than electrical microstimulation and because much of the area is buried in the arcuate sulcus in macaques, making targeting optical stimulation difficult.

In macaques, optogenetic stimulation of FEF axon terminals in the superior colliculus can generate saccades towards the receptive field of stimulated FEF cells (Inoue et al., 2015), indicating that technique can be used to determine the influence of long-range projections. However, the latencies of these optogenetically evoked saccades (Inoue et al., 2015) appear to be 150-170 ms longer than saccades evoked by electrical microstimulation (Schiller and Stryker, 1972; Bruce et al., 1985). This may be explained by the fact that optical suppression of axon terminals can have unintended consequences if suppressive opsins affect synaptic transmission in unpredictable and complex ways, especially when illuminated at high

intensities or for longer durations (Mahn et al., 2016; Wiegert et al., 2017). Stimulation of axon terminals may even cause some back-propagated activation of indirect pathways influencing saccades (Inoue et al., 2015) or it can depolarise both inhibitory and excitatory neurons (Jazayeri et al., 2012). Nassi et al., (2015) demonstrated this exact phenomenon, when attempting to optogenetically target excitatory neurons in the macaque V1, and indirectly exciting inhibitory neurons. As a means to overcome such a limitation, (Shewcraft et al., 2020) recently demonstrated the ability to optogenetically manipulate either excitatory or inhibitory activity alone, by carefully selecting stimulation parameters such as light pulse duration.

Marmosets are a promising animal model for studying how neural circuits give rise to certain complex brain states and behaviours, and this remains true for their use in optogenetic protocols. While optogenetic techniques have only recently been introduced in marmosets, the smaller size of marmoset brains (relative to other primates) is already showing to be a key advantage. Forelimb movements have been induced through blue-light optogenetic stimulation of the marmoset motor cortex (Ebina et al., 2019). Using a gene expression system that amplifies neuronal expression of a ChR2 opsin gene variant with fast kinetics, Ebina and colleagues stimulated the motor cortex through a relatively large cranial window. Given that this has previously been difficult to accomplish in macaques, due to the size of their motor cortex restricting light permeability through neural tissue, this demonstrates a unique benefit of the marmoset model. The size of the macaque cortex has also proven to be disadvantageous for optogenetic manipulation of behaviours, as the viral transfection range at the site of interaction is proportionally much smaller than what is required to elicit a behavioural effect from a population of neurons (Debes and Dragoi, 2023). Given the proportionately smaller size of the marmoset brain, it stands that they would be a more successful model for optogenetic perturbation of behaviours.

The smaller brain size of marmosets also shows promise for enabling long range transduction of optogenetic constructs. (MacDougall et al., 2016) developed a novel method to induce rapid photo stimulation in individual neurons, for several months, in awake behaving marmosets. They reported that along with successful transport of the virus, ChR2 opsins and fluorescent proteins were trafficked further along long-range pyramidal neuron projections in the marmoset, from the site of injection, enabling accurate tracing of neural circuits that are directly and causally activated during visual behaviours. In the months following injection, similar excitatory and inhibitory changes in neural activity during optogenetic stimulation in marmosets (MacDougall et al., 2016) as have been previously observed in mice (Sato et al., 2014) and macaques (Han et al., 2011). There have already been demonstrations of the success of optogenetics for investigating neural circuits in the visual cortex of marmosets. Recently, optogenetic suppression of the axon terminals of V2 feedback projections to V1, revealed an overall reduction in marmoset V1 responses to visual stimuli, as well as a

reduction in surround suppression, a property fundamental to V1 (Nurminen et al., 2018). In macaques, optogenetic stimulation of the koniocellular compartment of the macaque LGN, while recording from V1, they observed short latency neural responses evoked in the supragranular layers of V1, to which they are known to project anatomically (Klein et al., 2016). Similarly, recent work inhibiting specific FEF feedback inputs to M1 in macaques demonstrated a reduction in attentional modulation in MT, by third, without affecting the sensory response component here (Hüer et al., 2024). These studies demonstrate that optogenetics is a suitable technique for studying longer-range projections. The relatively smaller brain size of the marmoset compared to the macaque suggests that it will be particularly suitable for studying network interactions across cortical distances, including between areas of the frontal and parietal cortices. Extending the findings of this thesis, optogenetic inhibition of the terminals of FEF feedback projections to PPC in the superficial layers can clarify our speculation about its driving influence over the observed effects of attentional modulation here (Chapter 5).

Finally, coupling optogenetics with a powerful imaging technique like two-photon microscopy, can further improve investigations into neuronal circuit mechanisms. Two-photon microscopy permits *in vivo* visualisation of neural activity at high resolutions, deep into the cortex and for extended periods of time. Briefly, it is a fluorescence imaging technique that relies on the principle of a fluorophore absorbing two photons of light and emitting a longer wavelength of light which is known to scatter less and penetrate deeper through neural tissue. Two-photon imaging is already well established in rodents (Holtmaat et al., 2009; Drew et al., 2010), mainly due to their relatively thin dura, upper cortical layers, and amenability to transgenic technology - features shared by marmosets. While it has been attempted in the areas most exposed to the cortical surface in macaques, like V1 (Stettler et al., 2006; Heider et al., 2010), penetration depths in terms of anatomical layers are more limited owing to the cortical thickness and vascularisation. To date, fewer studies have attempted two-photon imaging in marmosets, however studies in somatosensory (Sadakane et al., 2015) and motor cortical areas (Ebina et al., 2018) have successfully imaged hundreds of neurons for several months, up to cortical depths of 500 μm (equating to layers 2/3) (Santisakultarm et al., 2016; Pattadkal et al., 2024). Given that like mice, marmosets have a relatively small brain size and a lissencephalic structure, it stands that the progress made in multi-area two-photon imaging in mice, using either multiple microscopes (Lecoq et al., 2014; Wagner et al., 2019) or a unique two-stage magnification process (Yang et al., 2019), is much more easily transferred to marmosets. That being said, to date, this technology has been limited to single area imaging in macaques and marmosets. Nonetheless, given that we observed attentional modulation in superficial layers of PPC (Chapter 5), two-photon imaging could provide further valuable insights into the nature of neural activity, as well as the spatial and temporal dynamics of attentional modulation in this layer, compared to deeper layers.

6.3 Conclusion

Non-human primates have been essential in studying the neural mechanisms of cognitive behaviours, such as visual attention. However, there are still many open questions about how such behaviours arise from interactions across brain areas. New electrode technologies and molecular techniques like optogenetics continually increase the toolbox with which researchers can probe these questions. While macaques have historically been the dominant model in such investigations, given their extensive behavioural repertoire and our knowledge of their neurophysiology and neuroanatomy, the sulcal structure of their brain has been limiting in the application of such techniques. I propose that the marmoset monkey is the ideal primate model for this arsenal, and shows much promise to help bridge the gap between our anatomical knowledge of the structure of cortex and understanding how this precise architecture across brain areas gives rise to cognitive visual behaviour. This thesis provides the foundational knowledge of the topographic and laminar organisation of the PPC. Extending this work by combining optogenetic methods in marmosets with existing behavioural, multi-area neurophysiological, and neuroimaging approaches could help uncover the functional architecture underlying visual and cognitive behaviours in primates.

References

.

Albright TD, Desimone R, Gross CG (1984) Columnar organization of directionally selective cells in visual area MT of the macaque. J Neurophysiol 51:16–31.

Andersen RA, Asanuma C, Essick G, Siegel RM (1990a) Corticocortical connections of anatomically and physiologically defined subdivisions within the inferior parietal lobule. J Comp Neurol 296:65–113.

Andersen RA, Bracewell RM, Barash S, Gnadt JW, Fogassi L (1990b) Eye position effects on visual, memory, and saccade-related activity in areas LIP and 7a of macaque. J Neurosci 10:1176–1196.

Andersen RA, Buneo CA (2002) Intentional maps in posterior parietal cortex. Annu Rev Neurosci 25:189–220.

Andersen RA, Essick GK, Siegel RM (1985) Encoding of spatial location by posterior parietal neurons. Science 230:456–458.

Anderson JC, Kennedy H, Martin KAC (2011) Pathways of Attention: Synaptic Relationships of Frontal Eye Field to V4, Lateral Intraparietal Cortex, and Area 46 in Macaque Monkey. J Neurosci 31:10872–10881.

Antoniades C, Ettinger U, Gaymard B, Gilchrist I, Kristjánsson A, Kennard C, John Leigh R, Noorani I, Pouget P, Smyrnis N, Tarnowski A, Zee DS, Carpenter RHS (2013) An internationally standardised antisaccade protocol. Vision Res 84:1–5.

Atallah BV, Scanziani M (2009) Instantaneous modulation of gamma oscillation frequency by balancing excitation with inhibition. Neuron 62:566–577.

Baizer JS, Ungerleider LG, Desimone R (1991) Organization of visual inputs to the inferior temporal and posterior parietal cortex in macaques. J Neurosci 11:168–190.

Baker JT, Patel GH, Corbetta M, Snyder LH (2006) Distribution of activity across the monkey cerebral cortical surface, thalamus and midbrain during rapid, visually guided saccades. Cereb Cortex 16:447–459.

Bakola S, Burman KJ, Rosa MGP (2015) The cortical motor system of the marmoset monkey (Callithrix jacchus). Neuroscience Research 93:72–81 Available at: http://dx.doi.org/10.1016/j.neures.2014.11.003.

Balaram P, Young NA, Kaas JH (2014) Histological features of layers and sublayers in cortical visual areas V1 and V2 of chimpanzees, macaque monkeys, and humans. Eye Brain 2014:5–18.

Barash S, Bracewell RM, Fogassi L, Gnadt JW, Andersen RA (1991) Saccade-related activity in the lateral intraparietal area. II. Spatial properties. J Neurophysiol 66:1109–1124.

Barbas H, Mesulam MM (1981) Organization of afferent input to subdivisions of area 8 in the rhesus monkey. J Comp Neurol 200:407–431.

Barton JJS, Cherkasova MV, Lindgren K, Goff DC, Intriligator JM, Manoach DS (2002) Antisaccades and task switching: studies of control processes in saccadic function in normal subjects and schizophrenic patients. Ann N Y Acad Sci 956:250–263.

Bastos AM, Loonis R, Kornblith S, Lundqvist M, Miller EK (2018) Laminar recordings in frontal cortex suggest distinct layers for maintenance and control of working memory. Proc Natl Acad Sci U S A 115:1117–1122.

Bastos AM, Vezoli J, Bosman CA, Schoffelen J-M, Oostenveld R, Dowdall JR, De Weerd P, Kennedy H, Fries P (2015a) Visual areas exert feedforward and feedback influences through distinct frequency channels. Neuron 85:390–401.

Bastos AM, Vezoli J, Bosman CA, Schoffelen J-M, Oostenveld R, Dowdall JR, De Weerd P, Kennedy H, Fries P (2015b) Visual areas exert feedforward and feedback influences through distinct frequency channels. Neuron 85:390–401.

Bell AH, Fecteau JH, Munoz DP (2004) Using auditory and visual stimuli to investigate the behavioral and neuronal consequences of reflexive covert orienting. J Neurophysiol 91:2172–2184.

Bendiksby MS, Platt ML (2006) Neural correlates of reward and attention in macaque area LIP. Neuropsychologia. 44(12):2411-20.

Ben Hamed S, Duhamel JR, Bremmer F, Graf W (2001) Representation of the visual field in the lateral intraparietal area of macaque monkeys: a quantitative receptive field analysis. Exp Brain Res 140:127–144.

Berens P (2009) CircStat: A MATLAB Toolbox for Circular Statistics. J Stat Softw 31:1–21.

Berman RA, Joiner WM, Cavanaugh J, Wurtz RH (2009) Modulation of presaccadic activity in the frontal eye field by the superior colliculus. J Neurophysiol 101:2934–2942.

Bisley JW, Goldberg ME (2003) Neuronal Activity in the Lateral Intraparietal Area and Spatial Attention. Science 299:81–86.

Bisley JW, Goldberg ME (2010) Attention, intention, and priority in the parietal lobe. Annu Rev Neurosci 33:1–21.

Blanke O, Spinelli L, Thut G, Michel CM, Perrig S, Landis T, Seeck M (2000) Location of the human frontal eye field as defined by electrical cortical stimulation: anatomical, functional and electrophysiological characteristics. Neuroreport 11:1907–1913.

Blatt GJ, Andersen RA, Stoner GR (1990) Visual receptive field organization and cortico-cortical connections of the lateral intraparietal area (area LIP) in the macaque. J Comp Neurol 299:421–445.

Blum B, Kulikowski JJ, Carden D, Harwood D (1982) Eye movements induced by electrical stimulation of the frontal fields of marmosets and squirrel monkeys. Brain Behav Evol 21:34–41.

Bollimunta A, Chen Y, Schroeder CE, Ding M (2008) Neuronal mechanisms of cortical alpha oscillations in awake-behaving macaques. J Neurosci 28:9976–9988.

Bosking WH, Crowley JC, Fitzpatrick D (2002) Spatial coding of position and orientation in primary visual cortex. Nat Neurosci 5:874–882.

Boyden ES, Zhang F, Bamberg E, Nagel G, Deisseroth K (2005) Millisecond-timescale, genetically targeted optical control of neural activity. Nat Neurosci 8:1263–1268.

Brainard DH (1997) The Psychophysics Toolbox. Spat Vis 10:433–436.

Bressler SL, Tang W, Sylvester CM, Shulman GL, Corbetta M (2008) Top-down control of human visual cortex by frontal and parietal cortex in anticipatory visual spatial attention. J Neurosci 28:10056–10061.

Bruce CJ, Goldberg ME (1985) Primate frontal eye fields. I. Single neurons discharging before saccades. J Neurophysiol 53:603–635.

Bruce CJ, Goldberg ME, Bushnell MC, Stanton GB (1985) Primate frontal eye fields. II. Physiological and anatomical correlates of electrically evoked eye movements. J Neurophysiol 54:714–734.

Buffalo EA, Fries P, Landman R, Buschman TJ, Desimone R (2011) Laminar differences in gamma and alpha coherence in the ventral stream. Proc Natl Acad Sci U S A 108:11262–11267.

Burman KJ, Bakola S, Richardson KE, Reser DH, Rosa MGP (2014a) Patterns of afferent input to the caudal and rostral areas of the dorsal premotor cortex (6DC and 6DR) in the marmoset monkey. J Comp Neurol 522:3683–3716.

Burman KJ, Bakola S, Richardson KE, Reser DH, Rosa MGP (2014b) Patterns of cortical input to the primary motor area in the marmoset monkey. J Comp Neurol 522:811–843.

Burman KJ, Palmer SM, Gamberini M, Rosa MGP (2006) Cytoarchitectonic subdivisions of the dorsolateral frontal cortex of the marmoset monkey (Callithrix jacchus), and their projections to dorsal visual areas. J Comp Neurol 495:149–172.

Buschman TJ, Miller EK (2007) Top-down versus bottom-up control of attention in the prefrontal and posterior parietal cortices. Science 315:1860–1862.

Buzsáki G, Anastassiou CA, Koch C (2012) The origin of extracellular fields and currents--EEG, ECoG, LFP and spikes. Nat Rev Neurosci 13:407–420.

Cardin JA, Carlén M, Meletis K, Knoblich U, Zhang F, Deisseroth K, Tsai L-H, Moore CI (2009) Driving fast-spiking cells induces gamma rhythm and controls sensory responses. Nature 459:663–667.

Cavanaugh J, Joiner WM, Wurtz RH (2012) Suppressive surrounds of receptive fields in monkey frontal eye field. Journal of Neuroscience 32:12284–12293.

Chafee MV, Goldman-Rakic PS (2000) Inactivation of parietal and prefrontal cortex reveals interdependence of neural activity during memory-guided saccades. J Neurophysiol 83:1550–1566.

Chaplin TA, Yu H-H, Soares JGM, Gattass R, Rosa MGP (2013) A conserved pattern of differential expansion of cortical areas in simian primates. J Neurosci 33:15120–15125.

Chen C-Y, Matrov D, Veale R, Onoe H, Yoshida M, Miura K, Isa T (2021) Properties of visually guided saccadic behavior and bottom-up attention in marmoset, macaque, and human. J Neurophysiol 125:437–457.

Chen M, Li B, Guang J, Wei L, Wu S, Liu Y, Zhang M (2016) Two subdivisions of macaque LIP process visual-oculomotor information differently. Proc Natl Acad Sci U S A 113:E6263–E6270.

Chen M, Liu Y, Wei L, Zhang M (2013) Parietal cortical neuronal activity is selective for express saccades. J Neurosci 33:814–823.

Chen SC, Morley JW, Solomon SG (2015) Spatial precision of population activity in primate area MT. J Neurophysiol 114:869–878.

Chen X, Zirnsak M, Moore T (2018) Dissonant Representations of Visual Space in Prefrontal Cortex during Eye Movements. Cell Rep 22:2039–2052.

Chen X, Zirnsak M, Vega GM, Govil E, Lomber SG, Moore T (2020) Parietal Cortex

Regulates Visual Salience and Salience-Driven Behavior. Neuron 106:177–187.e4.

Chen Y, Seidemann E (2012) Attentional modulations related to spatial gating but not to allocation of limited resources in primate V1. Neuron 74:557–566.

Cloherty SL, Yates JL, Graf D, DeAngelis GC, Mitchell JF (2020) Motion Perception in the Common Marmoset. Cereb Cortex 30:2658–2672.

Cohen MR, Maunsell JHR (2010) A neuronal population measure of attention predicts behavioral performance on individual trials. J Neurosci 30: 15241-15253

Colby CL, Duhamel JR, Goldberg ME (1996) Visual, presaccadic, and cognitive activation of single neurons in monkey lateral intraparietal area. J Neurophysiol 76:2841–2852.

Colby CL, Goldberg ME (1999) Space and attention in parietal cortex. Annu Rev Neurosci 22:319–349.

Collins CE, Lyon DC, Kaas JH (2005) Distribution across cortical areas of neurons projecting to the superior colliculus in new world monkeys. Anat Rec A Discov Mol Cell Evol Biol 285:619–627.

Connor CE, Preddie DC, Gallant JL, Van Essen DC (1997) Spatial attention effects in macaque area V4. J Neurosci 17:3201–3214.

Corbetta M (1998) Frontoparietal cortical networks for directing attention and the eye to visual locations: identical, independent, or overlapping neural systems? Proc Natl Acad Sci U S A 95:831–838.

Corbetta M, Akbudak E, Conturo TE, Snyder AZ, Ollinger JM, Drury HA, Linenweber MR, Petersen SE, Raichle ME, Van Essen DC, Shulman GL (1998) A common network of functional areas for attention and eye movements. Neuron 21:761–773.

Corbetta M, Shulman GL (2002) Control of goal-directed and stimulus-driven attention in the brain. Nat Rev Neurosci 3:201–215.

Crawford TJ, Muller HJ (1992) Spatial and temporal effects of spatial attention on human saccadic eye movements. Vision Res 32:293–304.

Dafoe JM, Armstrong IT, Munoz DP (2007) The influence of stimulus direction and eccentricity on pro- and anti-saccades in humans. Exp Brain Res 179:563–570.

Dai J, Brooks DI, Sheinberg DL (2014) Optogenetic and electrical microstimulation systematically bias visuospatial choice in primates. Curr Biol 24:63–69.

Davis ZW, Dotson NM, Franken TP, Muller L, Reynolds JH (2023) Spike-phase coupling patterns reveal laminar identity in primate cortex. Elife 12 Available at: http://dx.doi.org/10.7554/eLife.84512.

Davis ZW, Muller L, Martinez-Trujillo J, Sejnowski T, Reynolds JH (2020) Spontaneous travelling cortical waves gate perception in behaving primates. Nature 587:432–436.

Davis ZW, Muller L, Reynolds JH (2022) Spontaneous Spiking Is Governed by Broadband Fluctuations. J Neurosci 42:5159–5172.

De A, El-Shamayleh Y, Horwitz GD (2020) Fast and reversible neural inactivation in macaque cortex by optogenetic stimulation of GABAergic neurons. Elife 9 Available at: http://dx.doi.org/10.7554/eLife.52658.

Dean HL, Hagan MA, Pesaran B (2012) Only coherent spiking in posterior parietal cortex coordinates looking and reaching. Neuron 73:829–841.

Debes SR, Dragoi V (2023) Suppressing feedback signals to visual cortex abolishes attentional modulation. Science 379:468–473.

de Haan B, Morgan PS, Rorden C (2008) Covert orienting of attention and overt eye movements activate identical brain regions. Brain Res 1204:102–111.

Deisseroth K (2011) Optogenetics. Nat Methods 8:26–29.

Deisseroth K (2015) Optogenetics: 10 years of microbial opsins in neuroscience. Nat Neurosci 18:1213–1225.

DeSouza JFX, Menon RS, Everling S (2003) Preparatory set associated with pro-saccades and anti-saccades in humans investigated with event-related FMRI. J Neurophysiol 89:1016–1023.

Diester I, Kaufman MT, Mogri M, Pashaie R, Goo W, Yizhar O, Ramakrishnan C, Deisseroth K, Shenoy KV (2011) An optogenetic toolbox designed for primates. Nat Neurosci 14:387–397.

Douglas RJ, Martin KAC (2004) Neuronal circuits of the neocortex. Annu Rev Neurosci 27:419–451.

Douglas RJ, Martin KAC (2007) Recurrent neuronal circuits in the neocortex. Curr Biol 17:R496–R500.

Douglas RJ, Martin KAC, Whitteridge D (1989) A canonical microcircuit for neocortex. Neural Comput 1:480–488.

Drew PJ, Shih AY, Driscoll JD, Knutsen PM, Blinder P, Davalos D, Akassoglou K, Tsai PS, Kleinfeld D (2010) Chronic optical access through a polished and reinforced thinned skull. Nat Methods 7:981–984.

D'Souza JF, Price NSC, Hagan MA (2021) Marmosets: a promising model for probing the neural mechanisms underlying complex visual networks such as the frontal-parietal network. Brain Struct Funct 226:3007–3022.

Ebina T, Masamizu Y, Tanaka YR, Watakabe A, Hirakawa R, Hirayama Y, Hira R, Terada S-I, Koketsu D, Hikosaka K, Mizukami H, Nambu A, Sasaki E, Yamamori T, Matsuzaki M (2018) Two-photon imaging of neuronal activity in motor cortex of marmosets during upper-limb movement tasks. Nat Commun 9:1879.

Ebina T, Obara K, Watakabe A, Masamizu Y, Terada S-I, Matoba R, Takaji M, Hatanaka N, Nambu A, Mizukami H, Yamamori T, Matsuzaki M (2019) Arm movements induced by noninvasive optogenetic stimulation of the motor cortex in the common marmoset. Proc Natl Acad Sci U S A 116:22844–22850.

Edelman JA, Valenzuela N, Barton JJS (2006) Antisaccade velocity, but not latency, results from a lack of saccade visual guidance. Vision Res 46:1411–1421.

Ekstrom LB, Roelfsema PR, Arsenault JT, Bonmassar G, Vanduffel W (2008) Bottom-up dependent gating of frontal signals in early visual cortex. Science 321:414–417.

El-Shamayleh Y, Horwitz GD (2019) Primate optogenetics: Progress and prognosis. Proc Natl Acad Sci U S A Available at: http://dx.doi.org/10.1073/pnas.1902284116.

Everling S, Munoz DP (2000) Neuronal correlates for preparatory set associated with pro-saccades and anti-saccades in the primate frontal eye field. J Neurosci 20:387–400.

Fecteau JH, Bell AH, Munoz DP (2004) Neural correlates of the automatic and goal-driven biases in orienting spatial attention. J Neurophysiol 92:1728–1737.

Federer F, Ta'afua S, Merlin S, Hassanpour MS, Angelucci A (2021) Stream-specific feedback inputs to the primate primary visual cortex. Nature Communications 11;12(1):228.

Feizpour A, Majka P, Chaplin TA, Rowley D, Yu H-H, Zavitz E, Price NSC, Rosa MGP, Hagan MA (2021) Visual responses in the dorsolateral frontal cortex of marmoset monkeys. J Neurophysiol 125:296–304.

Ferrier D (1874) XVI. The Croonian Lecture.—experiments on the brain of monkeys (second series).

Ferro D, van Kempen J, Boyd M, Panzeri S, Thiele A (2021) Directed information exchange between cortical layers in macaque V1 and V4 and its modulation by selective attention. Proc Natl Acad Sci U S A 118 Available at: http://dx.doi.org/10.1073/pnas.2022097118.

Fiebelkorn IC, Kastner S (2019) A rhythmic theory of attention. Trends Cogn Sci Available at: https://www.cell.com/trends/cognitive-sciences/fulltext/S1364-6613(18)30281-X.

Fiebelkorn IC, Kastner S (2020) Functional Specialization in the Attention Network. Annu Rev Psychol 71:221–249.

Fiebelkorn IC, Pinsk MA, Kastner S (2018) A Dynamic Interplay within the Frontoparietal Network Underlies Rhythmic Spatial Attention. Neuron 99:842–853.e8.

Filali-Sadouk N, Castet E, Olivier E, Zenon A (2010) Similar effect of cueing conditions on attentional and saccadic temporal dynamics. J Vis 10:21.1–13.

Fries P (2015) Rhythms for Cognition: Communication through Coherence. Neuron 88:220–235.

Fries P, Reynolds JH, Rorie AE, Desimone R (2001) Modulation of oscillatory neuronal synchronization by selective visual attention. Science 291:1560–1563.

Fries P, Womelsdorf T, Oostenveld R, Desimone R (2008) The effects of visual stimulation and selective visual attention on rhythmic neuronal synchronization in macaque area V4. J Neurosci 28:4823–4835.

Fries W (1984) Cortical projections to the superior colliculus in the macaque monkey: a retrograde study using horseradish peroxidase. J Comp Neurol 230:55–76.

Gerits A, Farivar R, Rosen BR, Wald LL, Boyden ES, Vanduffel W (2012) Optogenetically induced behavioral and functional network changes in primates. Curr Biol 22:1722–1726.

Ghahremani M, Hutchison RM, Menon RS, Everling S (2017) Frontoparietal functional connectivity in the common marmoset. Cereb Cortex 27:3890–3905.

Ghahremani M, Johnston KD, Ma L, Hayrynen LK, Everling S (2019) Electrical microstimulation evokes saccades in posterior parietal cortex of common marmosets. J Neurophysiol 122:1765–1776.

Gnadt JW, Andersen RA (1988) Memory related motor planning activity in posterior parietal cortex of macaque. Exp Brain Res 70:216–220.

Goldberg ME, Colby CL, Duhamel JR (1990) Representation of visuomotor space in the parietal lobe of the monkey. Cold Spring Harb Symp Quant Biol 55:729–739.

Gold JI, Shadlen MN (2000) Representation of a perceptual decision in developing oculomotor commands. Nature 404:390–394.

Gottlieb J, Goldberg ME (1999) Activity of neurons in the lateral intraparietal area of the

monkey during an antisaccade task. Nat Neurosci 2:906–912.

Gottlieb JP, Kusunoki M, Goldberg ME (1998) The representation of visual salience in monkey parietal cortex. Nature 391:481–484.

Gregoriou GG, Gotts SJ, Zhou H, Desimone R (2009) High-frequency, long-range coupling between prefrontal and visual cortex during attention. Science 324:1207–1210.

Haegens S, Barczak A, Musacchia G, Lipton ML, Mehta AD, Lakatos P, Schroeder CE (2015) Laminar Profile and Physiology of the α Rhythm in Primary Visual, Auditory, and Somatosensory Regions of Neocortex. J Neurosci 35:14341–14352.

Hagan MA, Pesaran B (2022) Modulation of inhibitory communication coordinates looking and reaching. Nature 604:708–713.

Hanks TD, Ditterich J, Shadlen MN (2006) Microstimulation of macaque area LIP affects decision-making in a motion discrimination task. Nat Neurosci 9:682–689.

Hansen BJ, Chelaru MI, Dragoi V (2012) Correlated variability in laminar cortical circuits. Neuron 76:590–602.

Han X, Chow BY, Zhou H, Klapoetke NC, Chuong A, Rajimehr R, Yang A, Baratta MV, Winkle J, Desimone R, Boyden ES (2011) A high-light sensitivity optical neural silencer: development and application to optogenetic control of non-human primate cortex. Front Syst Neurosci 5:18.

Harris KD, Mrsic-Flogel TD (2013) Cortical connectivity and sensory coding. Nature 503:51–58.

Hawellek DJ, Wong YT, Pesaran B (2016a) Temporal coding of reward-guided choice in the posterior parietal cortex. Proceedings of the National Academy of Sciences 113:13492–13497.

Hawellek DJ, Wong YT, Pesaran B (2016b) Temporal coding of reward-guided choice in the posterior parietal cortex. Proc Natl Acad Sci U S A 113:13492–13497.

Heider B, Nathanson JL, Isacoff EY, Callaway EM, Siegel RM (2010) Two-photon imaging of calcium in virally transfected striate cortical neurons of behaving monkey. PLoS One 5:e13829.

Herrington TM, Assad JA (2009) Neural activity in the middle temporal area and lateral intraparietal area during endogenously cued shifts of attention. J Neurosci 29:14160–14176.

Holtmaat A, Bonhoeffer T, Chow DK, Chuckowree J, De Paola V, Hofer SB, Hübener M, Keck T, Knott G, Lee W-CA, Mostany R, Mrsic-Flogel TD, Nedivi E, Portera-Cailliau C, Svoboda K, Trachtenberg JT, Wilbrecht L (2009) Long-term, high-resolution imaging in the mouse neocortex through a chronic cranial window. Nat Protoc 4:1128–1144.

Hook MA, Rogers LJ (2008) Visuospatial reaching preferences of common marmosets (Callithrix jacchus): an assessment of individual biases across a variety of tasks. J Comp Psychol 122:41–51.

Hüer J, Saxena P, Treue S (2024) Pathway-selective optogenetics reveals the functional anatomy of top-down attentional modulation in the macaque visual cortex. Proc Natl Acad Sci U S A 121:e2304511121.

Huerta MF, Krubitzer LA, Kaas JH (1987) Frontal eye field as defined by intracortical microstimulation in squirrel monkeys, owl monkeys, and macaque monkeys. II. Cortical connections. J Comp Neurol 265:332–361.

Hung CC, Yen CC, Ciuchta JL, Papoti D, Bock NA, Leopold DA, Silva AC (2015) Functional MRI of visual responses in the awake, behaving marmoset. Neuroimage 120:1–11.

Inoue K-I, Takada M, Matsumoto M (2015) Neuronal and behavioural modulations by pathway-selective optogenetic stimulation of the primate oculomotor system. Nat Commun 6:8378.

Isaacson JS, Scanziani M (2011) How inhibition shapes cortical activity. Neuron 72:231–243.

Isa T (2017) Using the common marmoset for neurophysiological studies of neocortical functions. J Physiol 595:7013.

Jazayeri M, Lindbloom-Brown Z, Horwitz GD (2012) Saccadic eye movements evoked by optogenetic activation of primate V1. Nat Neurosci 15:1368–1370.

Jerde TA, Curtis CE (2013) Maps of space in human frontoparietal cortex. J Physiol Paris 107:510–516.

Johnston K, Everling S (2006) Neural activity in monkey prefrontal cortex is modulated by task context and behavioral instruction during delayed-match-to-sample and conditional prosaccade-antisaccade tasks. J Cogn Neurosci 18:749–765.

Johnston K, Everling S (2008) Neurophysiology and neuroanatomy of reflexive and voluntary saccades in non-human primates. Brain Cogn 68:271–283.

Johnston K, Everling S (2011) Frontal cortex and flexible control of saccades. The Oxford handbook of eye movements Available at: https://books.google.com/books?hl=en&lr=&id=GctzmDb3xmMC&oi=fnd&pg=PA279&dq=Johnston+and+Everling+(2011)&ots=bb1IwOyAHT&sig=eqsqylcLKjCVueTqE22BMsvKZi8.

Johnston K, Ma L, Schaeffer L, Everling S (2019) Alpha Oscillations Modulate Preparatory Activity in Marmoset Area 8Ad. J Neurosci 39:1855–1866.

Kaas JH (1997) Topographic maps are fundamental to sensory processing. Brain Res Bull 44:107–112.

Kaschube M (2014) Neural maps versus salt-and-pepper organization in visual cortex. Curr Opin Neurobiol 24:95–102.

Khan AZ, Heinen SJ, McPeek RM (2010) Attentional cueing at the saccade goal, not at the target location, facilitates saccades. J Neurosci 30:5481–5488.

Klein C, Evrard HC, Shapcott KA, Haverkamp S, Logothetis NK, Schmid MC (2016) Cell-Targeted Optogenetics and Electrical Microstimulation Reveal the Primate Koniocellular Projection to Supra-granular Visual Cortex. Neuron 90:143–151.

Kleiner M, Brainard D, Pelli D (2007) What's new in Psychtoolbox-3?

Koyama M, Hasegawa I, Osada T, Adachi Y, Nakahara K, Miyashita Y (2004) Functional magnetic resonance imaging of macaque monkeys performing visually guided saccade tasks: comparison of cortical eye fields with humans. Neuron 41:795–807.

Kustov AA, Robinson DL (1996) Shared neural control of attentional shifts and eye movements. Nature 384:74–77.

Kusunoki M, Gottlieb J, Goldberg ME (2000) The lateral intraparietal area as a salience map: the representation of abrupt onset, stimulus motion, and task relevance. Vision Res 40:1459–1468.

Lakatos P, Karmos G, Mehta AD, Ulbert I, Schroeder CE (2008) Entrainment of neuronal oscillations as a mechanism of attentional selection. Science 320:110–113.

Leathers ML, Olson CR (2012) In monkeys making value-based decisions, LIP neurons encode cue salience and not action value. Science 338(6103):132-5

Lecoq J, Savall J, Vučinić D, Grewe BF, Kim H, Li JZ, Kitch LJ, Schnitzer MJ (2014) Visualizing mammalian brain area interactions by dual-axis two-photon calcium imaging. Nat Neurosci 17:1825–1829.

Lewis JW, Van Essen DC (2000) Corticocortical connections of visual, sensorimotor, and multimodal processing areas in the parietal lobe of the macaque monkey. J Comp Neurol 428:112–137.

Lu T, Liang L, Wang X (2001) Temporal and rate representations of time-varying signals in the auditory cortex of awake primates. Nat Neurosci 4:1131–1138.

Lynch JC, Graybiel AM, Lobeck LJ (1985) The differential projection of two cytoarchitectonic subregions of the inferior parietal lobule of macaque upon the deep layers of the superior colliculus. J Comp Neurol 235:241–254.

MacDougall M, Nummela SU, Coop S, Disney A, Mitchell JF, Miller CT (2016) Optogenetic manipulation of neural circuits in awake marmosets. J Neurophysiol 116:1286–1294.

Mahn M, Prigge M, Ron S, Levy R, Yizhar O (2016) Biophysical constraints of optogenetic inhibition at presynaptic terminals. Nat Neurosci 19:554–556.

Maier A, Adams GK, Aura C, Leopold DA (2010) Distinct superficial and deep laminar domains of activity in the visual cortex during rest and stimulation. Front Syst Neurosci 4 Available at: http://dx.doi.org/10.3389/fnsys.2010.00031.

Majaj NJ, Carandini M, Movshon JA (2007) Motion integration by neurons in macaque MT is local, not global. J Neurosci 27:366–370.

Majka P, Bai S, Bakola S, Bednarek S, Chan JM, Jermakow N, Passarelli L, Reser DH, Theodoni P, Worthy KH, Wang X-J, Wójcik DK, Mitra PP, Rosa MGP (2020) Open access resource for cellular-resolution analyses of corticocortical connectivity in the marmoset monkey. Nat Commun 11:1133.

Majka P, Chaplin TA, Yu H-H, Tolpygo A, Mitra PP, Wójcik DK, Rosa MGP (2016) Towards a comprehensive atlas of cortical connections in a primate brain: Mapping tracer injection studies of the common marmoset into a reference digital template. J Comp Neurol 524:2161–2181.

Malach R, Schirman TD, Harel M, Tootell RB, Malonek D (1997) Organization of intrinsic connections in owl monkey area MT. Cereb Cortex 7:386–393.

Ma L, Selvanayagam J, Ghahremani M, Hayrynen LK, Johnston KD, Everling S (2020) Single-unit activity in marmoset posterior parietal cortex in a gap saccade task. J Neurophysiol 123:896–911.

Marple L (1999) Computing the discrete-time “analytic” signal via FFT. IEEE Trans Signal Process 47:2600–2603.

Mazzoni P, Bracewell RM, Barash S, Andersen RA (1996) Motor intention activity in the macaque’s lateral intraparietal area. I. Dissociation of motor plan from sensory memory. J Neurophysiol 76:1439–1456.

McDowell JE, Dyckman KA, Austin BP, Clementz BA (2008) Neurophysiology and neuroanatomy of reflexive and volitional saccades: evidence from studies of humans.

Brain Cogn 68:255–270.

Meister MLR, Hennig JA, Huk AC (2013) Signal multiplexing and single-neuron computations in lateral intraparietal area during decision-making. J Neurosci 33:2254–2267.

Mendoza-Halliday D, Major AJ, Lee N, Lichtenfeld MJ, Carlson B, Mitchell B, Meng PD, Xiong YS, Westerberg JA, Jia X, Johnston KD, Selvanayagam J, Everling S, Maier A, Desimone R, Miller EK, Bastos AM (2024) A ubiquitous spectrolaminar motif of local field potential power across the primate cortex. Nat Neurosci 27:547–560.

Miller CT, Freiwald WA, Leopold DA, Mitchell JF, Silva AC, Wang X (2016) Marmosets: A Neuroscientific Model of Human Social Behavior. Neuron 90:219–233.

Miller CT, Wren Thomas A (2012) Individual recognition during bouts of antiphonal calling in common marmosets. J Comp Physiol A Neuroethol Sens Neural Behav Physiol 198:337–346.

Mitchell JF, Leopold DA (2015) The marmoset monkey as a model for visual neuroscience. Neurosci Res 93:20–46.

Mitchell JF, Priebe NJ, Miller CT (2015) Motion dependence of smooth pursuit eye movements in the marmoset. J Neurophysiol 113:3954–3960.

Mitchell JF, Reynolds JH, Miller CT (2014) Active vision in marmosets: a model system for visual neuroscience. J Neurosci 34:1183–1194.

Mitra PP, Pesaran B (1999) Analysis of dynamic brain imaging data. Biophys J 76:691–708.

Mitzdorf U (1985) Current source-density method and application in cat cerebral cortex: investigation of evoked potentials and EEG phenomena. Physiol Rev 65:37–100.

Mitzdorf U, Singer W (1979) Excitatory synaptic ensemble properties in the visual cortex of the macaque monkey: a current source density analysis of electrically evoked potentials. J Comp Neurol 187:71–83.

Mohler CW, Goldberg ME, Wurtz RH (1973) Visual receptive fields of frontal eye field neurons. Brain Res 61:385–389.

Moore T, Fallah M (2004) Microstimulation of the frontal eye field and its effects on covert spatial attention. J Neurophysiol 91:152–162.

Moran J, Desimone R (1985) Selective attention gates visual processing in the extrastriate cortex. Science 229:782–784.

Motter BC (1993) Focal attention produces spatially selective processing in visual cortical areas V1, V2, and V4 in the presence of competing stimuli. J Neurophysiol 70:909–919.

Mott FW, Schuster E, Halliburton WD (1910) Cortical lamination and localisation in the brain of the marmoset. Proc R Soc Lond B Biol Sci 82:124–134.

Mountcastle VB (1997) The columnar organization of the neocortex. Brain 120 (Pt 4):701–722.

Munoz DP, Everling S (2004) Look away: the anti-saccade task and the voluntary control of eye movement. Nat Rev Neurosci 5:218–228.

Nagel-Leiby S, Buchtel HA, Welch KM (1990) Cerebral control of directed visual attention and orienting saccades. Brain 113 (Pt 1):237–276.

Nandy AS, Nassi JJ, Reynolds JH (2017) Laminar Organization of Attentional Modulation in Macaque Visual Area V4. Neuron 93:235–246.

Nassi JJ, Avery MC, Cetin AH, Roe AW, Reynolds JH (2015) Optogenetic Activation of Normalization in Alert Macaque Visual Cortex. Neuron 86:1504–1517.

Nobre AC, Gitelman DR, Dias EC, Mesulam MM (2000) Covert visual spatial orienting and saccades: overlapping neural systems. Neuroimage 11:210–216.

Nummela SU, Jovanovic V, de la Mothe L, Miller CT (2017) Social Context-Dependent Activity in Marmoset Frontal Cortex Populations during Natural Conversations. J Neurosci 37:7036–7047.

Nurminen L, Merlin S, Bijanzadeh M, Federer F, Angelucci A (2018) Top-down feedback controls spatial summation and response amplitude in primate visual cortex. Nat Commun 9:2281.

O'Driscoll GA, Alpert NM, Matthysse SW, Levy DL, Rauch SL, Holzman PS (1995) Functional neuroanatomy of antisaccade eye movements investigated with positron emission tomography. Proc Natl Acad Sci U S A 92:925–929.

Ohayon S, Grimaldi P, Schweers N, Tsao DY (2013) Saccade modulation by optical and electrical stimulation in the macaque frontal eye field. J Neurosci 33:16684–16697.

Paré M, Wurtz RH (1997) Monkey posterior parietal cortex neurons antidromically activated from superior colliculus. J Neurophysiol 78:3493–3497.

Parker AJ, Newsome WT (1998) Sense and the single neuron: probing the physiology of perception. Annu Rev Neurosci 21:227–277.

Pattadkal JJ, Zemelman BV, Fiete I, Priebe NJ (2024) Primate neocortex performs balanced sensory amplification. Neuron 112:687–688.

Peck CJ, Jangraw DC, Suzuki M, Efem R, Gottlieb J (2009) Reward modulates attention independently of action value in posterior parietal cortex. Journal of Neuroscience. 29(36):11182-91

Perry RJ, Zeki S (2000) The neurology of saccades and covert shifts in spatial attention: an event-related fMRI study. Brain 123 (Pt 11):2273–2288.

Pesaran B, Nelson MJ, Andersen RA (2008) Free choice activates a decision circuit between frontal and parietal cortex. Nature 453:406–409.

Pesaran B, Pezaris JS, Sahani M, Mitra PP, Andersen RA (2002) Temporal structure in neuronal activity during working memory in macaque parietal cortex. Nat Neurosci 5:805–811.

Pesaran B, Vinck M, Einevoll GT, Sirota A, Fries P, Siegel M, Truccolo W, Schroeder CE, Srinivasan R (2018) Investigating large-scale brain dynamics using field potential recordings: analysis and interpretation. Nat Neurosci 21:903–919.

Petrides M, Cadoret G, Mackey S (2005) Orofacial somatomotor responses in the macaque monkey homologue of Broca's area. Nature 435:1235–1238.

Petrides M, Pandya DN (2002) Comparative cytoarchitectonic analysis of the human and the macaque ventrolateral prefrontal cortex and corticocortical connection patterns in the monkey. Eur J Neurosci 16:291–310.

Pettine WW, Steinmetz NA, Moore T (2019) Laminar segregation of sensory coding and behavioral readout in macaque V4. Proc Natl Acad Sci U S A 116:14749–14754.

Platt ML, Glimcher PW (1998) Response fields of intraparietal neurons quantified with multiple saccadic targets. Exp Brain Res 121:65–75.

Platt ML, Glimcher PW (1999) Neural correlates of decision variables in parietal cortex. Nature 400:233–238.

Pomberger T, Hage SR (2019) Semi-chronic laminar recordings in the brainstem of behaving marmoset monkeys. J Neurosci Methods 311:186–192.

Posner MI, Cohen Y (1984) Components of visual orienting. In: Attention and performance X: Control of language processes (Bouma H, Bouwhuis DG, eds), pp 531–556. Hillsdale, NJ: Erlbaum.

Premereur E, Janssen P, Vanduffel W (2013) FEF-microstimulation causes task-dependent modulation of occipital fMRI activity. Neuroimage 67:42–50.

Redinbaugh MJ, Phillips JM, Kambi NA, Mohanta S, Andryk S, Dooley GL, Afrasiabi M, Raz A, Saalmann YB (2020) Thalamus Modulates Consciousness via Layer-Specific Control of Cortex. Neuron 106:66–75.e12.

Reser DH, Burman KJ, Yu HH, Chaplin TA, Richardson KE, Worthy KH, Rosa MGP (2013) Contrasting patterns of cortical input to architectural subdivisions of the area 8 complex: A retrograde tracing study in marmoset monkeys. Cereb Cortex 23:1901–1922.

Rockland KS, Pandya DN (1979) Laminar origins and terminations of cortical connections of the occipital lobe in the rhesus monkey. Brain research. 21;179(1):3-20.

Robinson DA, Fuchs AF (1969) Eye movements evoked by stimulation of frontal eye fields. J Neurophysiol 32:637–648.

Rosa MGP, Palmer SM, Gamberini M, Burman KJ, Yu HH, Reser DH, Bourne JA, Tweedale R, Galletti C (2009) Connections of the dorsomedial visual area: Pathways for early integration of dorsal and ventral streams in extrastriate cortex. Journal of Neuroscience 29:4548–4563.

Rubino D, Robbins KA, Hatsopoulos NG (2006) Propagating waves mediate information transfer in the motor cortex. Nat Neurosci 9:1549–1557.

Saalmann YB, Pigarev IN, Vidyasagar TR (2007) Neural mechanisms of visual attention: how top-down feedback highlights relevant locations. Science 316:1612–1615.

Saalmann YB, Pinsk MA, Wang L, Li X, Kastner S (2012) The pulvinar regulates information transmission between cortical areas based on attention demands. Science 337:753–756.

Sadakane O, Masamizu Y, Watakabe A, Terada S-I, Ohtsuka M, Takaji M, Mizukami H, Ozawa K, Kawasaki H, Matsuzaki M, Yamamori T (2015) Long-Term Two-Photon Calcium Imaging of Neuronal Populations with Subcellular Resolution in Adult Non-human Primates. Cell Rep 13:1989–1999.

Sakata S, Harris KD (2009) Laminar structure of spontaneous and sensory-evoked population activity in auditory cortex. Neuron 64:404–418.

Sanes JN, Donoghue JP (1993) Oscillations in local field potentials of the primate motor cortex during voluntary movement. Proceedings of the National Academy of Sciences 90:4470–4474.

Santisakultarm TP, Kersbergen CJ, Bandy DK, Ide DC, Choi S-H, Silva AC (2016) Two-photon imaging of cerebral hemodynamics and neural activity in awake and anesthetized marmosets. J Neurosci Methods 271:55–64.

Sasaki E et al. (2009) Generation of transgenic non-human primates with germline transmission. Nature 459:523–527.

Sato TK, Häusser M, Carandini M (2014) Distal connectivity causes summation and division across mouse visual cortex. Nat Neurosci 17:30–32.

Schaeffer DJ, Gilbert KM, Hori Y, Hayrynen LK, Johnston KD, Gati JS, Menon RS, Everling S (2019) Task-based fMRI of a free-viewing visuo-saccadic network in the marmoset monkey. Neuroimage 202:116147.

Schall JD (1991) Neuronal activity related to visually guided saccades in the frontal eye fields of rhesus monkeys: comparison with supplementary eye fields. J Neurophysiol 66:559–579.

Schall JD (1995) Neural basis of saccade target selection. Rev Neurosci 6:63–85.

Schall JD (1997) Visuomotor Areas of the Frontal Lobe. In: Extrastriate Cortex in Primates (Rockland KS, Kaas JH, Peters A, eds), pp 527–638. Boston, MA: Springer US.

Schall JD, Morel A, King DJ, Bullier J (1995a) Topography of visual cortex connections with frontal eye field in macaque: convergence and segregation of processing streams. J Neurosci 15:4464–4487.

Schall JD, Morel A, King DJ, Bullier J (1995b) Topography of visual cortex connections with frontal eye field in macaque: convergence and segregation of processing streams. J Neurosci 15:4464 4487.

Schall JD, Zinke W, Cosman JD, Schall MS, Paré M, Pouget P (2020) On the Evolution of the Frontal Eye Field: Comparisons of Monkeys, Apes, and Humans. In: Evolutionary Neuroscience, pp 861–890. Elsevier.

Schiller PH, Stryker M (1972) Single-unit recording and stimulation in superior colliculus of the alert rhesus monkey. J Neurophysiol 35:915–924.

Schlag-Rey M, Amador N, Sanchez H, Schlag J (1997) Antisaccade performance predicted by neuronal activity in the supplementary eye field. Nature 390:398–401.

Schluppeck D, Curtis CE, Glimcher PW, Heeger DJ (2006) Sustained activity in topographic areas of human posterior parietal cortex during memory-guided saccades. J Neurosci 26:5098–5108.

Schluppeck D, Glimcher P, Heeger DJ (2005) Topographic organization for delayed saccades in human posterior parietal cortex. J Neurophysiol 94:1372–1384.

Schmitt LI, Wimmer RD, Nakajima M, Happ M, Mofakham S, Halassa MM (2017) Thalamic amplification of cortical connectivity sustains attentional control. Nature 545:219–223.

Schmolesky MT, Wang Y, Hanes DP, Thompson KG, Leutgeb S, Schall JD, Leventhal AG (1998) Signal Timing Across the Macaque Visual System. J Neurophysiol 79:3272–3278.

Schroeder CE, Lakatos P (2009) Low-frequency neuronal oscillations as instruments of sensory selection. Trends Neurosci 32:9–18.

Schroeder CE, Mehta AD, Givre SJ (1998) A spatiotemporal profile of visual system activation revealed by current source density analysis in the awake macaque. Cereb Cortex 8:575–592.

Self MW, van Kerkoerle T, Supèr H, Roelfsema PR (2013) Distinct roles of the cortical layers of area V1 in figure-ground segregation. Curr Biol 23:2121–2129.

Selvanayagam J, Johnston KD, Schaeffer DJ, Hayrynen LK, Everling S (2019) Functional Localization of the Frontal Eye Fields in the Common Marmoset Using Microstimulation. J Neurosci 39:9197–9206.

Selvanayagam J, Johnston K, Everling S (2023) Laminar dynamics of target selection in the posterior parietal cortex of the common marmoset. bioRxiv Available at: http://biorxiv.org/lookup/doi/10.1101/2023.08.15.553425.

Senzai Y, Fernandez-Ruiz A, Buzsáki G (2019) Layer-Specific Physiological Features and Interlaminar Interactions in the Primary Visual Cortex of the Mouse. Neuron 101:500–513.e5.

Serences JT, Yantis S (2006) Selective visual attention and perceptual coherence. Trends Cogn Sci 10:38–45.

Shepherd GM (2011) The microcircuit concept applied to cortical evolution: from three-layer to six-layer cortex. Front Neuroanat 5:30.

Shewcraft RA, Dean HL, Fabiszak MM, Hagan MA, Wong YT, Pesaran B (2020) Excitatory/Inhibitory Responses Shape Coherent Neuronal Dynamics Driven by Optogenetic Stimulation in the Primate Brain. J Neurosci 40:2056–2068.

Shibutani H, Sakata H, Hyvärinen J (1984) Saccade and blinking evoked by microstimulation of the posterior parietal association cortex of the monkey. Exp Brain Res 55:1–8.

Siegel M, Buschman TJ, Miller EK (2015) Cortical information flow during flexible sensorimotor decisions. Science 348:1352–1355.

Silver MA, Kastner S (2009) Topographic maps in human frontal and parietal cortex. Trends Cogn Sci 13:488–495.

Silver MA, Ress D, Heeger DJ (2005) Topographic maps of visual spatial attention in human parietal cortex. J Neurophysiol 94:1358–1371.

Snyder LH, Batista AP, Andersen RA (1997) Coding of intention in the posterior parietal cortex. Nature 386:167–170.

Solomon SG, Rosa MGP (2014) A simpler primate brain: the visual system of the marmoset monkey. Front Neural Circuits 8:96.

Solomon SG, White AJR, Martin PR (2002) Extraclassical receptive field properties of parvocellular, magnocellular, and koniocellular cells in the primate lateral geniculate nucleus. J Neurosci 22:338–349.

Solomon SS, Chen SC, Morley JW, Solomon SG (2015) Local and Global Correlations between Neurons in the Middle Temporal Area of Primate Visual Cortex. Cereb Cortex 25:3182–3196.

Solomon SS, Morley JW, Solomon SG (2017) Spectral Signatures of Feedforward and Recurrent Circuitry in Monkey Area MT. Cereb Cortex 27:2793–2808.

Sommer MA, Wurtz RH (2006) Influence of the thalamus on spatial visual processing in frontal cortex. Nature 444:374–377.

Spadacenta S, Dicke PW, Thier P (2019) Reflexive gaze following in common marmoset monkeys. Sci Rep 9:15292.

Stanton GB, Bruce CJ, Goldberg ME (1995) Topography of projections to posterior cortical areas from the macaque frontal eye fields. J Comp Neurol 353:291–305.

Stanton GB, Deng SY, Goldberg ME, McMullen NT (1989) Cytoarchitectural characteristic of the frontal eye fields in macaque monkeys. J Comp Neurol 282:415–427.

Stettler DD, Yamahachi H, Li W, Denk W, Gilbert CD (2006) Axons and synaptic boutons are highly dynamic in adult visual cortex. Neuron 49:877–887.

Sugrue LP, Corrado GS, Newsome WT (2004) Matching behavior and the representation of value in the parietal cortex. Science 304:1782–1787.

Swanson LW, Newman E, Araque A, Dubinsky JM. The beautiful brain: the drawings of Santiago Ramón y Cajal. Seattle, WA: Abrams, 2017.Szczepanski SM, Konen CS, Kastner S (2010) Mechanisms of spatial attention control in frontal and parietal cortex. J Neurosci 30:148–160.

Thier P, Andersen RA (1998) Electrical microstimulation distinguishes distinct saccade-related areas in the posterior parietal cortex. J Neurophysiol 80:1713–1735.

Thompson KG, Hanes DP, Bichot NP, Schall JD (1996) Perceptual and motor processing stages identified in the activity of macaque frontal eye field neurons during visual search. J Neurophysiol 76:4040–4055.

Thomson AM, Bannister AP (2003) Interlaminar connections in the neocortex. Cereb Cortex 13:5–14.

Treue S, Maunsell JH (1999) Effects of attention on the processing of motion in macaque middle temporal and medial superior temporal visual cortical areas. J Neurosci 19:7591–7602.

Ungerleider LG, Galkin TW, Desimone R, Gattass R (2008) Cortical connections of area V4 in the macaque. Cereb Cortex 18:477–499.

van Kerkoerle T, Self MW, Dagnino B, Gariel-Mathis M-A, Poort J, van der Togt C, Roelfsema PR (2014) Alpha and gamma oscillations characterize feedback and feedforward processing in monkey visual cortex. Proc Natl Acad Sci U S A 111:14332–14341.

Wagner MJ, Kim TH, Kadmon J, Nguyen ND, Ganguli S, Schnitzer MJ, Luo L (2019) Shared Cortex-Cerebellum Dynamics in the Execution and Learning of a Motor Task. Cell 177:669–682.e24.

Walker AE (1940) A cytoarchitectural study of the prefrontal area of the macaque monkey. J Comp Neurol 73:59–86.

Wandell BA, Dumoulin SO, Brewer AA (2007) Visual field maps in human cortex. Neuron 56:366–383.

Wardak C, Ibos G, Duhamel J-R, Olivier E (2006) Contribution of the monkey frontal eye field to covert visual attention. J Neurosci 26:4228–4235.

Wardak C, Olivier E, Duhamel J-R (2002) Saccadic target selection deficits after lateral intraparietal area inactivation in monkeys. J Neurosci 22:9877–9884.

Wardak C, Olivier E, Duhamel J-R (2011) The relationship between spatial attention and saccades in the frontoparietal network of the monkey. Eur J Neurosci 33:1973–1981.

Wardak C, Vanduffel W, Orban GA (2010) Searching for a salient target involves frontal regions. Cereb Cortex 20:2464–2477.

Westerberg JA, Sigworth EA, Schall JD, Maier A (2021) Pop-out search instigates beta-gated feature selectivity enhancement across V4 layers. Proc Natl Acad Sci U S A 118

Available at: http://dx.doi.org/10.1073/pnas.2103702118.

Whissell PD, Tohyama S, Martin LJ (2016) The Use of DREADDs to Deconstruct Behavior. Front Genet 7:70.

Wiegert JS, Mahn M, Prigge M, Printz Y, Yizhar O (2017) Silencing Neurons: Tools, Applications, and Experimental Constraints. Neuron 95:504–529.

Wiesel TN, Hubel DH, Lam DM (1974) Autoradiographic demonstration of ocular-dominance columns in the monkey striate cortex by means of transneuronal transport. Brain Res 79:273–279.

Wietek J, Nozownik A, Pulin M, Saraf-Sinik I, Matosevich N, Gowrishankar R, Gat A, Malan D, Brown BJ, Dine J, Imambocus BN (2024) A bistable inhibitory OptoGPCR for multiplexed optogenetic control of neural circuits. Nature Methods 29:1-3.

Wimmer RD, Schmitt LI, Davidson TJ, Nakajima M, Deisseroth K, Halassa MM (2015) Thalamic control of sensory selection in divided attention. Nature 526:705–709.

Wong YT, Fabiszak MM, Novikov Y, Daw ND, Pesaran B (2016) Coherent neuronal ensembles are rapidly recruited when making a look-reach decision. Nat Neurosci 19:327–334.

Wu Z, Chen A, Cai X (2023) Neuronal response to reward and luminance in macaque LIP during saccadic choice. Neuroscience Bulletin. 39(1):14-28

Wurtz RH, Mohler CW (1976) Enhancement of visual responses in monkey striate cortex and frontal eye fields. J Neurophysiol 39:766–772.

Yang M, Zhou Z, Zhang J, Li T, Guan J, Liao X, Leng B, Lyu J, Yan J, Zhang K, Gong Y, Tang Y, Zhu Z, Varga Z, Konnerth A, Gao J, Chen X, Jia H (2019) MATRIEX Imaging: Multi-Area Two-photon Real-time In-vivo Explorer. bioRxiv:510545 Available at: https://www.biorxiv.org/content/10.1101/510545v2 [Accessed July 23, 2021].

Yates JL, Coop SH, Sarch GH, Wu R-J, Butts DA, Rucci M, Mitchell JF (2023) Detailed characterization of neural selectivity in free viewing primates. Nat Commun 14:3656.

Yu H-H, Rowley DP, Price NSC, Rosa MGP, Zavitz E (2020) A twisted visual field map in the primate dorsomedial cortex predicted by topographic continuity. Sci Adv 6 Available at: http://dx.doi.org/10.1126/sciadv.aaz8673.

Zavitz E, Yu H-H, Rowe EG, Rosa MGP, Price NSC (2016) Rapid Adaptation Induces Persistent Biases in Population Codes for Visual Motion. Journal of Neuroscience 36:4579–4590.

Zhang M, Barash S (2000) Neuronal switching of sensorimotor transformations for antisaccades. Nature 408:971–975.

Zhang M, Barash S (2004) Persistent LIP activity in memory antisaccades: working memory for a sensorimotor transformation. J Neurophysiol 91:1424–1441.

Zhu Q, Vanduffel W (2019) Submillimeter fMRI reveals a layout of dorsal visual cortex in macaques, remarkably similar to New World monkeys. Proc Natl Acad Sci U S A 116:2306–2311.